



**Politecnico  
di Torino**

Master of Science degree in Mechanical Engineering  
Academic Year 2022/2023

**Integrated design of Autonomous System  
Brake and Emergency Brake System for a  
Formula Student prototype**

**Supervisors**

Prof. Nicola Amati

Co-Sup. Gennaro Sorrentino

**Candidate**

Matteo Dalla Stella

# Abstract

In recent years, the field in which the automotive industry researched most is the autonomous driving. As a consequence, also the motorsport world embraced the concept of autonomous driving vehicles. Formula Student, a motorsport competition in which students design, manufacture and race their own vehicles, founded its Driverless competition in 2017, so that young engineers could develop knowledge on self-driving vehicles.

From the mechanical point of view the main difference between a human operated vehicle and a driverless vehicle is the presence of mechanical actuators that have to emulate the driver actions. The object of this thesis is the brake actuator, which is divided into two subsystems: Autonomous System Brake (ASB), that can perform ordinary braking manoeuvres, and Emergency Brake System (EBS), that can perform emergency braking manoeuvres.

At first it was necessary to evaluate the target force needed by the braking actuators to perform braking with the maximum possible deceleration. The EBS consists in a pneumatic actuator, which was sized on the target force calculated. The ASB is an electromechanical actuator, composed by an electric motor, a gear train and a ball screw mechanism. Differently from the previous version of ASB/EBS mounted on the vehicle, the braking system actuators' case is designed to support both the ASB and the EBS in a compact volume.

After the sizing both systems have been tested. The ASB performance has been evaluated by means of a Simulink model, while experiments on test bench have been performed on the EBS actuator. Results are promising and the system is compatible with a driverless motorsport application.

# Acknowledgements

I would like to thank Professor Nicola Amati and Engineer Gennaro Sorrentino for offering me the opportunity to research in the innovative field of autonomous driving vehicles and, in particular, with a driverless motorsport prototype.

A special thanks also to Squadra Corse Driverless PoliTO team, to the mech guys and, in particular, to Stefano and James. Being part of this wonderful team has been an incredible journey that I will always remember in my heart.

I am grateful to my parents and my brother Enrico who always supported me and always listened to my thinking aloud. Now (finally) everybody in the family knows what a ball screw is.

A special thought also to my grandpa Cele, who made me passionate about cars and motorsport. You followed me throughout my path, with a short phone call every time something good happened, always congratulating and at the same time pushing to pursue my dreams.

My deepest thank also to my girlfriend Arianna, who sustained and pushed me during these wonderful years. It is because of you that I sent my application to Squadra Corse Driverless in 2021, with everything that followed that decision. With all the times spent talking to you about the issues (a lot) and the solutions (a few) you probably know this thesis as good as I do.

And finally I would like to finish this section with a quote that everyone near me knows that I use and abuse:

*"Oh no!  
Anyway..."*

*Jeremy Clarkson*

# Contents

<b>1</b>	<b>Introduction</b>	<b>9</b>
1.1	Road safety . . . . .	9
1.2	Autonomous driving . . . . .	10
1.3	Formula Student and Formula Student Driverless . . . . .	11
1.4	Squadra Corse Driverless . . . . .	13
1.5	Autonomous System Brake and Emergency Brake System . . . . .	14
1.6	Thesis outline . . . . .	16
<b>2</b>	<b>Actuation targets</b>	<b>17</b>
2.1	Braking system architecture . . . . .	17
2.1.1	SCD22 ASB and EBS . . . . .	19
2.1.2	Integrated design of ASB and EBS . . . . .	21
2.1.3	SCD23 ASB and EBS . . . . .	23
2.2	Performance requirements . . . . .	24
2.3	Vehicle braking dynamics . . . . .	25
2.4	Master cylinders selection . . . . .	28
2.5	Actuation targets calculation . . . . .	30
<b>3</b>	<b>Mechanical design</b>	<b>34</b>
3.1	EBS design . . . . .	35
3.1.1	EBS actuator . . . . .	35
3.1.2	EBS canister . . . . .	36
3.1.3	EBS joint . . . . .	38
3.2	ASB design . . . . .	38
3.2.1	Ball screw . . . . .	40
3.2.2	Electric motor . . . . .	47
3.2.3	Gear train . . . . .	48
3.2.4	Ball screw - gear train joint . . . . .	52
3.2.5	ASB bar . . . . .	55
3.2.6	Pneumatic cylinder fork . . . . .	61
3.2.7	Master cylinder rod end . . . . .	62
3.2.8	Balance bar . . . . .	63
3.2.9	Kinematic analysis . . . . .	66
3.3	Case design . . . . .	69

3.3.1	Base . . . . .	70
3.3.2	Rear column . . . . .	70
3.3.3	Front column . . . . .	71
3.3.4	Front column connections . . . . .	75
3.3.5	Bearing supports . . . . .	75
3.3.6	Gear train support . . . . .	76
3.3.7	Case assembly structural analysis . . . . .	77
3.4	Assembly pictures . . . . .	83
<b>4</b>	<b>Modelling</b>	<b>85</b>
4.1	Electric motor . . . . .	86
4.2	Gear train . . . . .	87
4.3	Ball screw . . . . .	88
4.4	ASB bar and master cylinders . . . . .	89
4.5	Controller . . . . .	90
4.6	Step response analysis . . . . .	91
4.7	Frequency response analysis . . . . .	93
<b>5</b>	<b>EBS experimental campaign</b>	<b>96</b>
5.1	Test setup . . . . .	97
5.2	Data analysis . . . . .	98
<b>6</b>	<b>Conclusions and future steps</b>	<b>103</b>
<b>A</b>	<b>Abbreviations</b>	<b>109</b>
<b>B</b>	<b>Simulink model</b>	<b>110</b>

# List of Figures

1.1	SAE J3016 six levels of automation[9]	10
1.2	Skidpad track layout[14]	13
1.3	SC19 Formula Student Electric prototype	14
1.4	Steering actuator[18]	15
1.5	Schematic of the Shutdown Circuit[14]	16
2.1	Hydraulic brake lines without autonomous actuators	17
2.2	Brake pedal assembly	18
2.3	Brembo master cylinders[20]	18
2.4	Braking system architecture of SCD22, including manual braking, ASB and EBS. For a better visualization hydraulic lines are represented in bold	20
2.5	EBS (left) and ASB (top right) mounted on the vehicle	21
2.6	New braking system architecture, including manual braking, ASB and EBS. For a better visualization hydraulic lines are represented in bold	22
2.7	Braking system architecture of SCD23	23
2.8	SCD23 ASB analysis	24
2.9	Vehicle free body diagram	25
2.10	Wheels free body diagram	26
2.11	Changes in vehicle braking dynamics with different MC setups	30
2.12	Variation of vehicle deceleration, wheels' angular deceleration, normal forces and tangential forces as a function of the force generated by the ASB	31
2.13	Variation of brake fluid pressure as a function of the force generated by the ASB and variation of deceleration as a function of brake fluid pressure	32
2.14	Deceleration as a function of the force generated by the ASB (or the EBS in case of emergency braking) in case of failure in one line	33
3.1	Render of the ASB/EBS assembly	34
3.2	Festo pneumatic cylinder[27] used as EBS actuator	35
3.3	Braking kinematic due to EBS actuation at different speeds	37
3.4	High pressure canister	37
3.5	SKF Uniballs	39
3.6	Ball screws[30]	40
3.7	Bosch Rexroth ball screw efficiency as a function of the pitch angle[30]	42
3.8	Bosch Rexroth indications on safety factor[30]	42
3.9	Bosch Rexroth SEB-F bearing[30]	43

3.10	Hiwin FK08 bearing[32]	44
3.11	SKF BA 8 thrust ball bearing[33]	45
3.12	Hwin FF10 bearing[32]	46
3.13	Spacer	47
3.14	Maxon EC 45 flat electric motor[35]	49
3.15	Characteristic curve of Maxon EC 45 flat brushless motor[35]	50
3.16	Maxon Planetary Gearhead GP 32 C[40]	51
3.17	Bolt joint between gear train and ball screw	54
3.18	ASB bar	55
3.19	Hertzian contact between the ASB bar and the two master cylinders	56
3.20	ASB bar free body diagram (XZ plane)	56
3.21	ASB bar free body diagram (YZ plane)	57
3.22	Free body diagrams in brake line fail condition (vertical forces on the bushing free body diagram are omitted)	58
3.23	ASB bar stress distribution when the maximum force is generated by the ASB	60
3.24	ASB bar displacement when the maximum force is generated by the ASB	60
3.25	ASB bar stress distribution in case of hydraulic fail in one brake line and maximum force generated by the ASB	61
3.26	Pneumatic cylinder forks	62
3.27	Master cylinders' rod ends	63
3.28	Balance bar free body diagram	64
3.29	Balance bar free body diagram in horizontal position	65
3.30	The two linear guides for the pneumatic cylinder forks, each one composed by a bushing and a shaft	65
3.31	ASB kinematic analysis scheme	67
3.32	Simplified model for balance bar and master cylinders	68
3.33	Kinematic analysis with simultaneous activation of the brake lines	69
3.34	Kinematic analysis with right brake line activated with a delay	70
3.35	Kinematic analysis with right brake line in fail	71
3.36	Base 3D model	72
3.37	Rear column	72
3.38	Rear column holes for the bearing supports and the gear train support	73
3.39	Rear column flanges for the bushings' shafts	73
3.40	Balance bar's Uniball housing on the rear column	74
3.41	Front column	74
3.42	Front column connections	75
3.43	Bearing supports	76
3.44	gear train support	76
3.45	ASB operation: stress distribution	80
3.46	ASB operation: displacement	80
3.47	ASB/EBS assembly seen from the front bulkhead of the vehicle	83
3.48	ASB/EBS assembly mounted on the vehicle	84
3.49	Rear of the ASB/EBS assembly	84

4.1	ASB model block diagram . . . . .	85
4.2	Electric motor equivalent circuit[44] . . . . .	86
4.3	ASB bar model . . . . .	89
4.4	ASB step response at different sets of pressure . . . . .	91
4.5	ASB step response analysis . . . . .	92
4.6	ASB Bode diagram . . . . .	94
4.7	Bandwidth as a function of the signal amplitude . . . . .	95
5.1	SCD23 EBS mounted on the vehicle . . . . .	96
5.2	EBS actuator test setup . . . . .	97
5.3	EBS actuator test bench pneumatic circuit . . . . .	97
5.4	Experimental data of force and pressure during the test to evaluate the force developed . . . . .	99
5.5	Graphics from test on the pneumatic actuator whose target is to define the order of magnitude of rising time and decreasing time . . . . .	100
5.6	Graphics from test on the pneumatic actuator whose target is to define rising time and decreasing time . . . . .	101
5.7	Rising time and decreasing time as a function of the number of actuations	102
B.1	ASB model . . . . .	110
B.2	ASB controller subsystem . . . . .	110
B.3	ASB subsystem . . . . .	111
B.4	Electric motor subsystem . . . . .	111
B.5	Gear train subsystem . . . . .	112
B.6	Ball screw subsystem . . . . .	112
B.7	ASB bar and master cylinders subsystem . . . . .	113

# List of Tables

- 2.1 Braking system architecture parameters . . . . . 19
- 2.2 Constants . . . . . 29
- 2.3 ASB and EBS targets considering a safety factor of 1.5 . . . . . 32
  
- 3.1 EBS sizing data . . . . . 36
- 3.2 Comparison between rotative to linear mechanisms[31] . . . . . 40
- 3.3 Comparison between three ball screw mechanisms[30][32] . . . . . 43
- 3.4 Bosch Rexroth SEB-F bearing data and calculations[30] . . . . . 44
- 3.5 Hiwin FK08 bearing data and calculations[32] . . . . . 45
- 3.6 SKF BA 8 bearing data and calculations[33] . . . . . 46
- 3.7 Ball screw assembly details[32][33] . . . . . 48
- 3.8 Maxon EC 45 flat brushless motor datasheet[35] . . . . . 49
- 3.9 Custom gear train parameters . . . . . 52
- 3.10 Maxon Planetary Gearhead GP 32 C datasheet[40] . . . . . 53
- 3.11 Aluminium case with weight reducing holes FEM analysis . . . . . 79
- 3.12 Aluminium case without weight reducing holes FEM analysis . . . . . 79
- 3.13 Steel case with weight reducing holes FEM analysis . . . . . 81
- 3.14 Steel case with weight reducing holes FEM analysis . . . . . 82

# Chapter 1

## Introduction

### 1.1 Road safety

Since their invention in the late 1800s the automobiles had a huge impact on everyday life[1]. While before 1900 most people spent their lives within a few miles of where they were born, the invention of cars changed all that, allowing people to travel easily[2]. From International Organization of Motor Vehicle Manufacturers (OICA) data 1.59 billion of vehicles were registered in 2020 all around the world, in other words 209 vehicles for every 1000 inhabitants[3].

Because of the high number of vehicles on the road the automotive field always researches solutions to overcome new challenges. Nowadays the automotive R&D program is focused on two main targets: reduction of the environmental impact of vehicles and safety increase for road users. With regards to the last point, in 2016 the World Health Organization registered 1.35 million death caused by road traffic injuries, that is to say the 8<sup>th</sup> leading cause of death for people of all ages[4]. In 2022 in Italy Istat registered that 166 thousand road accidents that caused 223 thousand of injured and 3159 deaths[5]. The main three causes of accidents were distraction (15.0 %), failure to comply precedence rules (13.7 %) and speeding (9.3 %).

In order to increase road safety two types of safety feature are developed:

- *passive safety features*, which are parts of the vehicle that mitigates the effect of an accident during and after impact (for example seat belts and airbags)[6];
- *active safety features*, which are mechanisms that avoid or mitigates an accident pre-impact, for example Anti-lock Brake System (ABS) or Advanced Driver Assistance Systems[7].

Nowadays the evolution of autonomous driving is considered to have a huge potential on the reduction of road accidents[8]. In fact self-driving vehicles reduce the effects of human errors, which is the cause of 90 % of road accidents. However, the field is still in evolution and only it is expected to see the first results in road safety only in 2030.

## 1.2 Autonomous driving

The first ideas on autonomous driving were born in the first decades when General Motors, with its 1939 Futurama installation, showed the first vision of autonomous vehicles. Differently from today's driverless cars, in Futurama the vehicles were not self-driving, but it was the highway to be automated: vehicle entering the highway will be automatically driven to the desired exit by the highway itself.

**SAE J3016™ LEVELS OF DRIVING AUTOMATION™**  
 Learn more here: [sae.org/standards/content/j3016\\_202104](http://sae.org/standards/content/j3016_202104)

Copyright © 2021 SAE International. The summary table may be freely copied and distributed AS-IS provided that SAE International is acknowledged as the source of the content.

	SAE LEVEL 0™	SAE LEVEL 1™	SAE LEVEL 2™	SAE LEVEL 3™	SAE LEVEL 4™	SAE LEVEL 5™
What does the human in the driver's seat have to do?	You <b>are</b> driving whenever these driver support features are engaged – even if your feet are off the pedals and you are not steering			You <b>are not</b> driving when these automated driving features are engaged – even if you are seated in “the driver’s seat”		
	You must constantly supervise these support features; you must steer, brake or accelerate as needed to maintain safety			When the feature requests, you must drive	These automated driving features will not require you to take over driving	
Copyright © 2021 SAE International.						
What do these features do?	These are driver support features			These are automated driving features		
	These features are limited to providing warnings and momentary assistance	These features provide steering OR brake/acceleration support to the driver	These features provide steering AND brake/acceleration support to the driver	These features can drive the vehicle under limited conditions and will not operate unless all required conditions are met	This feature can drive the vehicle under all conditions	
Example Features	<ul style="list-style-type: none"> <li>• automatic emergency braking</li> <li>• blind spot warning</li> <li>• lane departure warning</li> </ul>	<ul style="list-style-type: none"> <li>• lane centering OR</li> <li>• adaptive cruise control</li> </ul>	<ul style="list-style-type: none"> <li>• lane centering AND</li> <li>• adaptive cruise control at the same time</li> </ul>	<ul style="list-style-type: none"> <li>• traffic jam chauffeur</li> </ul>	<ul style="list-style-type: none"> <li>• local driverless taxi</li> <li>• pedals/steering wheel may or may not be installed</li> </ul>	<ul style="list-style-type: none"> <li>• same as level 4, but feature can drive everywhere in all conditions</li> </ul>

**Figure 1.1:** SAE J3016 six levels of automation[9]

The evolution of autonomous driving in the last two decades led to the definition of levels for autonomous driving with the introduction of the taxonomy SAE J3016 defined by the Society of Automotive Engineers[9]. The normative defines 6 levels of automation[10] (Figure 1.1):

- *level 0*: the driver is fully responsible for driving while the system provides momentary assistance with warnings or emergency interventions;
- *level 1*: the driver is fully responsible for driving while the system provides continuous assistance with acceleration/braking or steering;

- *level 2*: the driver is fully responsible for driving while the system provides continuous assistance with acceleration/braking and steering;
- *level 3*: the system handles all aspects of driving while the driver must remain alert to intervene if the system cannot operate;
- *level 4*: the system is fully responsible for driving within controlled environment while the driver is not needed on the vehicle;
- *level 5*: the system is fully responsible for driving in all conditions while the driver is not needed on the vehicle.

European laws allows autonomous driving only till SAE level 3[11], but the majority of autonomous vehicle available in the market has only up to SAE level 2. However some exceptions allow the test of SAE level 4 vehicles on European roads[12].

### 1.3 Formula Student and Formula Student Driverless

Formula Student is an international competition founded in 1981 by the Society of Automotive Engineers[13]. The competition challenges teams of university students to design, manufacture, develop and compete with small formula style race cars[14]. Formula Student was born in the United States but has soon spread with races all over the world. In Europe the most important competition is Formula Student Germany (FSG). The rules wrote by FSG organizers are adopted by most of European competitions, with some additions defined by other races' organizers.

Until 2017 the events were divided in two different competitions depending on the vehicle propulsion system: Formula Student Combustion, for prototypes with internal combustion engine, and Formula Student Electric, for prototypes with electric propulsion. Motorsport has always been a test bench for the automotive industry[15] and this also applies to Formula Student. In fact, due to the evolution of autonomous driving, a third competition was created by FSG in 2017: Formula Student Driverless.

Prototypes competing in the Driverless competition are fully autonomous driving vehicles. The heart of a Formula Student Driverless prototype is the Autonomous System (AS) which is the system that has to substitute the driver inside the vehicle. Like a driver the AS has first to identify the track, delimited by blue and yellow cones, by means of sensors like cameras, LiDAR and radar. Afterwards the AS has to compute the best trajectory thanks to path planning algorithms and it has to evaluate the amount of steering and torque or braking needed to follow the trajectory using control algorithms. At the end the AS has to substitute the physical action of a driver thanks to mechanical actuators. It is important to underline that the prototype is not operated by remote control but it is self-driving; the only remote commands are the starting procedure order and the emergency manoeuvre, explained in detail in Section 1.5. Since the vehicle can

move autonomously but in a controlled environment (the track) the prototypes can be associated to a SAE level 4 of automation (Figure 1.1).

To be compliant with FSG rules a Formula Driverless prototype must be able to be driven by a human driver. The result of this rule is that driverless vehicles are very similar to Formula Electric or Formula Combustion prototypes, with the only difference consisting in the Autonomous System, not present in non-driverless vehicles.

A single Formula Student Driverless competition is divided into multiple events, both Static and Dynamic. During Dynamic Events vehicles have to complete the event in the shortest time possible; car to car battles are not allowed by the rules. The Dynamic Events for the Driverless competition are the following:

- *Acceleration Event* (maximum score = 75 points): the track is a straight line with a length of 75 meters;
- *Skidpad Event* (maximum score = 50 points): the track consist of two pair of concentric circles (Figure 1.2) and each car has to take two laps on the right circle and two laps on the left circle, while only the last lap on each circle is timed;
- *Autocross Event* (maximum score = 100 points): the autocross event is a handling track built following some guidelines specified on the rules and every prototype has to complete one lap;
- *Trackdrive Event* (maximum score = 200 points): the track for the Trackdrive Event is the same as the one used for the Autocross Event, but each vehicle has to complete ten laps.

It is important to underline that, except for Acceleration and Skidpad events, the track is previously unknown and therefore perception sensors are fundamental.

Besides Dynamic Events, the team ability to design an efficient, low cost car and to develop a business model around it are evaluated during Static Events:

- *Business Plan Presentation Event* (maximum score = 75 points): the objective of the event is to evaluate the team's ability to develop and deliver a business model offering the vehicle or its component as a product or selling a service that relates to it;
- *Cost and Manufacturing Event* (maximum score = 95 points): the objective of the event is to evaluate the team's understanding of the manufacturing process and costs associated;
- *Engineering Design Event* (maximum score = 150 points): the objective of the event is to evaluate the team's engineering process for the design of the prototype.

As it is possible to calculate in each event it is possible to collect up to 745 points. 43 % of the points available come from Static Events, meaning that to aim to a race win it is necessary to build a fast and reliable vehicle, but also efficient, low cost and designed following the best engineering practice.

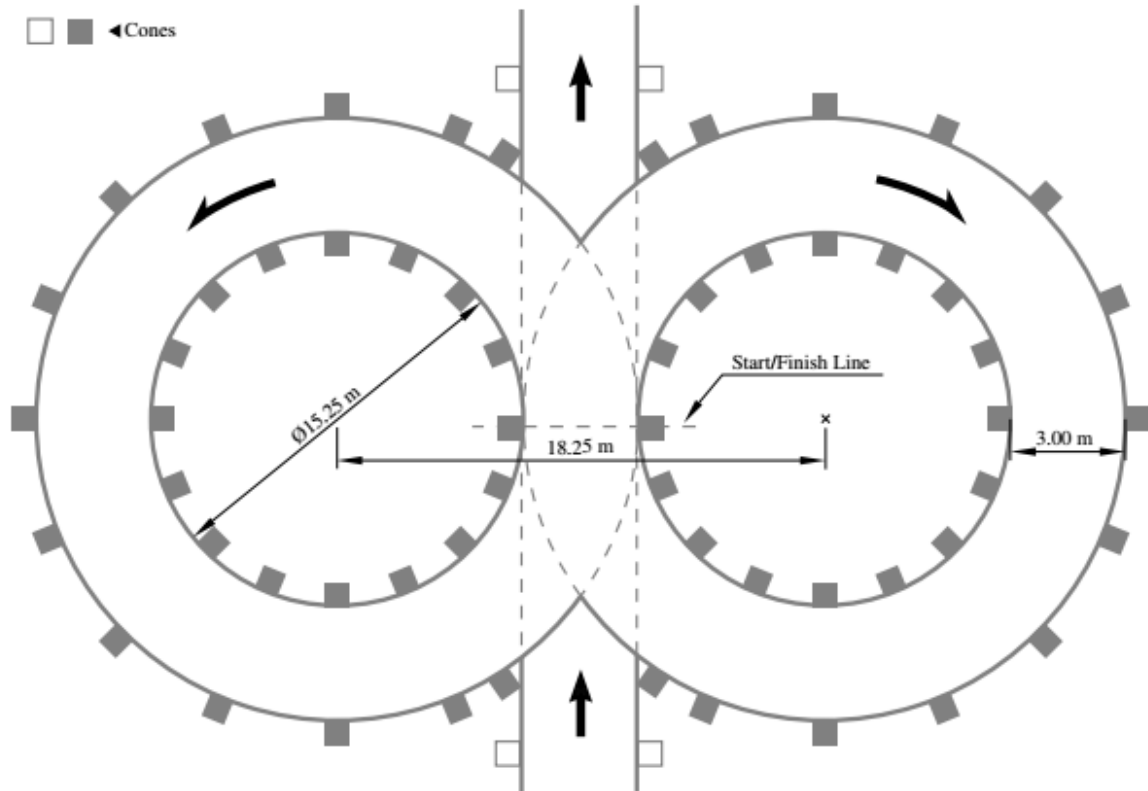


**Figure 1.2:** Skidpad track layout[14]

Since its introduction in 2017 the Formula Student Driverless has grown through the years. In 2022, for the first time ever, Formula Student Germany merged the Driverless competition with Formula Student Electric and Formula Student Combustion. This means that teams aiming to win the competition have to develop a prototype designed both for manual and driverless driving. This situation allowed Formula Student to approach the automotive world, where cars are designed to be driven first by a human driver and in some cases also by the Autonomous System.

## 1.4 Squadra Corse Driverless

Squadra Corse Driverless is the Formula Student Driverless team of Politecnico di Torino[16]. The team was founded in 2021 and it inherited the SC19 prototype, a Formula Student Electric vehicle designed and manufactured in 2019 (Figure 1.3). The car has a carbon fiber monocoque, with a total mass of around 200 kg. It has four in-wheel electric motors with a total maximum power limited to 80 kW and a total maximum torque limited to 84 Nm. When driven by a driver the SC19 accelerates from 0 km/h to 100 km/h in 2.6 s.

The vehicle has been modified in order to add the Autonomous System, including



**Figure 1.3:** SC19 Formula Student Electric prototype

both software and hardware updates. In 2022 the prototype, with codename SCD22, took part at its first driverless competition, achieving the third place overall in Formula SAE Italy[17].

The prototype used in 2023, codename SCD23, was the evolution of the SCD22. The sensors used by the AS for the perception of the track are two cameras and a LiDAR, that with a sensor fusion algorithm are able to detect the cones that represent the track. The steering actuator is composed by a ball screw mechanism actuated by an electric motor and in parallel to the previously existing steering rack[18] (Figure 1.4), while the acceleration actuator is not needed since the electric motors can be controlled directly through the inverters. The brake actuators, object of this thesis, are explained in detail in the following chapters.

## 1.5 Autonomous System Brake and Emergency Brake System

The Autonomous System Brake (ASB) is the brake actuator needed by the rules to run in autonomous mode (FSG T15 rules[14]). The Emergency Brake System (EBS) is the part of the ASB that guarantees the emergency braking manoeuvre. Therefore the ASB should guarantee ordinary braking but also, thanks to the EBS, emergency braking. The

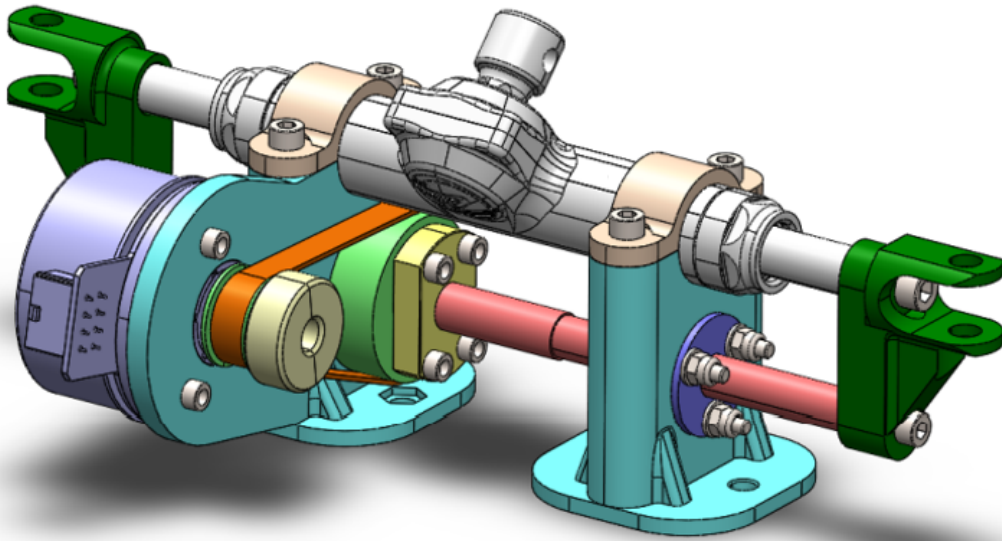


**Figure 1.4:** Steering actuator[18]

EBS is a part of the ASB but, for sake of clarity, hereafter ASB will refer only to the actuator that performs the ordinary braking and EBS will refer to the actuator that performs the emergency manoeuvre.

Since the EBS is a safety component of the vehicle several rules specify how the system should work. First of all the EBS should use only passive systems with mechanical energy storage in order to operate if an electrical power loss occurs (T15.2.1). The vehicle safety status is carried out by the Shutdown Circuit (SDC) an electrical circuit that runs across all the vehicle and supply different buttons, switches and relays (Figure 1.5). If the SDC is closed the vehicle is in a safe condition; if the SDC is open the vehicle is in an unsafe condition: the car has to stop immediately thanks to the EBS and the high voltage battery that supplies the electric motor is disconnected.

One of the relays that maintain the SDC closed is the Remote Emergency System (RES) relay[19]. The system is a radio component with two functions (rule T14.3.3):

- when the “Go” button is pressed, the autonomous mission is started;
- when the remote emergency stop button is pressed, it must open the RES relay on the SDC.

The RES signals are the only remote commands allowed in Formula Student Driverless.

To sum up, while the ASB operates in regular braking manoeuvres during races, the EBS is activated only by malfunctions of the vehicle. The SDC opens if failures are detected or if the RES’ emergency stop button is pressed. If the SDC is open the vehicle will stop immediately by means of the EBS.

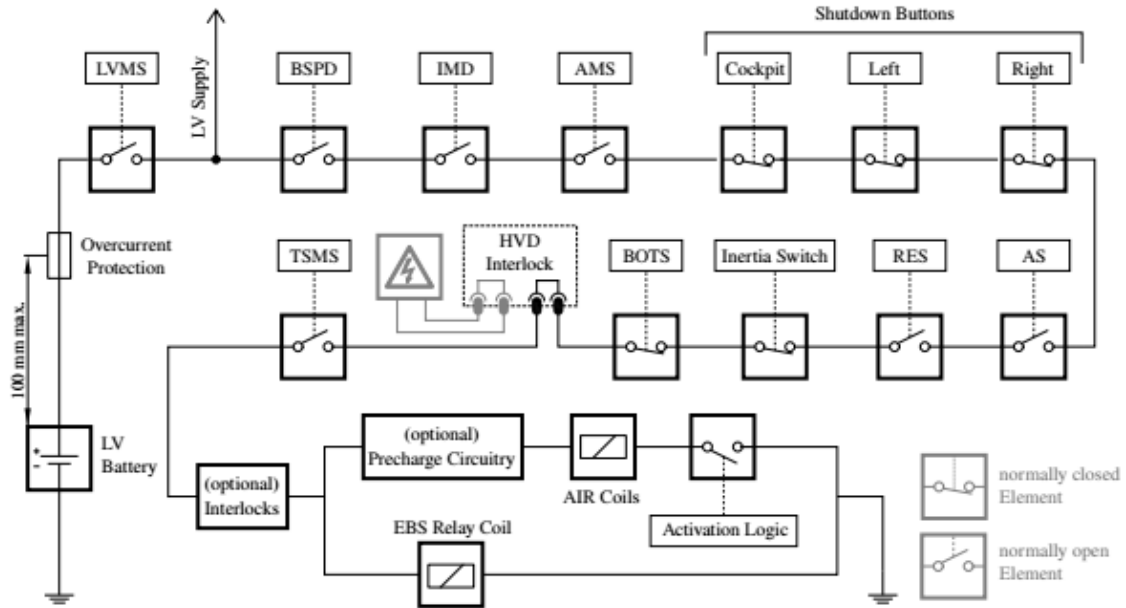


Figure 1.5: Schematic of the Shutdown Circuit[14]

## 1.6 Thesis outline

The target of this thesis is the design and the validation of a system able to work as Autonomous System Brake and Emergency Brake System for Squadra Corse Driverless' prototype. At first, the braking targets have been defined in order to guarantee the performance required by the Formula Student rulebook. Once the optimal brake lines layout has been chosen, the system has then been sized.

Since the rules specify that the EBS has to use only passive energy systems[14], a pneumatic system has been chosen. On the other hand, in order to guarantee enough control on the braking force during non-emergency braking maneuver an electromechanical system has been chosen as ASB. The two systems are independent but they both have in common some elements. Each component of the two systems has been sized, as well as the case of the systems.

The ASB performance has been evaluated by means of a Simulink model. The analysis focused both on the time response, in order to calculate the static performance of the system, and on the frequency response, in order to calculate the dynamic performance. The EBS has then been tested on a test bench, in order to evaluate the force generated as well as the rising time of the system.

# Chapter 2

## Actuation targets

The aim of this chapter is to give an overview on the braking system of the vehicle and to calculate the actuation forces required.

### 2.1 Braking system architecture

The ASB and the EBS are designed to be implemented in an existing Formula Student prototype. The braking system architecture of the SCD23, without the autonomous actuators, is reported in Figure 2.1.

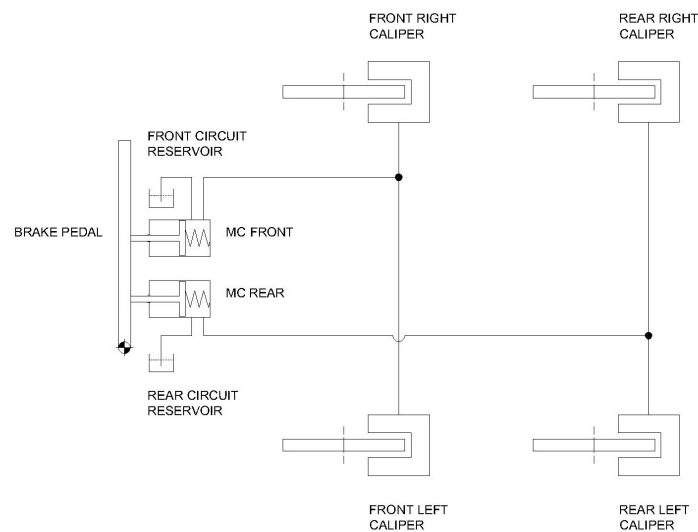


**Figure 2.1:** Hydraulic brake lines without autonomous actuators

The brake lines are divided into front line and rear line. Two master cylinders, one for each line, convert the force applied on the brake pedal into fluid pressure. The master cylinders are in parallel configuration in order to guarantee redundancy as required by FSG rule T6.1.2[14]. While the brake pedal is custom made (Figure 2.2), the master

cylinders are manufactured by Brembo (Figure 2.3); the front master cylinder has a bore of 17.5 mm, while the rear one has a bore of 16 mm.

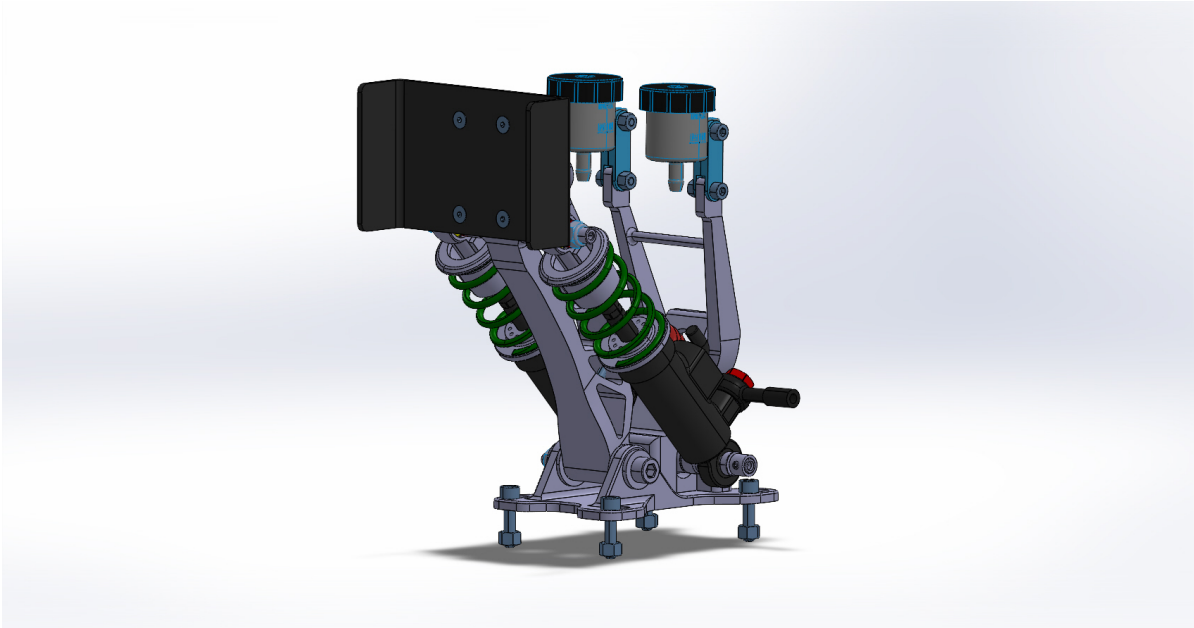


Figure 2.2: Brake pedal assembly

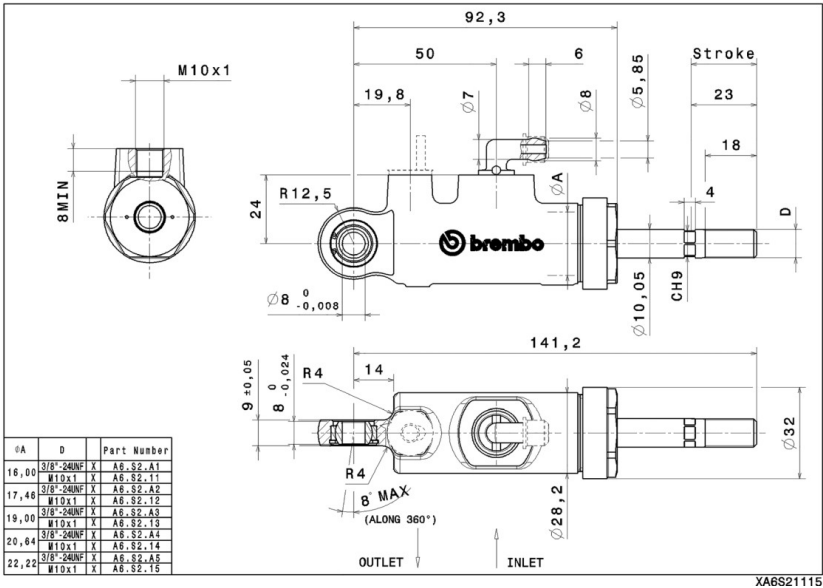


Figure 2.3: Brembo master cylinders[20]

After the master cylinders each line is divided into right and left calipers. Each caliper presents pistons that, thanks to the fluid pressure, generate a force on the braking pads. The friction between pads and disc produces the braking torque on the wheel. Like the

master cylinders, also calipers and pads are manufactured by Brembo. The bore of the piston is of 24 mm either on the front and on the rear of the vehicle, but while on the front there are four pistons per caliper (Brembo P4 24), on the rear there are only two pistons per caliper (Brembo P2 24)[21]. The discs are custom made and present a radius at pads level of 94 mm at the front and of 83 mm at the rear. Table 2.1 summarize the already existing braking system architecture.

	Front	Rear
MC bore	17.46 mm	16 mm
Number of pistons per caliper	4	2
Caliper pistons bore	24 mm	24 mm
Brake disc radius	94 mm	83 mm

**Table 2.1:** Braking system architecture parameters

In addition to the hydraulic braking system, the vehicle is able to perform regenerative braking. The four electric motors of the vehicle can work as generators, converting the kinetic energy of the vehicle into electrical energy that is going to be stored in the Tractive System Energy Storage, in other words the High Voltage Battery. FSG rule T6.1.11 specifies that maximum 90 % of the brake pedal travel may be used for regenerative braking without actuating hydraulic brake system[14]. However regenerative braking will be considered null for the design of the Autonomous System Brake.

### 2.1.1 SCD22 ASB and EBS

In 2022 the vehicle, named SCD22, had a fully functional Autonomous System Brake and Emergency Brake System. The schematic of the braking system architecture is reported in Figure 2.4.

The ASB of the prototype is implemented with an electric servo-motor[22] (Figure 2.5). Its shaft is attached to a pulley that rotates a steel cable directly connected to the brake pedal. Therefore the kinematic chain allows to transform the torque generated by the servo-motor in a force acting on the master cylinders and, as a result, in brake fluid pressure.

Since the ASB uses electric power the system cannot be used also for emergency braking because only passive systems are allowed (T15.2.1). Therefore the Emergency Brake System of the vehicle is a separated device that uses compressed air as energy source[23]. Two air canisters, one for the front line and one for the rear line, supply air at 200 bar. In each line a pressure regulator sets the maximum pressure at 10 bar, the maximum pressure allowed by the rules[14]. Two 3/2 normally open solenoid valves, one for each line, manage the emergency braking:

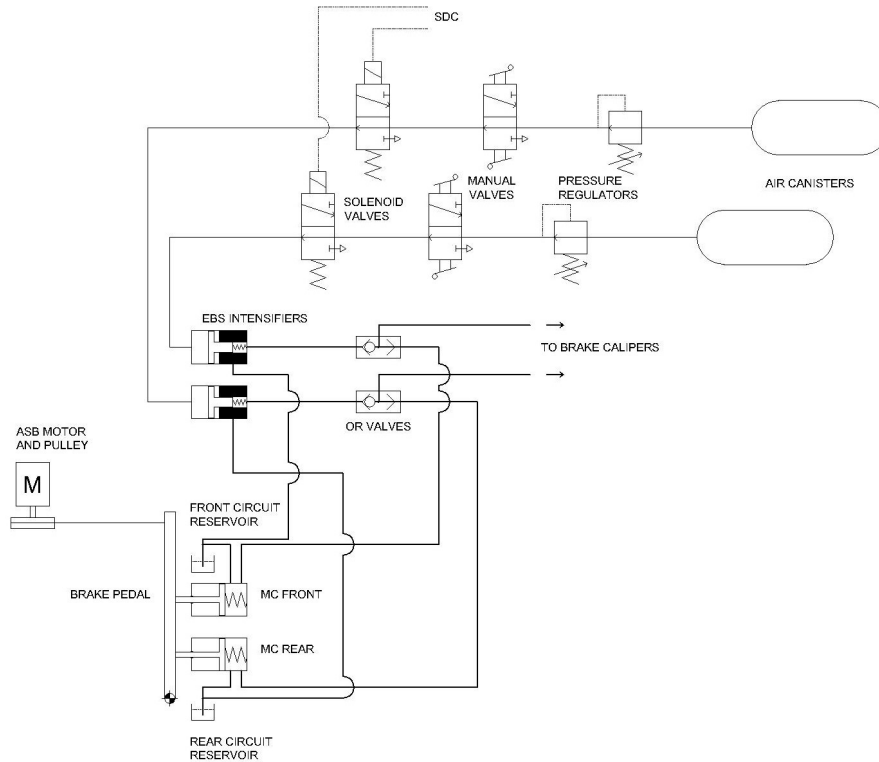


**Figure 2.4:** Braking system architecture of SCD22, including manual braking, ASB and EBS. For a better visualization hydraulic lines are represented in bold

- if the Shut Down Circuit is closed, and therefore no emergency is detected, the valves are in the closed position and the actuators are at ambient pressure;
- if an emergency is detected the Shut Down Circuit will open and the pneumatic pressure in the actuators will rise.

The actuators are pressure intensifiers with one chamber connected to the pneumatic circuit and the other chamber connected to the hydraulic braking system. The pneumatic chamber has an higher bore than the hydraulic chamber, therefore the pressure in the hydraulic braking system is higher than the pressure in the pneumatic system[23] (Figure 2.5).

To guarantee the functioning of both emergency braking and manual braking simultaneously as requested by rule T15.1.4 two or valves are connected in the hydraulic system, one for each line. ASB and EBS simultaneous activation could also be possible considering the braking architecture, but it is not a realistic situation since the activation of the EBS disconnect the ASB power supply. Another function of the or valves is to avoid the rising of fluid pressure in the actuators' line or master cylinders' line if these are not actuated, preventing the damaging of the components[24].

Manual valves activate or deactivate the EBS. If the valves are in the open position the EBS could be activated, since line pressure is at 10 bar; if the valves are in



**Figure 2.5:** EBS (left) and ASB (top right) mounted on the vehicle

closed position EBS' lines are at ambient pressure and the actuators cannot be activated. Another function of the manual valves is the deactivation point required by the rules (T15.1.7 and T15.1.8): after the EBS activation the turning of the valve to the closed position allows to connect the intensifiers to ambient pressure, deactivating the emergency braking.

The system as presented was used during 2022 Formula ATA event. However some drawbacks of the system have been discovered. As regards to the EBS the main problems was a leakage of oil from the oil chamber to the air chamber, causing the corrosion of the seals and the rising of the internal friction of the actuators, and the use of a small area on the pneumatic chamber, which lead to low brake fluid pressure. Moreover the ASB had an issue with the tensioning of the steel cable that absorbed part of the force generated by the servo-motor. Another issue was the volume occupied by the two systems that made maintenance operations on the front of the vehicle more difficult.

### **2.1.2 Integrated design of ASB and EBS**

The objective of this thesis is the evolution of the SCD22's ASB and EBS. In this new solution ASB and EBS are no longer divided into two different components but they are integrated into a single device, solving the problem regarding the volume of the system. In Figure 2.6 it is shown a schematic of the braking system.

In this brake architecture each line has two master cylinders, one dedicated only for the manual braking and the other one for autonomous braking, including both ASB and

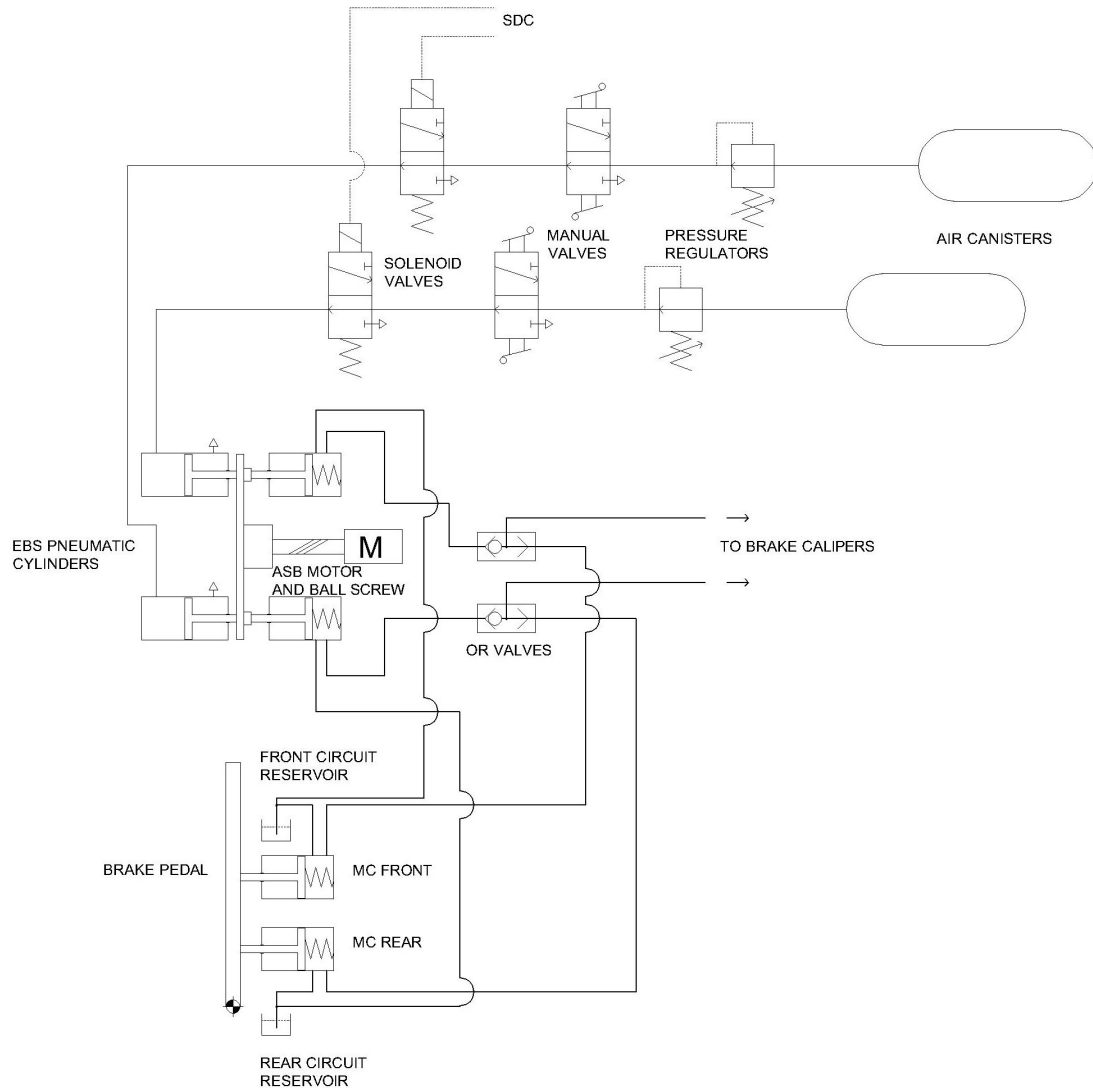


**Figure 2.6:** New braking system architecture, including manual braking, ASB and EBS. For a better visualization hydraulic lines are represented in bold

EBS. In order to prevent the oil leaking as described in Section 2.1.1 the evolution of the EBS is composed by a pneumatic cylinder and a master cylinder, per brake line, connected with a joint. Thanks to this solution the hydraulic line cannot come into contact with the pneumatic line. The EBS design is better explained in Section 3.1.

The ASB consists of an electric motor connected to a ball screw in order to transform the motion from rotating to linear. The ball screw's nut is connected to the master cylinders of the autonomous actuators, therefore a force on the ball screw generates pressure in the brake lines. It is important to underline that ball screw and master cylinders are not jointed together but the contact is removable: in this case the force given by the EBS acts only on the master cylinders and not on the ASB and therefore

the system has an higher efficiency and the ball screw will not be damaged because of impulsive forces. The ASB design is better explained in Section 3.2.

### 2.1.3 SCD23 ASB and EBS

Since the ASB object of this thesis is a complex mechanism which could not be manufactured for the 2023 season, the SCD23 had a different brake actuators setup (Figure 2.7).

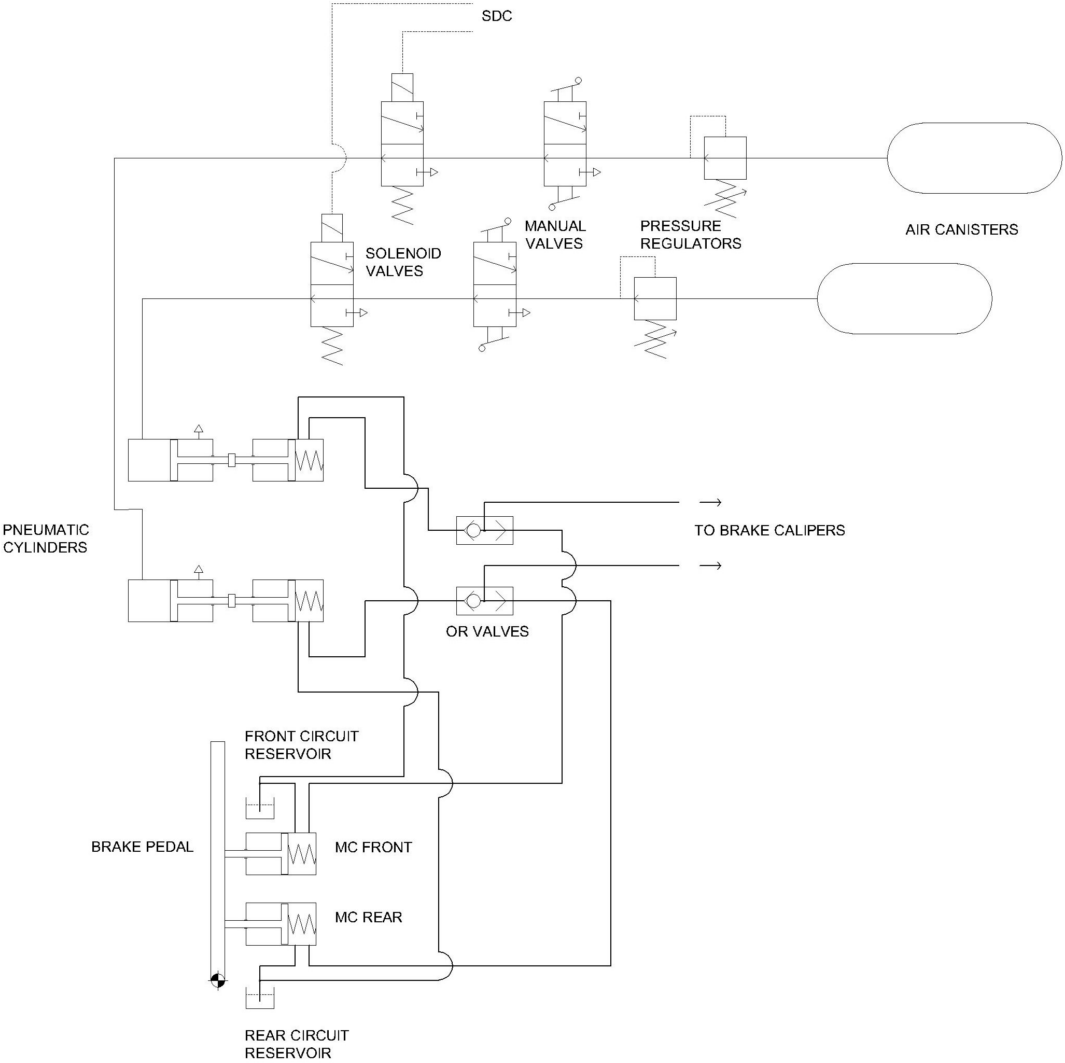


**Figure 2.7:** Braking system architecture of SCD23

In this solution the same device is used both as ASB and EBS actuator. The actuator is the same as the one designed in this thesis for the EBS. In case of EBS operation the solenoid valves are controlled with the SDC as specified in Section 2.1.2, while in case

of ASB operation the solenoid valves are controlled by means of a PWM signal with switching frequency of 10 Hz and duty cycle depending on the braking force needed.

Experimental and numerical tests have been performed and the results are reported in the following Figure 2.8, where the pressure specified is the brake fluid pressure generated.

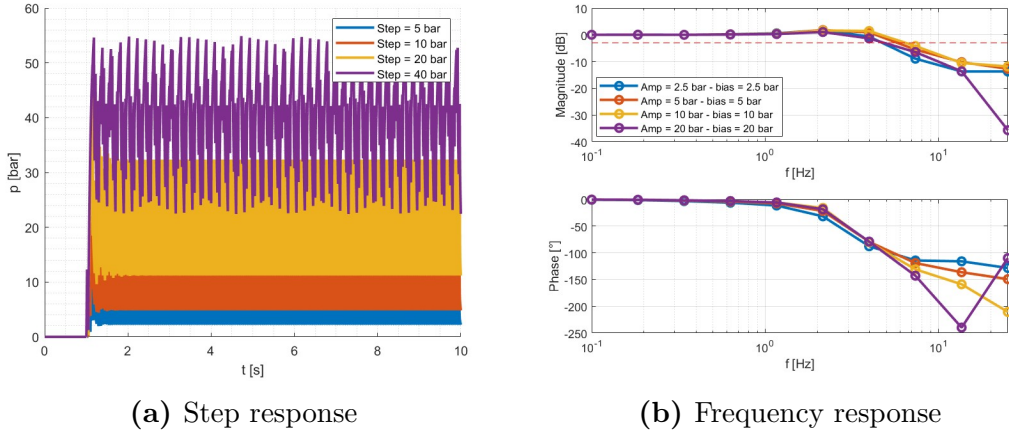


**Figure 2.8:** SCD23 ASB analysis

As it is possible to see in Figure 2.8a, the system is very responsive but it has high oscillations around the desired value. The oscillations reduce with higher sets of pressure, since the ASB reaches its force limit. In Figure 2.8b it is possible to see the frequency response of the system. The bandwidth of the system is between 4.9 Hz and 6.6 Hz, acceptable values for a braking system.

## 2.2 Performance requirements

Formula Student Germany rule-book[14] sets rules on the performance of the Emergency Brake System:

- T15.4.1: The system reaction time (the time between opening of the SDC and the start of the deceleration) must not exceed 200 ms.
- T15.4.2: The average deceleration must be greater than  $8 \text{ m/s}^2$  under dry track conditions.
- T15.4.3: In case of a single failure the ASB should be designed to achieve at least half of the performance specified in T15.4.2.
- T15.4.4: Whilst decelerating, the vehicle must remain in a stable driving condition.

Another set of rules specifies how the EBS will be tested:

- IN11.2.1 The EBS performance will be tested dynamically and must demonstrate the performance described in T15.4.

IN11.2.2 The test will be performed in a straight line marked with cones similar to acceleration.

IN11.2.3 During the brake test, the vehicle must accelerate in autonomous mode up to at least  $40\text{km/h}$  within 20 m. From the point where the RES is triggered, the vehicle must come to a safe stop within a maximum distance of 10 m.

IN11.2.4 In case of wet track conditions, the stopping distance will be scaled by the officials dependent on the friction level of the track.

IN11.2.5 The EBS test is conducted after all other elements of IN11 have been passed.

There are no explicit rules for the Autonomous System Brake on FSG rule-book, while Formula Student East handbook[25] specifies that the vehicle has to lock all four wheels during a brake test procedure.

### 2.3 Vehicle braking dynamics

To calculate the actuation forces needed it is necessary to analyse the dynamic of the vehicle under braking. For simplicity a two-dimensional model is used. The prototype is divided into three subsystems[26]: the whole vehicle, front axle and rear axle. It is important to notice that aerodynamic forces as well as regenerative braking forces are neglected.

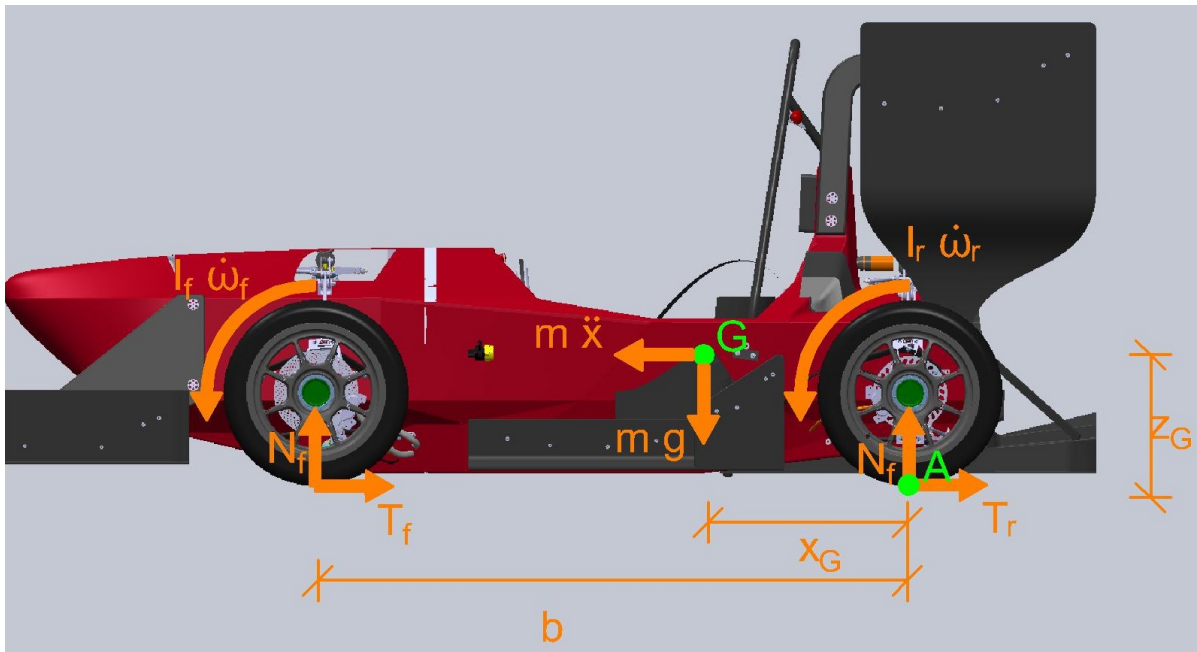
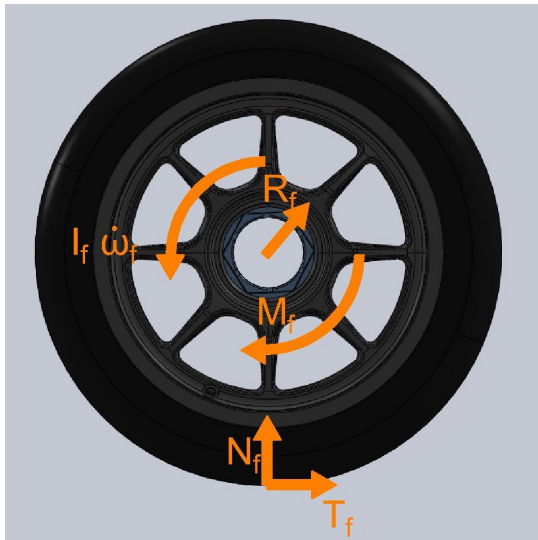
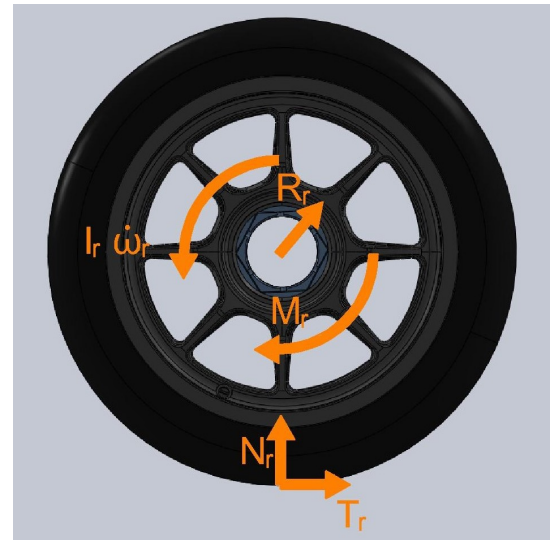


Figure 2.9: Vehicle free body diagram

Forces and constants in the free body diagrams are:



(a) Front wheel free body diagram



(b) Rear wheel free body diagram

**Figure 2.10:** Wheels free body diagram

- $m$ : mass of the vehicle;
- $I_f$ : moment of inertia of the front axle;
- $I_r$ : moment of inertia of the rear axle;
- $z_G$ : height from the road of the center of gravity;
- $x_G$ : horizontal distance from the rear axle to the center of gravity;
- $b$ : wheelbase;
- $\ddot{x}$ : deceleration of the vehicle;
- $\dot{\omega}_f$ : angular deceleration of the front axle;
- $\dot{\omega}_r$ : angular deceleration of the rear axle;
- $N_f$ : force parallel to Z axis acting on the front axle;
- $N_r$ : force parallel to Z axis acting on the rear axle;
- $T_f$ : force parallel to X axis acting on the front axle;
- $T_r$ : force parallel to X axis acting on the rear axle;
- $M_f$ : braking force acting on the front axle;
- $M_r$ : braking force acting on the rear axle.

From the balance of translation along Y and Z axis and from the balance of rotation around the point A (Figure 2.9) it is possible to obtain equations 2.2, 2.1 and 2.3 respectively.

$$N_f + N_r = mg \quad (2.1)$$

$$T_f + T_r = m\ddot{x} \quad (2.2)$$

$$I_f\dot{\omega}_f + I_r\dot{\omega}_r + m\ddot{x}z_G - mgx_G + N_rb = 0 \quad (2.3)$$

Considering the front axle and from the balance of rotation around the axle (Figure 2.10a) it is possible to obtain equation 2.4.

$$T_f + I_f\dot{\omega}_f = M_f \quad (2.4)$$

Similarly to the front axle it is possible to obtain equation 2.5 for the rear axle (Figure 2.10b).

$$T_r + I_r\dot{\omega}_r = M_r \quad (2.5)$$

As it is possible to analyse there are seven variables ( $\ddot{x}$ ,  $\dot{\omega}_f$ ,  $\dot{\omega}_r$ ,  $N_f$ ,  $N_r$ ,  $T_f$ ,  $T_r$ ,  $M_f$ ,  $M_r$ ) but only five equations. It is necessary to add other two equations regarding the kinematics of the vehicle, in particular taking into account the variable grip condition of the wheels[26]. Taking the front axle as an example, in order to have pure motion inequality 2.6 must be satisfied, where  $\mu$  is the friction coefficient between tyre and asphalt.

$$T_f \leq \mu N_f \quad (2.6)$$

If inequality 2.6 is true, then the sixth equation is going to be equation 2.7, where  $r = 237 \text{ mm}$  is the radius of the wheels.

$$\ddot{x} = r\dot{\omega}_f \quad (2.7)$$

If inequality 2.6 is not satisfied the sixth equation is going to be equation 2.8 and the force  $T_f$  is calculated with equation 2.9, where  $\mu_k$  is the kinetic friction coefficient between tyre and asphalt.

$$\dot{\omega}_f = 0 \quad (2.8)$$

$$T_f = \mu_k N_f \quad (2.9)$$

Similarly to the front axle, if  $T_r \leq \mu N_r$  then the seventh equation will be equation 2.10.

$$\ddot{x} = r\dot{\omega}_r \quad (2.10)$$

If the inequality is not satisfied the seventh equation will be equation 2.11, and the force  $T_r$  is calculated with equation 2.12.

$$\dot{\omega}_r = 0 \quad (2.11)$$

$$T_r = \mu_k N_r \quad (2.12)$$

For sake of simplicity the wheels are considered in pure rolling motion or fully locked but not in any intermediate condition. The static friction coefficient between tyres and asphalt, evaluated during tests held in 2019, has a value of  $\mu = 1.3$ ; a reduction of 80 % has been used to calculate the kinetic friction coefficient  $\mu_k$ . Thanks to other tests it has been possible to evaluate the friction coefficient between brake pads and brake discs, and the value calculated is  $\mu_{brake} = 0.4$ . The friction coefficients' values are reported in Table 2.2.

The force generated by the ASB is divided into two equal forces acting on the front line's master cylinder and on the rear line's master cylinder. Therefore the oil pressure in the front brake line is calculated with equation 2.13 and the pressure in the rear line with Equation 2.14.

$$p_f = \frac{F_{ASB}}{2A_{MC,f}} \quad (2.13)$$

$$p_r = \frac{F_{ASB}}{2A_{MC,r}} \quad (2.14)$$

$A_{MC,f}$  and  $A_{MC,r}$  depend on master cylinders' bore that are going to be evaluated in Section 2.4. Knowing the fluid pressure inside the braking system and the total area of the calipers' pistons at the front axle  $A_{cal,f}$  and at the rear axle  $A_{cal,r}$ , reported in Table 2.2, it is possible to calculate the braking forces acting on the front axle (equation 2.15) and rear axle (equation 2.16).

$$F_f = p_f A_{cal,f} \quad (2.15)$$

$$F_r = p_r A_{cal,r} \quad (2.16)$$

Knowing the medium distance  $r_{brake}$  from the wheel center to the brake pad it is possible to calculate the braking torque acting on the front axle[26] (equation 2.17) and the one acting on the rear axle (equation 2.18).

$$M_f = r_{brake,f} \mu_{brake} F_f = \frac{r_{brake,f} F_{ASB} A_{cal,f} \mu_{brake}}{2A_{MC,f}} \quad (2.17)$$

$$M_r = r_{brake,r} \mu_{brake} F_r = \frac{r_{brake,r} F_{ASB} A_{cal,r} \mu_{brake}}{2A_{MC,r}} \quad (2.18)$$

Thanks to a Matlab script it is possible to evaluate the vehicle braking dynamics and how the braking performance changes with several forces applied by the Autonomous System Brake. In Table 2.2 are reported the values of the constants used.

## 2.4 Master cylinders selection

The first thing to evaluate is the optimal master cylinders setup. The master cylinders could have bore of 16 mm, 17.46 mm or 19 mm[20]. Using a Matlab script it has been possible to analyse how the different setups affect the braking dynamics; the results are reported in Figure 2.11. The force with which maximum deceleration is obtained is going to be used as the target force for the ASB, while for the EBS, where front line and rear

Description		Value
Mass of the vehicle	$m$	200 <i>kg</i>
Moment of inertia of the front axle	$I_f$	$8.53 \cdot 10^{-1} \text{ kg m}^2$
Moment of inertia of the rear axle	$I_r$	$8.49 \cdot 10^{-1} \text{ kg m}^2$
Height from the road of the center of gravity	$z_G$	241 <i>mm</i>
Distance parallel to X axis from the rear axle to the center of gravity	$x_G$	878 <i>mm</i>
Wheelbase	$b$	1525 <i>mm</i>
Wheel radius	$r$	237 <i>mm</i>
Tyre - asphalt static friction coefficient	$\mu$	1.30
Tyre - asphalt kinetic friction coefficient	$\mu_k$	1.04
Brake pads - brake discs friction coefficient	$\mu_{brake}$	0.40
Front calipers' pistons total area[21]	$A_{cal,f}$	$3.62 \cdot 10^{-3} \text{ m}^2$
Rear calipers' pistons total area[21]	$A_{cal,r}$	$1.81 \cdot 10^{-3} \text{ m}^2$
Front brake radius	$r_{brake,f}$	94 <i>mm</i>
Rear brake radius	$r_{brake,r}$	83 <i>mm</i>

**Table 2.2:** Constants

line are independent, the target is the oil pressure with which maximum deceleration is obtained.

Figure 2.11 shows the deceleration obtained by a certain amount of force generated by the ASB. Each curve presents two discontinuity point, the first of which is caused by the locking of the front wheels while the second is caused by the lock of the rear wheels. As it was possible to imagine the locking of the wheels causes a reduction in deceleration of the vehicle. Two factor has been taken into account to choose the optimal setup:

- maximum deceleration performed;
- initial slope of the curve, because a curve with an higher slope requires less force to perform the same deceleration.

Considering only the initial slope the setup with bore of 16 mm both at the front and at the rear master cylinder is the best option, but the maximum deceleration performed is too low. Therefore the optimal option is with  $d_{MC,f} = 17.46 \text{ mm}$  and  $d_{MC,r} = 16 \text{ mm}$ , which is a setup that can guarantee the maximum deceleration with an excellent initial

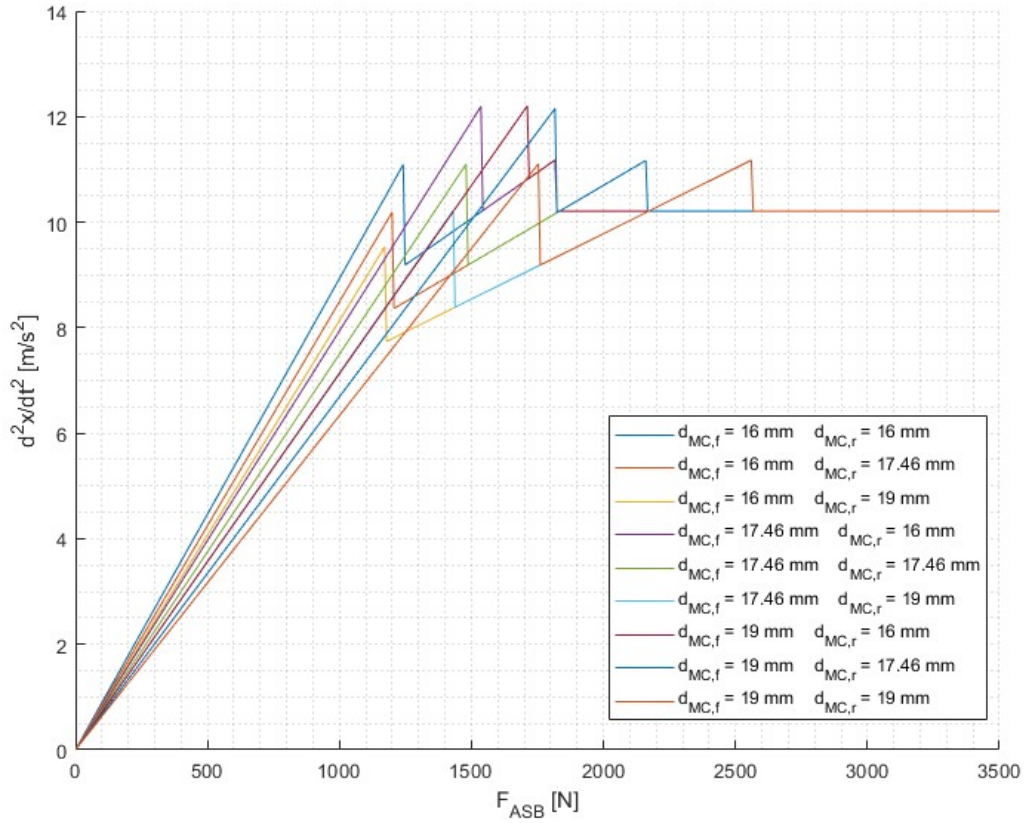


**Figure 2.11:** Changes in vehicle braking dynamics with different MC setups

slope. The setup chosen is also the same setup chosen in 2019 for the manual braking system.

## 2.5 Actuation targets calculation

Considering  $d_{MC,f} = 16\text{ mm}$  and  $d_{MC,r} = 17.46\text{ mm}$  it is possible to evaluate the actuation targets. Thanks to a Matlab script it is possible to analyse the effects of the variation of the force of the ASB on the dynamics of the vehicle. The results are reported in Figure 2.12 and Figure 2.13.

The maximum deceleration obtained is of  $12.20\text{ m/s}^2$ , which is higher than  $8\text{ m/s}^2$  as required by T15.4.2; also the deceleration achieved if all the wheels are locked is higher than the minimum requirement. The force needed to achieve the maximum deceleration is of 1536 N. From the wheels' angular deceleration graphic it is also possible to observe that the vehicle lock first the front wheels, remaining in a stable driving condition as required by T15.4.4.

From Figure 2.13 it is possible to evaluate the brake fluid pressure that the EBS

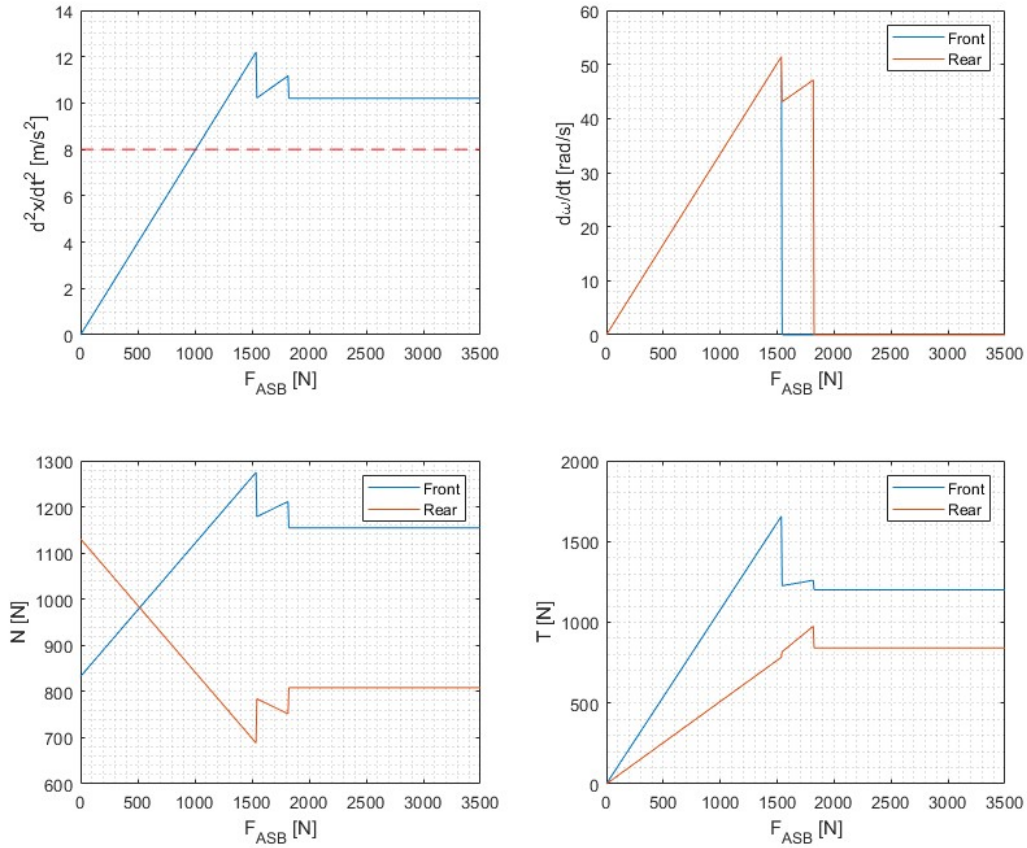


**Figure 2.12:** Variation of vehicle deceleration, wheels’ angular deceleration, normal forces and tangential forces as a function of the force generated by the ASB

has to achieve to obtain the maximum deceleration, that is  $p_f = 32.50 \text{ bar}$  for the front line and  $p_r = 38.71 \text{ bar}$  for the rear line. As it is possible to see the oil pressure on the front line is always lower than the pressure on the rear line because of the higher master cylinder bore (equations 2.13 and 2.14).

In Figure 2.14 it is possible to analyse the braking dynamics in case of fail of one of the braking lines. As specified in T15.4.3 in case of failure the vehicle has to decelerate with a minimum deceleration of  $4 \text{ m/s}^2$ . To guarantee the compliance of the rule the ASB (or the EBS in case of emergency braking) has to generate at least 729 N if the rear line has a failure or 765 N if the front line has a failure. These values are not used as targets for the design of ASB and EBS but they are going to be used as a check for the rule compliance of the system.

The targets calculated are reported in Table 2.3. In order to take into account the stiffness of the master cylinder spring and the friction between the components a safety factor of 1.5 has been taken into account.

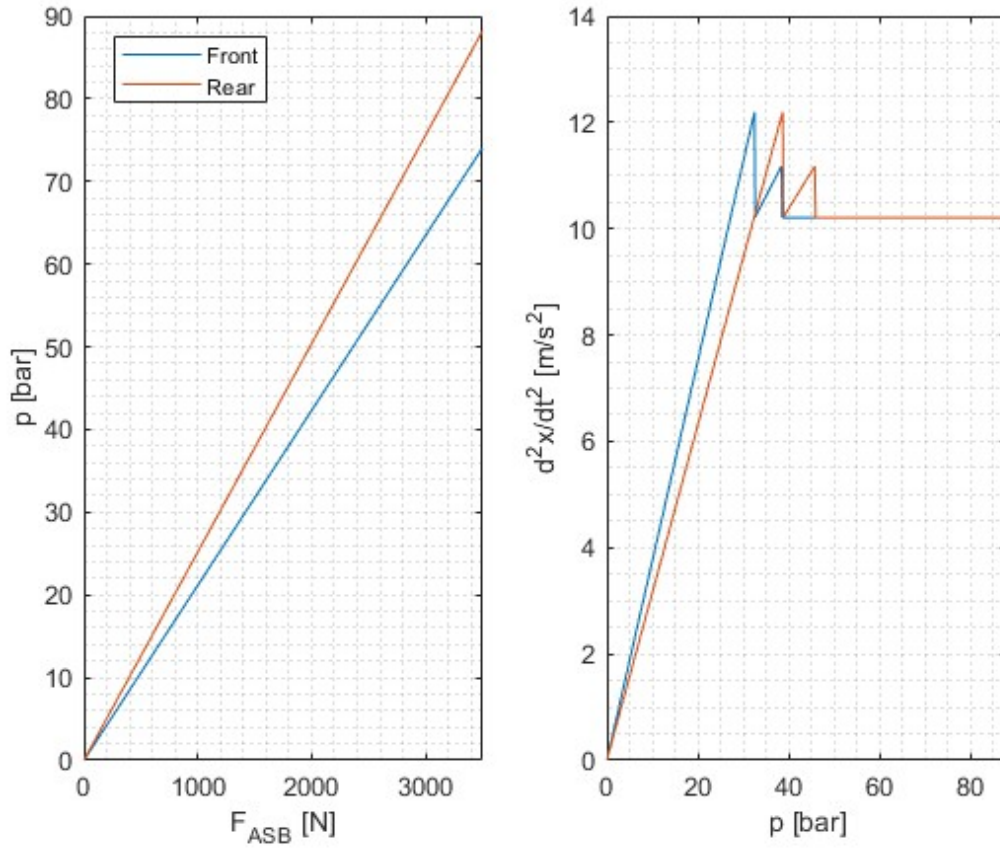


**Figure 2.13:** Variation of brake fluid pressure as a function of the force generated by the ASB and variation of deceleration as a function of brake fluid pressure

Description	Target without SF	Target with SF = 1.5
ASB maximum force	1536 N	2304 N
EBS front brake fluid pressure	32.50 bar	48.75 bar
EBS rear brake fluid pressure	38.71 bar	58.07 bar

**Table 2.3:** ASB and EBS targets considering a safety factor of 1.5

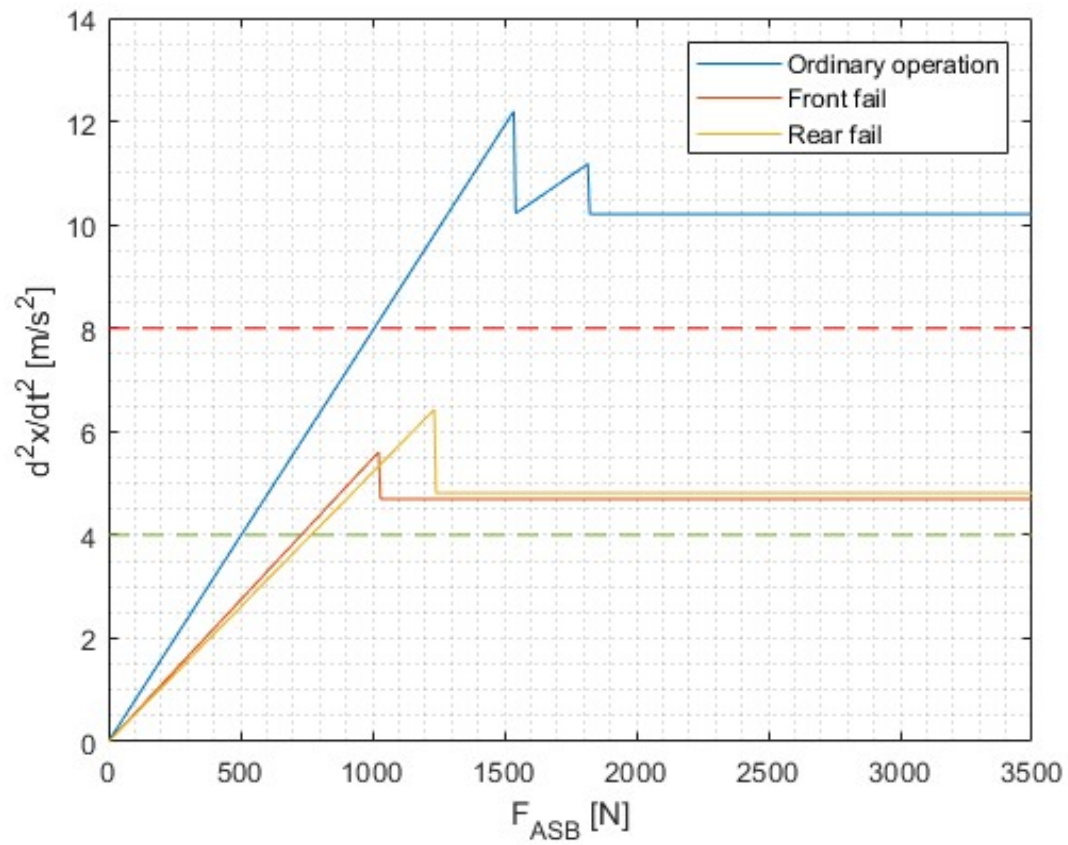


**Figure 2.14:** Deceleration as a function of the force generated by the ASB (or the EBS in case of emergency braking) in case of failure in one line

# Chapter 3

## Mechanical design

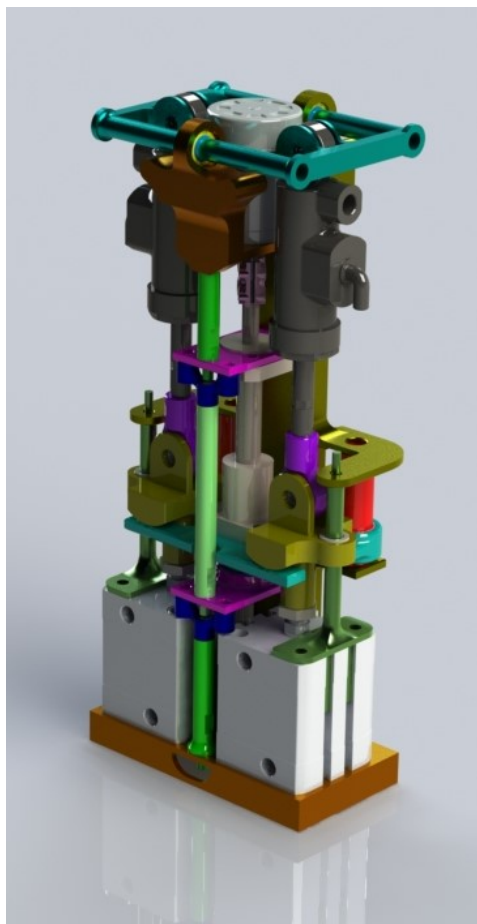


**Figure 3.1:** Render of the ASB/EBS assembly

The mechanical design of the autonomous brake actuators has been divided into three main subassemblies:

- EBS subassembly;

- ASB subassembly;
- case subassembly.

In this chapter the mechanical design of the three subassemblies is explained in detail. With regard to the EBS the system is composed by pneumatic cylinders that have to generate enough brake fluid pressure to satisfy the one calculated in Section 2.5. For the ASB the system consists in an electromechanical actuator, composed by an electric motor, a gear train and a ball screw. In the latter section it is also explained the design of the case for EBS and ASB.

### 3.1 EBS design

#### 3.1.1 EBS actuator

The Emergency Brake System actuator is composed by a pneumatic actuator. The shaft of the cylinder is then jointed to the shaft of the master cylinder. Each line, front and rear, is independent to the other, as specified in Section 2.1.2. Using equation 3.1 it is possible to calculate the minimum bore of the pneumatic cylinder.  $p_{MC}$  is the pressure target evaluated in Section 2.5 while  $p_{EBS}$  is limited by rule T9.1.1 at 10 bar.

$$d = d_{MC} \sqrt{\frac{p_{MC}}{p_{EBS}}} \quad (3.1)$$

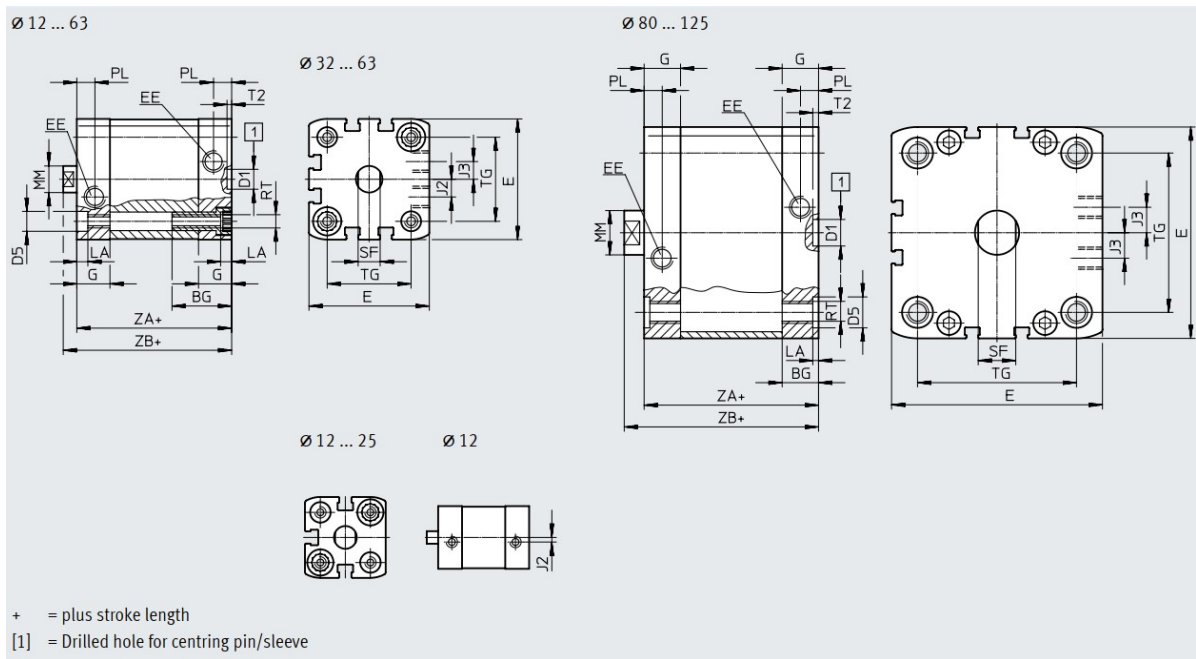


Figure 3.2: Festo pneumatic cylinder[27] used as EBS actuator

The minimum bore evaluated is of 38.64 mm at the front cylinder and of 38.55 mm at the rear cylinder. The pneumatic cylinders are not custom made and therefore the dimension of the bore is standardised. The maximum stroke of the master cylinder is very short (23 mm[20]), for this reason the best option found is the compact cylinder from Festo's ADN series[27] (Figure 3.2). The EBS could work with single acting cylinder, but since the master cylinder connected in series already has a return spring, the double acting cylinder has been chosen so that the force generated by the cylinder does not have to overcome the spring internal to the pneumatic cylinder. The bore chosen for both front and rear EBS is of 40 mm, while the stroke is 20 mm, lower than the maximum stroke of the master cylinder but enough to perform the emergency braking.

It is possible to evaluate the force generated by each cylinder using equation 3.2, where  $p_{EBS} = 10 \text{ bar}$  and  $d_{EBS} = 40 \text{ mm}$ .

$$F_{EBS} = p_{EBS} \frac{\pi d_{EBS}^2}{4} = 1273 \text{ N} \quad (3.2)$$

The force generated by the pneumatic actuators is higher than the minimum force in case of failure calculated in Section 2.5 (729 N for the front line and 765 N for the rear line). Results for EBS actuator selection are reported in Table 3.1.

	Front EBS	Rear EBS
$p_{MC}$ target	48.75 bar	58.07 bar
$\varnothing_{MC}$	16 mm	17.46 mm
$\varnothing_{EBS,min}$	38.64 mm	38.55 mm
$\varnothing_{EBS}$	40 mm	40 mm
$F_{EBS}$	1273 N	1273 N

**Table 3.1:** EBS sizing data

In order to verify the compliance of the EBS to rule IN11.2.3 (Section 2.2) a Matlab script has been used. The results are reported in Figure 3.3.

If the RES is triggered while the vehicle is moving at 40 km/h the vehicle comes to a safe stop within 6 m, less than 10 m as specified in IN11.2.3. However it is important to underline that electronic delays (opening of the SDC) and mechanical delays (rise of pressure inside the EBS actuator chamber) have not been considered .

### 3.1.2 EBS canister

As shown in Section 2.1.2 the ESB actuators are supplied by a canister for each line. Each canister has a volume of 0.15 l and a filling pressure of 200 bar[23] (Figure 3.4).

It is important to evaluate how many actuation the canister can provide. The maximum pressure of the canister is of 200 bar but, because of the compressor used by

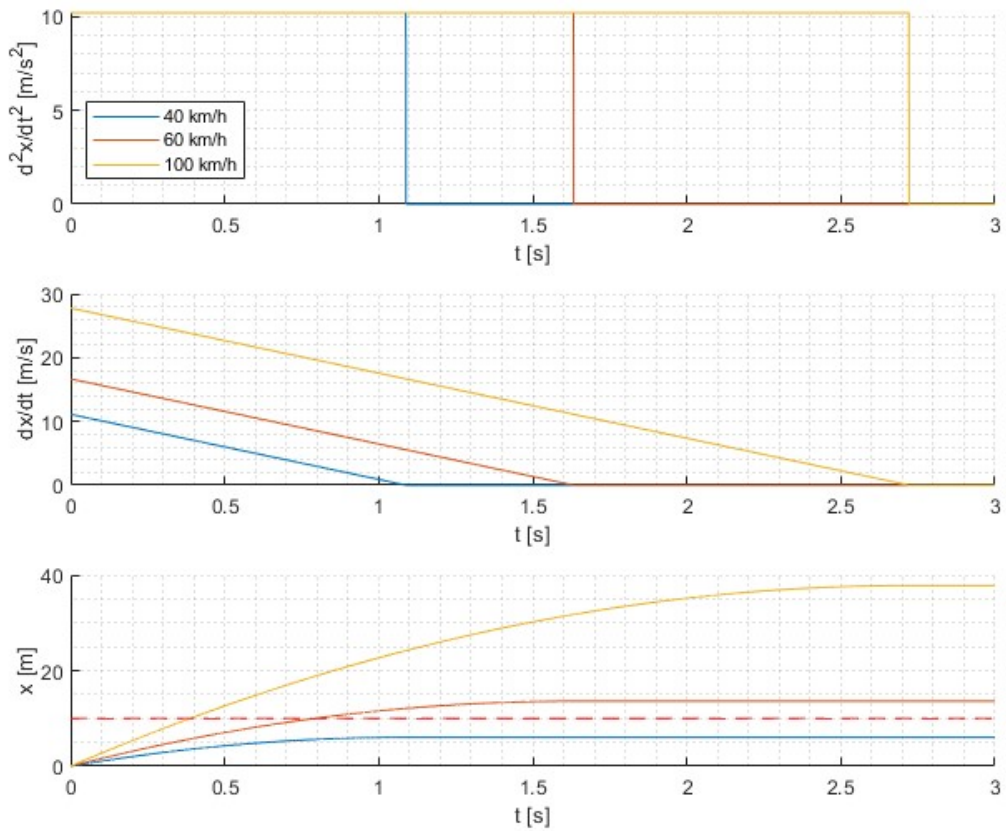


**Figure 3.3:** Braking kinematic due to EBS actuation at different speeds



**X- SHORT PAINTBALL HP SYSTEM**

Internal filling volume	0.15 l
Filling pressure	200 bar
Length (with regulator)	215 mm
Built-in regulator minimum pressure	56 bar
Diameter	50 mm

**Figure 3.4:** High pressure canister

Squadra Corse Driverless, the maximum available pressure is of 2000 psi = 138 bar. Thanks to equation 3.3 it is possible to calculate the mass used in every actuation, while equation 3.4 allows to calculate the total mass of the canister if it is charged up to 2000 psi. The masses are calculated using the ideal gas law, where  $R = 287 \text{ J}/(\text{kg K})$  is the gas constant for the air and  $T = 30 \text{ }^\circ\text{C}$  is the average temperature of the air.

$$m_{EBS} = \frac{P_{EBS}V_{EBS}}{RT} = 6.36 \cdot 10^{-4} \text{ kg} \quad (3.3)$$

$$m_{canister} = \frac{P_{canister}V_{canister}}{RT} = 2.40 \cdot 10^{-2} \text{ kg} \quad (3.4)$$

For sake of simplicity it is considered that, for every actuation, the pneumatic cylinder will move to the end stroke, whilst the stiffness of the oil should stop the motion before the end stroke. This means that the calculations are conservative, since the effective volume and mass used in every actuation are lower than the one calculated. The volume  $V_{EBS}$  used in equation 3.3 is the sum of the total volume of the pneumatic cylinder and the volume of the pneumatic line from the solenoid valve to the pneumatic cylinders (the tube is 500 mm long and it has a diameter of 8 mm). It is also important to underline that the pressure in equations 3.3 and 3.4 is an absolute pressure, therefore  $P_{EBS} = 1.10 \cdot 10^6 \text{ Pa}$  and  $P_{canister} = 1.39 \cdot 10^7 \text{ Pa}$ .

The number of actuations is calculated with equation 3.5. The EBS will work until the canister has a pressure higher than the pressure required by the EBS (10 bar). Therefore the number of actuations is calculated subtracting this final condition (canister at 10 bar) to the initial condition (canister at 2000 psi) and dividing it by the mass used in every actuation ( $m_{EBS}$ ).

$$actuations = \frac{m_{canister} - \frac{V_{canister}P_{EBS}}{RT}}{m_{EBS}} = 34 \quad (3.5)$$

### 3.1.3 EBS joint

Festo pneumatic cylinder has to be jointed to Brembo master cylinder. The connection has to guarantee the functioning also in case of small angular misalignment and not to stress the pneumatic cylinder and master cylinder shafts with flexion. Therefore a connection with SKF Uniball[28] has been chosen (Figure 3.5). Details and sizing of the joint are reported in Sections 3.2.6 and 3.2.7.

## 3.2 ASB design

The Autonomous System Brake is composed by an electric motor, a gear train, a joint, a ball screw, a linear guide, a balance bar and a bar connecting the ball screw to both master cylinders. In this section the mechanical design of each component of the ASB will be investigated.

It is important to underline that the ASB braking dynamics is divided into two main phases:



**Figure 3.5:** SKF Uniballs

1. the brake pads approach the discs: the speed of the actuator is at its maximum, while the force generated is almost null, since the only resistances to the motion are the spring of the master cylinder and the inertia of the moving parts;
2. the brake pads are in contact with the discs: the speed is almost null while the force generated is at its maximum.

The first phase determines the reaction time of the system. With the hypothesis of incompressible fluid, the volume of fluid moved by the master cylinder is equal to the displaced volume on braking pads. Therefore, considering a distance pads-disc of  $\Delta = 0.5 \text{ mm}$ , it is possible to evaluate the stroke of the master cylinder needed to finish the first phase thanks to equation 3.6, where  $d_{cal} = 24 \text{ mm}$  is the diameter of caliper's pistons,  $n$  is the number of pistons per caliper and the factor 2 is due to the fact that each brake line is connected to two calipers (right side and left side).

$$s = 2 \frac{\pi d_{cal}^2 n}{4} \Delta \quad (3.6)$$

The stroke calculated is of 7.56 mm at the front line and 4.50 mm at the rear line. The strokes are different because of the hypothesis of incompressible fluid. For the design of the ASB only the stroke of 7.56 mm has been taken into account because the results are conservative. The different stroke will not be a problem during braking since the balance bar will have the effect of equalizing the strokes of the master cylinders. Experimental analysis shown that the mean total reaction time for a driver is of 435 ms[29], therefore the speed of the actuator in order to be compared with a human driver has to be at least 17.38 mm/s.

The second phase is the one where the ASB has to generate the target force calculated in Section 2.5, that is  $F_{ASB} = 2304 \text{ N}$ .

### 3.2.1 Ball screw

The first ASB component to be designed is the ball screw (Figure 3.6). Since a rotative electric motor is used it is necessary to have a component that can guarantee the transformation of the motion from rotative to linear. Different options have been analysed and they are reported in Table 3.2.



**Figure 3.6:** Ball screws[30]

	Advantages	Disadvantages
Rack and pinion	The pinion could be part of the gear train and therefore no joint is needed	High cost
Trapezoidal screw	Low-cost	Low efficiency
Ball screw	High efficiency and more simple to assemble than a rack and pinion	More expensive than trapezoidal screw mechanism

**Table 3.2:** Comparison between rotative to linear mechanisms[31]

For the ASB the ball screw mechanism has been chosen for its high efficiency and because it is easier to assemble compared to the rack and pinion mechanism.

Three different options have been considered:

- Bosch Rexroth BASA miniaturized series ball screw[30], diameter = 12 mm, pitch = 5 mm;

- Bosch Rexroth BASA miniaturized series ball screw[30], diameter = 16 mm, pitch = 5 mm;
- Hiwin high load ball screw[32], diameter = 12 mm, pitch = 5 mm.

Only small diameters ball screw have been considered in order to reduce the mass and, more important, the volume occupied by the ASB. It is indeed important to remember that a ball screw with a larger diameter needs larger bearings that will hardly fit into the ASB/EBS case. Ball screw with pitch higher than 5 mm are not considered because the reduction ratio of the ball screw will be too low and an higher torque electric motor will be required.

The minimum length of the thread of the ball screw, according to Hiwin catalogue[32], has to be calculated as the sum of the nut length, the stroke required (23 mm, the stroke of the master cylinder) and the length of a nominal diameter  $d_0$  for each thread terminal. The different lengths are reported in Table 3.3 and it is possible to see that in any case the nut length is higher than the maximum stroke, therefore realizing the so called "short stroke condition"[30]. This condition requires caution in lubrication of the ball screw, since the spheres do not perform a complete revolution and it is impossible to form an adequate lubricant film. For this reason it is important to inspect the lubrication state more often.

From the conservation of energy between input (ball screw shaft rotation) and output (ball screw nut translation) it is possible to calculate the torque needed (equation 3.7).  $F_{ASB} = 2304$  N is the target force required calculated in Section 2.5,  $p = 5$  mm is the pitch and  $\eta$  is the efficiency of the ball screw mechanism which is extracted from graphics like the one reported in Figure 3.7, where the pitch angle  $\beta$  is calculated with equation 3.8.

$$T_{ASB} = \frac{F_{ASB} p}{2 \pi \eta} \quad (3.7)$$

$$\beta = \arctan\left(\frac{p}{\pi d_0}\right) \quad (3.8)$$

From Figure 3.7 it is also possible to see the difference in efficiency between ball screw mechanism and trapezoidal screw mechanism underlined in Table 3.2.

Each ball screw has a static load rating  $C_0$  and a dynamic load rating  $C$ . Since the variation of force and speed during time is unknown because it depends on the track layout, the ball screw is sized for its static behaviour.

The static safety factor  $SF_0$  is evaluated with equation 3.9. According to Bosch Rexroth manual[30] the safety factor should be at least 5, since not all the parameters are fully known and the system is not vibration-free (Figure 3.8).

$$SF_0 = \frac{C_0}{F_{ASB}} \quad (3.9)$$

It is also important to verify that the speed of the ball screw is lower than the maximum speed allowed by the mechanism. The minimum speed of the mechanism

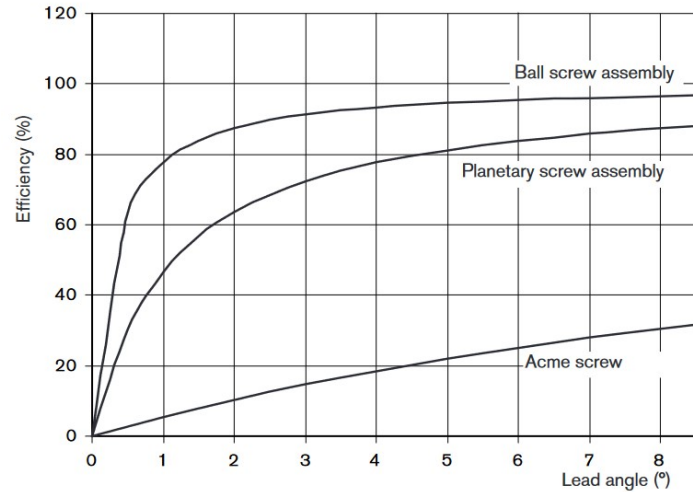


**Figure 3.7:** Bosch Rexroth ball screw efficiency as a function of the pitch angle[30]

Operating conditions	Static load safety factor $S_0$
Overhead arrangements and applications representing a high hazard potential	$\geq 12$
High dynamic load when at standstill, contamination.	8 - 12
Normal design of machinery and plant without full knowledge of the load parameters or connection details.	5 - 8
Full knowledge of all the load data. Vibration-free operation is ensured.	3 - 5

**Figure 3.8:** Bosch Rexroth indications on safety factor[30]

to be compliant with the target is of 17.30 mm/s (calculated in Section 3.2), while the maximum speed of the ball screw is reported in manuals. Differently to the Bosch Rexroth ball screws, Hiwin ball screw has no maximum speed but its bearings does, therefore the maximum speed is verified in the next subsection. The speed has also to be lower than the critical speed of the ball screw, but the length of the ball screw is too low and the critical speed is higher than the maximum speed allowed.

Calculation results are reported in Table 3.3.

The Bosch Rexroth 12 ball screw has a static safety factor lower than 5, which is the safety factor required, therefore it is not suitable for the ASB. Bosch Rexroth 16 and Hiwin 12 ball screws have both the minimum safety factor required. Both Bosch ball screws have a maximum speed much higher than the speed required, while for the Hiwin ball screw it is necessary to analyse its bearings first.

### Ball screw's bearings

Since the Bosch Rexroth 12 ball screw has a static safety factor too low for the application the only bearings to be sized are for the Bosch Rexroth 16 and Hiwin 12 ball screws. At first the vibrations caused by the motion of the vehicle led to choose a setup where both bearings are fixed.

	Bosch Rexroth 12	Bosch Rexroth 16	Hwini 12
$d_0$	12 mm	16 mm	12 mm
$p$	5 mm	5 mm	5 mm
$\beta$	7.55°	5.68°	7.55°
$\eta$	96 %	95 %	96 %
$C_0$	5800 N	14490 N	11772 N
$C$	4560 N	13320 N	5494 N
$v_{MAX}$	500 mm/s	500 mm/s	-
$v_{ASB}$	17.30 mm/s	17.30 mm/s	17.30 mm/s
$F_{ASB}$	2304 N	2304 N	2304 N
$T_{ASB}$	1.91 Nm	1.93 Nm	1.91 Nm
$SF_0$	2.52	6.29	5.11

**Table 3.3:** Comparison between three ball screw mechanisms[30][32]

For the Bosch Rexroth 16 ball screw SEB-F bearings have been chosen[30] (Figure 3.9), since they are a good compromise in strength and reduced volume. Every bearing has a static load rating  $C_0 = 18800$  N and a dynamic load rating  $C = 13400$  N.

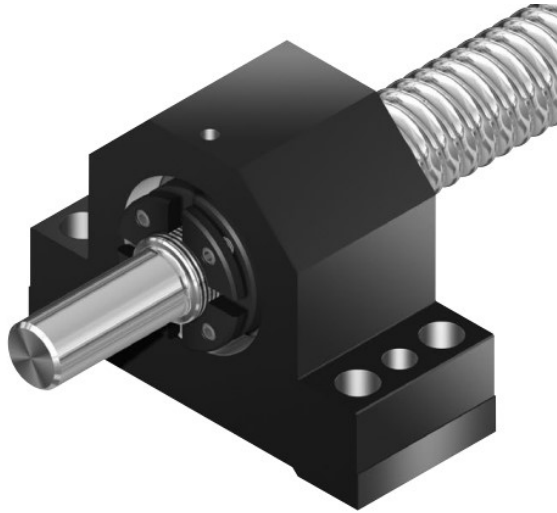


**Figure 3.9:** Bosch Rexroth SEB-F bearing[30]

Similar to the ball screw also the bearings have been sized on their static behaviour. Considering that the force acting on each bearing is half of the total force it is possible

to evaluate the static safety factor with equation 3.10. Bearing data and calculations are reported in Table 3.4.

$$SF_0 = \frac{F_{ASB}}{2C_0} = 16.32 \quad (3.10)$$

Parameter	Value
$C_0$	18800 N
$C$	13400 N
$SF_0$	16.32

**Table 3.4:** Bosch Rexroth SEB-F bearing data and calculations[30]

The safety factor obtained is very high and not justified for motorsport application considering the higher volume occupied by a 16 mm ball screw instead of a 12 mm mechanism.

For the Hiwin 12 ball screw FK08 bearings have been chosen[32] (Figure 3.10). Differently from Bosch Rexroth manual, Hiwin manual provide static and dynamic load ratings and a maximum axial force admissible  $C_{ax,MAX} = 1000$  N. Since the bearings support only axial force and its value is half of the force generated by the ASB it is possible to calculate the static safety factor using equation 3.11. Moreover it is possible to evaluate if the maximum speed of the ball screw is compatible with the maximum speed allowed by the bearings. FK08 data and calculations are reported in Table 3.5.

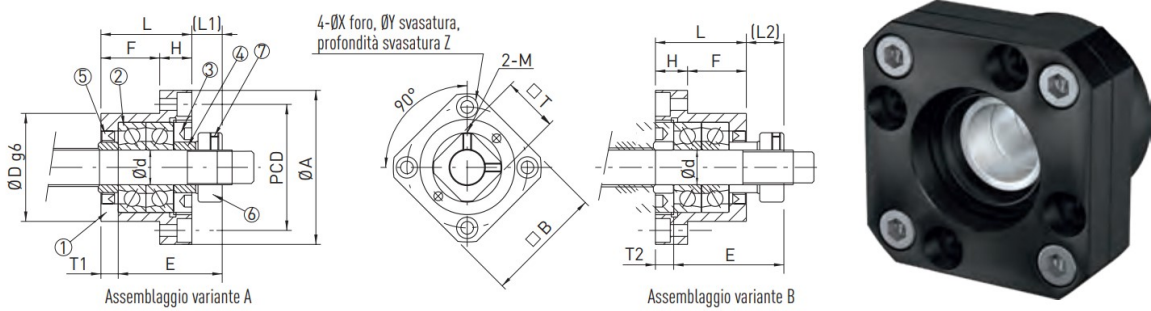


**Figure 3.10:** Hiwin FK08 bearing[32]

$$SF_0 = \frac{F_{ASB}}{2C_{ax,MAX}} = 0.87 \quad (3.11)$$

The maximum angular speed of 40000 rpm, or equivalently a linear speed of 531 mm/s, is much greater than the speed required by the actuator (17.30 mm/s). However

Parameter	Value
$C_0$	4800 N
$C$	2800 N
$C_{ax,MAX}$	1000 N
$v_{MAX}$	40000 rpm
$SF_0$	0.87

**Table 3.5:** Hiwin FK08 bearing data and calculations[32]

the maximum axial force allowed is lower than the actual force ( $SF_0 < 1$ ) therefore this bearing setup is not compliant with the application.

Both solutions provided by the manufacturers are not suitable for the ASB application. Therefore an hybrid solution has been chosen: one of the bearing will be provided by the ball screw manufacturer while the second bearing will be a thrust bearing, able to withstand all the axial load generated by the ASB. In order to have all the load supported only by the thrust bearing the second bearing will be a radial floating bearing.

The Hiwin 12 has been chosen as ASB ball screw since it requires a lower volume and the inertia of the actuator will be lower compared to the Bosch Rexroth 16 ball screw. The shank of the ball screw has a diameter of 8 mm, therefore an SKF 8 mm thrust bearing has been chosen (Figure 3.11)[33]. Since the bearing requires a shoulder of at least 14.5 mm but the ball screw is only 12 mm large a spacer has been designed; details on the spacer design process can be found in the next subsection.

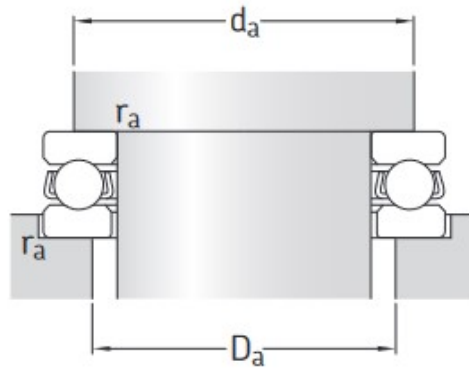


**Figure 3.11:** SKF BA 8 thrust ball bearing[33]

SKF manual provides static and dynamic load rating and therefore it is possible to evaluate the safety factor of the bearing with equation 3.12. It is necessary to underline

that in this configuration the total force generated by the ASB is supported only by the thrust bearing. BA 8 data and calculations are reported in Table 3.6.

$$SF_0 = \frac{C_0}{F_{ASB}} = 1.65 \quad (3.12)$$

Parameter	Value
$C_0$	3800 N
$C$	3190 N
$v_{MAX}$	17000 rpm
$SF_0$	1.65

**Table 3.6:** SKF BA 8 bearing data and calculations[33]

The maximum speed of 17000 rpm or equivalently of 1417 mm/s is compliant with the actual speed of 17.30 mm/s. Also the safety factor of 1.65 is enough for a motorsport application, being the ASB not a safety system. Moreover it is important to underline that  $F_{ASB}$  is not the actual force of the actuator but it is increased by 50 % in order to take into account the master cylinder spring and potential friction (Section 2.5); if the force would not have been increased the safety factor would be 2.47.

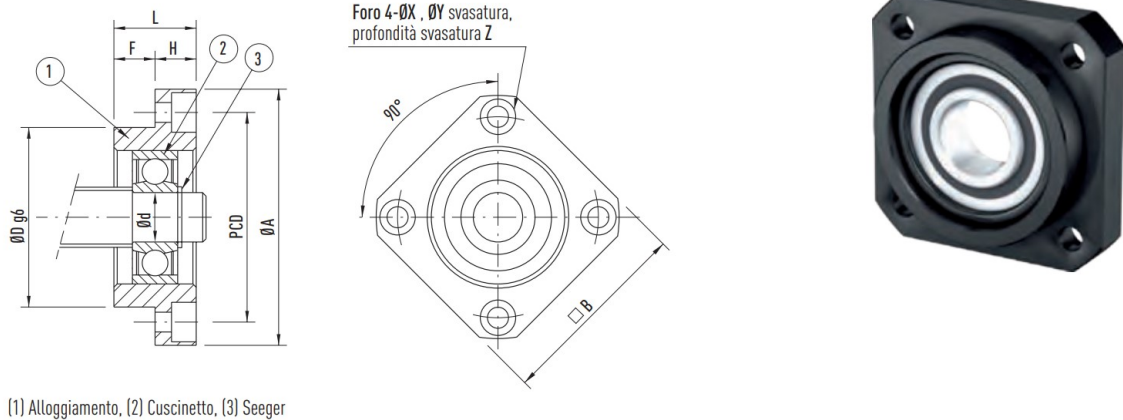


**Figure 3.12:** Hwin FF10 bearing[32]

The second bearing will be the Hiwin FF10 floating bearing (Figure 3.12). This bearing is not able to withstand any axial load. No safety factor has been calculated in this case since the radial load caused by misalignment is supported by the linear guides sized in Section 3.2.5.

In conclusion, the ball screw is supported by a thrust bearing manufactured by SKF and a radial floating bearing manufactured by Hiwin.

## Spacer

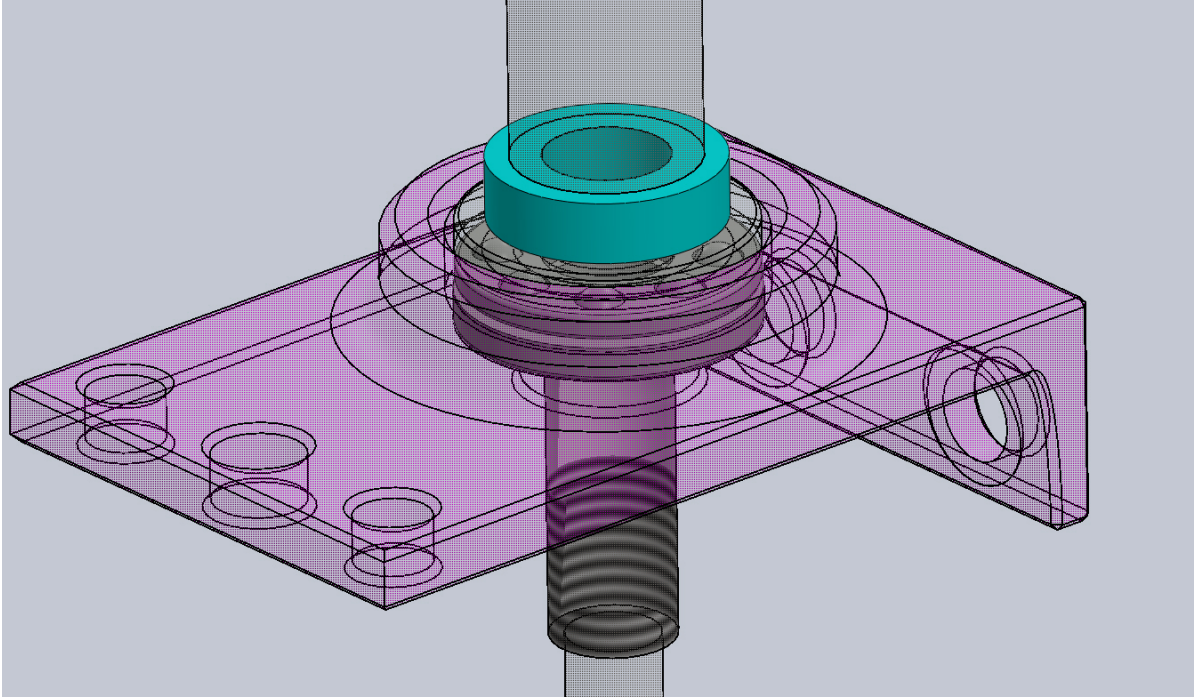


**Figure 3.13:** Spacer

Since the thrust bearing needs a shoulder of at least 14.5 mm but the ball screw is only 12 mm large a spacer has been designed (Figure 3.13). The outer diameter chosen is of 15 mm. The spacer is subjected to compression stress, calculated with equation 3.13[34]. Considering a safety factor  $SF$  of 2, thanks to equation 3.14 it has been possible to evaluate the minimum yield stress  $R_{p0.2}$  required.

$$\sigma = \frac{4 F_{ASB}}{\pi (D^2 - d^2)} = 18 \text{ MPa} \quad (3.13)$$

$$R_{p0.2,min} = \sigma \cdot SF = 36 \text{ MPa} \quad (3.14)$$

The material to be used for the spacer requires a minimum yield stress of 36 MPa. In Table 3.7 it is reported a summary of the ball screw assembly parameters.

### 3.2.2 Electric motor

The force of the ASB acting on the master cylinders is generated by an electric motor. For its sizing the power required by the ASB has been calculated with equation 3.15, where  $v_{ASB} = 17.30$  mm/s is the maximum speed and  $F_{ASB} = 2304$  N is the maximum force required. As highlighted in Section 3.2 maximum force and maximum speed are conditions that will not happen simultaneously, therefore the power calculated with

Parameter	Value
<b>Ball screw</b>	Hiwin high load ball screw
Nominal diameter	12 mm
Pitch	5 mm
Efficiency	96 %
Thread length	94 mm
Ball screw static load rating	11772 N
Ball screw static safety factor	5.11
<b>Thrust bearing</b>	SKF BA 8 thrust bearing
Static load rating	3800 N
Static safety factor	1.65
Maximum speed	17000 rpm
<b>Radial bearing</b>	Hiwin FF10 support

**Table 3.7:** Ball screw assembly details[32][33]

equation 3.15 is conservative.

$$P_{ASB} = F_{ASB} \cdot v_{ASB} = 39.86 W \quad (3.15)$$

The best motor found with a minimum power of 39.86 W is the EC 45 flat brushless motor manufactured by Maxon[35] (Figure 3.14). The maximum power of the motor is of 60 W which is much higher than the minimum power required; however electric motors with lower power would require a gear train with an higher reduction ratio and therefore more costly and voluminous.

Parameters of the motor are reported in Table 3.8, while in Figure 3.15 it is represented the characteristic curve of the electric motor[36] realized thanks to datasheet parameters.

### 3.2.3 Gear train

As it is possible to see in Table 3.8 the maximum torque generated by the electric motor is  $T_{IN} = 0.11$  Nm, but in Section 3.2.1 the calculated torque needed at the ball screw shaft was  $T_{ASB} = 1.91$  Nm, therefore it is necessary to use a gear train with a minimum reduction ratio calculated with equation 3.16.

$$u_{TOT,min} = \frac{T_{ASB}}{T_{IN}} = 17.64 \quad (3.16)$$

**EC 45 flat** Ø43.5 mm, brushless, 60 watt  
Open Rotor

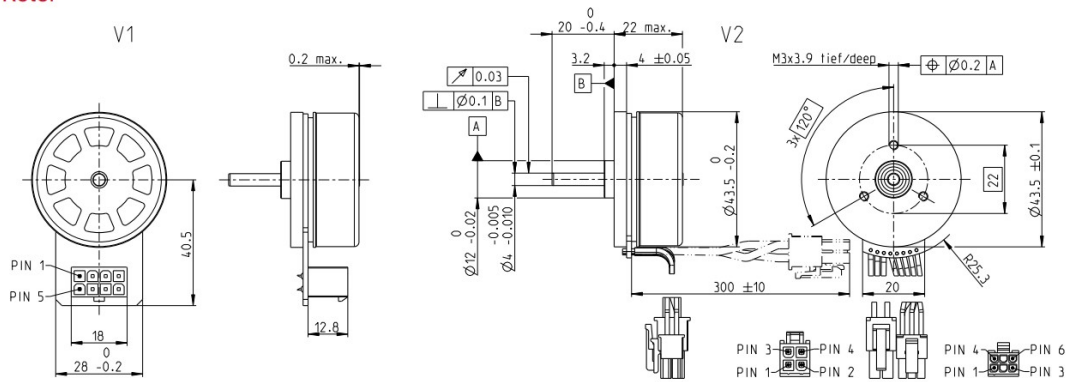


**Figure 3.14:** Maxon EC 45 flat electric motor[35]

Parameter	Value
Nominal voltage	24 V
No load speed	6250 rpm
No load current	238 mA
Nominal speed	4970 rpm
Nominal torque	110 mNm
Nominal current	2.97 A
Stall torque	918 mNm
Stall current	26 A
Max efficiency	32 %
Terminal resistance phase to phase	0.942 Ω
Terminal inductance phase to phase	0.363 mH
Torque constant	36 mNm/A
Speed constant	265 rpm/V
Mechanical time constant	9.790 ms
Rotor inertia	135 gcm <sup>2</sup>

**Table 3.8:** Maxon EC 45 flat brushless motor datasheet[35]

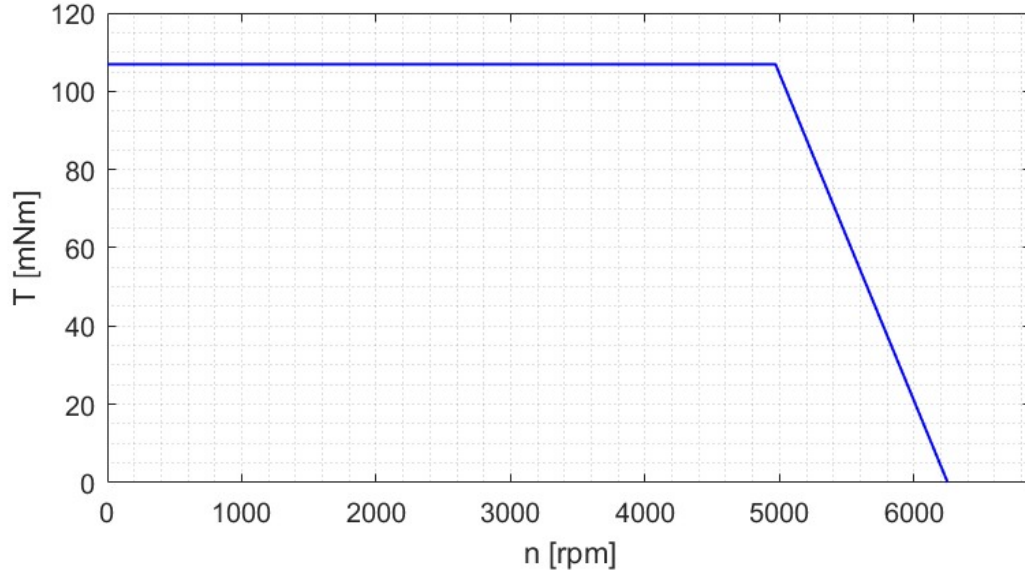


**Figure 3.15:** Characteristic curve of Maxon EC 45 flat brushless motor[35]

At first the idea was to design a custom two stage gear train, with a reduction ratio per stage of  $u_{stage} = 4.20$ . The material chosen is 16MnCr5 steel, a case-hardening steel with high strength and high core toughness[37]; the material has a yield stress  $R_{p0.2}$  of 735 MPa, an ultimate tensile stress  $R_m$  of 1030 MPa and a Brinell hardness  $HB$  of 654. For the sizing of each stage the minimum number of teeth for the pinion  $z_{min}$  has been calculated with equation 3.17, where  $\alpha = 20^\circ$  is the pressure angle[38].

$$z_{min} = \frac{2}{\sin^2 \alpha} = 18 \quad (3.17)$$

To size the modulus of each stage of the gear train the minimum modulus has been calculated with Lewis' theory (equation 3.18) and Hertz's theory (equation 3.19)[38][39]. The modulus of the stage will be the minimum standard modulus higher than the one evaluated with equations 3.18 and 3.19.

$$m_{Lewis,min} = \sqrt[3]{\frac{2T_{IN} Y SF_{Lewis}}{\lambda z_p R_{p0.2}}} \quad (3.18)$$

$$m_{Hertz,min} = 0.418 \sqrt[3]{\frac{4T_{IN} E SF_{Hertz}}{z_p^2 \lambda \cos \alpha \sin \alpha \sigma_{H0}^2} \cdot \frac{u_{stage} + 1}{u_{stage}}} \quad (3.19)$$

The parameters reported in equations 3.18 and 3.19 are the following:

- $T_{IN}$ : torque at stage input;
- $Y$ : Lewis factor, evaluated thanks to tables;

- $SF_{Lewis} = 2$ : safety factor used for the sizing with Lewis' theory, it can assume values between 1.5 to 3;
- $\lambda = b/m = 10$ : it is the ratio between the face width  $b$  and the modulus  $m$ , it can assume values between 8 to 14;
- $z_p = 18$ : number of teeth of the pinion, assumed equal to the minimum number of teeth (equation 3.17);
- $R_{p0.2} = 735$  MPa: material yield stress;
- $E = 210$  GPa: steel Young Modulus;
- $SF_{Hertz} = 1.5$ : safety factor used for the sizing with Hertz's theory, it can assume values between 1.3 to 1.6;
- $\alpha = 20^\circ$ : pressure angle;
- $\sigma_{H0} = 2.5 HB = 1635$  MPa: pitting resistance;
- $u_{stage} = z_g/z_p$ : resuction ratio of the stage, where  $z_g$  is the number of teeth of the gear chosen in order to be compatible to the total reduction ratio  $u_{TOT}$  required.

The results of the calculations are reported in Table 3.9.

The total reduction ratio is compatible with the reduction ratio required, but the device would require a large volume that will potentially decrease thanks to the use of helical wheels instead of cylindrical wheels. However the optimal option is to buy a planetary gear train compatible with the motor. The gear train found is made by Maxon[40] (Figure 3.16) and it has a reduction ratio of 18. This solution is preferable since it is cheaper, less volume consuming and potentially more efficient. Datasheet of the gear train is reported in Table 3.10 and it is also possible to see that the maximum torque at gear train output is higher than the torque required by the ASB.

### Planetary Gearhead GP 32 C $\varnothing 32$ mm, 1.0–6.0 Nm Ceramic Version

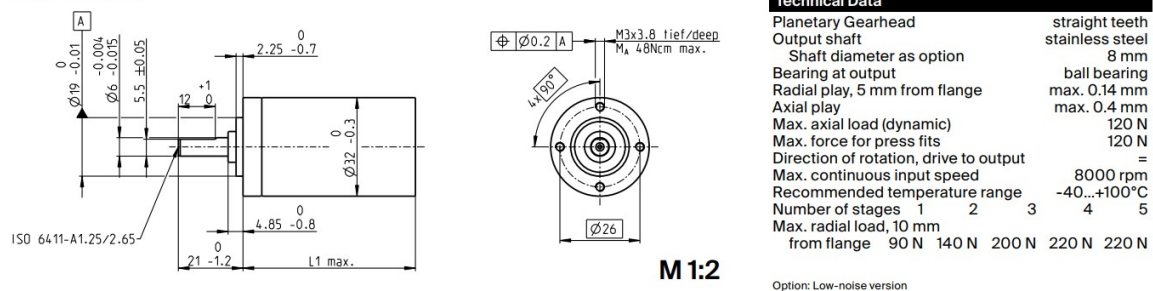


Figure 3.16: Maxon Planetary Gearhead GP 32 C[40]

Gear	Parameter	Value
<b>First stage</b>	Minimum modulus (Lewis)	0.22 mm
	Minimum modulus (Hertz)	0.25 mm
	Modulus	0.5 mm
	Reduction ratio	4.33
	Face width	5 mm
Pinion 1	Number of teeth	18
	Pitch diameter	9 mm
Gear 2	Number of teeth	78
	Pitch diameter	39 mm
<b>Second stage</b>	Minimum modulus (Lewis)	0.36
	Minimum modulus (Hertz)	0.42 mm
	Modulus	0.5 mm
	Reduction ratio	4.17
	Face width	5 mm
Pinion 3	Number of teeth	18
	Pitch diameter	9 mm
Gear 4	Number of teeth	75
	Pitch diameter	37.5 mm
	<b>Total reduction ratio</b>	<b>18.06</b>

**Table 3.9:** Custom gear train parameters

### 3.2.4 Ball screw - gear train joint

A joint has been designed in order to connect the gear train shaft to the ball screw. Unfortunately the ball screw shaft end is not provided with a keyseat, therefore other type of joints have been taken into consideration.

At first a forced mating has been evaluated[41]. With a joint length  $b$  of 9 mm it is possible to evaluate the pressure needed for the torque transmission with equation 3.20, where  $T_{ASB} = 1.94$  Nm is the torque transmitted to the ball screw,  $d = 6$  mm is the inner diameter of the joint and  $f = 0.11$  is the friction coefficient for steel-steel in case

Parameter	Value
Reduction	18:1
Number of stages	1
Max continuous torque	3 Nm
Max intermittent torque at gear output	3.75 Nm
Max efficiency	75 %
Weight	162 g
Mass inertia	162 gcm <sup>2</sup>

**Table 3.10:** Maxon Planetary Gearhead GP 32 C datasheet[40]

of lubricated press fit.

$$p = \frac{2T_{ASB}}{\pi d^2 b f} = 35 \text{ MPa} \quad (3.20)$$

After the calculation of the hub deformability  $\delta_h$  (equation 3.21) and of the shaft deformability  $\delta_s$  (equation 3.22), it is possible to evaluate the interference needed by the forced mating with equation 3.23.

$$\delta_h = \frac{(1 + \nu) + \beta_h^2 (1 - \nu)}{E (1 - \beta_h^2)} = 6.51 \cdot 10^{-6} \text{ MPa}^{-1} \quad (3.21)$$

$$\delta_s = \frac{1 - \nu}{E} = 6.19 \cdot 10^{-6} \text{ MPa}^{-1} \quad (3.22)$$

$$i = p d (\delta_h + \delta_s) = 2.64 \text{ } \mu\text{m} \quad (3.23)$$

The parameters in equations 3.21, 3.22 and 3.23 are the following:

- $\nu = 0.3$ : steel Poisson Modulus;
- $\beta_h = D/d = 2$ , where  $d = 6$  mm is the inner diameter and  $D = 12$  mm is the outer diameter of the hub;
- $E = 210$  GPa: steel Young Modulus.

The minimum interference for the forced mating  $i_0$  is calculated with equation 3.26 taking into account the loss of interference due to surface roughness  $\Delta i^R$  (equation 3.24) and centrifugal forces  $\Delta i^\omega$  (equation 3.25); the temperature variation does not affect the interference since hub and shaft are both made in steel.

$$\Delta i^R = 2 \cdot 0.4 (R_a^{shaft} + R_a^{hub}) = 1.28 \text{ } \mu\text{m} \quad (3.24)$$

$$\Delta i^\omega = \frac{d \rho \omega^2 D^2}{4 E} = 3.89 \cdot 10^{-6} \text{ } \mu\text{m} \quad (3.25)$$

$$i_0 = i + \Delta i^R + \Delta i^\omega = 3.92 \mu\text{m} \quad (3.26)$$

The parameters in equations 3.24, 3.25 and 3.26 are the following:

- $R_a^{shaft} = 0.8$ : surface roughness of the shaft;
- $R_a^{hub} = 0.8$ : surface roughness of the hub;
- $\rho = 8000 \text{ kg/m}^3$ : steel density;
- $\omega = 22 \text{ rad/s}$ : angular speed of the ball screw.

The ball screw shaft end is  $\varnothing 6 \text{ j6}$ , which means  $\varnothing 6_{-0.002}^{+0.006}$ , therefore the diameter of the chosen hub is  $\varnothing 6_{-0.015}^{-0.006}$ . The minimum interference will be  $i_{min} = 4 \mu\text{m}$ , while the maximum interference will be  $i_{MAX} = 21 \mu\text{m}$ . The tolerance required by the hub is very low (the maximum error permitted is of  $9 \mu\text{m}$ ) and the realization will be expensive. Therefore a bolt joint has been evaluated (Figure 3.17).

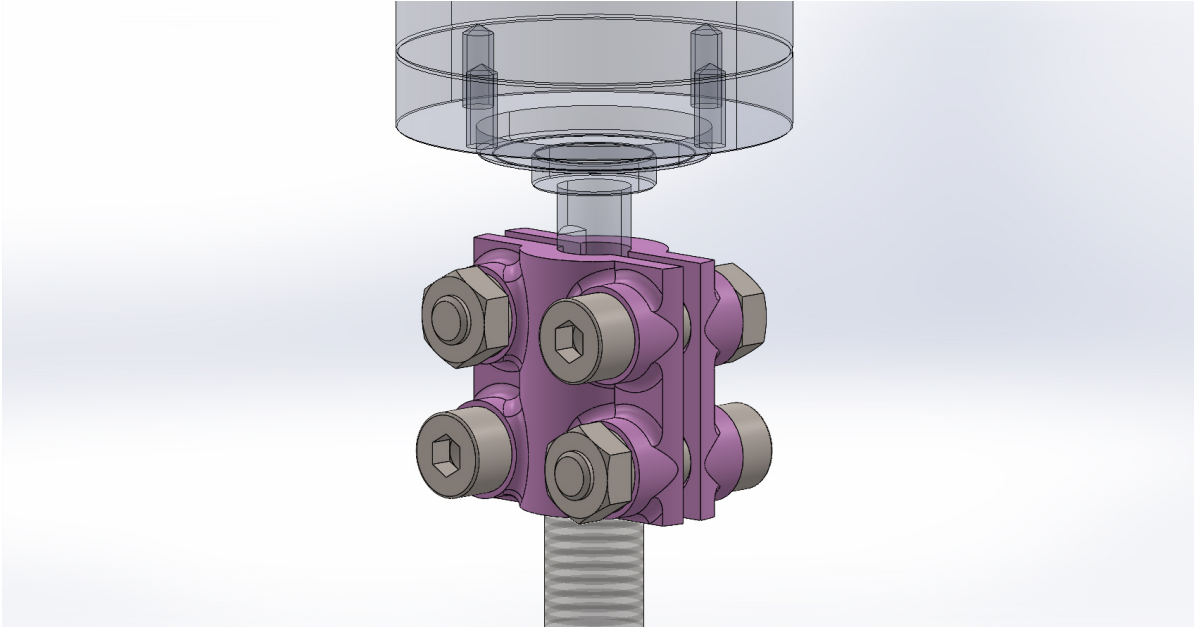


**Figure 3.17:** Bolt joint between gear train and ball screw

The pressure needed for the torque transmission is  $p = 35 \text{ MPa}$  as calculated in equation 3.20, but this time is obtained with four M4 bolts. After calculating the axial force that each bolt needs to perform with equation 3.27[41], it is necessary to evaluate the tightening torque needed for the bolts with equation 3.28[42].  $b = 9 \text{ mm}$  is the length of the joint,  $n = 4$  is the number of bolts,  $\alpha = \arctan[P \cdot (\pi d_2)] = 3.6^\circ$ ,  $P = 0.7 \text{ mm}$  is the thread pitch,  $d_2 = 3.55 \text{ mm}$  is the mean thread diameter,  $\phi = 7.2^\circ$  is the friction angle,  $f = 0.11$  is the friction coefficient[41] and  $D_m = 5.5 \text{ mm}$  is the screw mean head diameter.

$$F_{ax} = \frac{p d b}{n} = 468 \text{ N} \quad (3.27)$$

$$M = F_{ax} \tan(\alpha + \varphi) \frac{d_2}{2} + F_{ax} f \frac{D_m}{2} = 0.30 \text{ Nm} \quad (3.28)$$

### 3.2.5 ASB bar

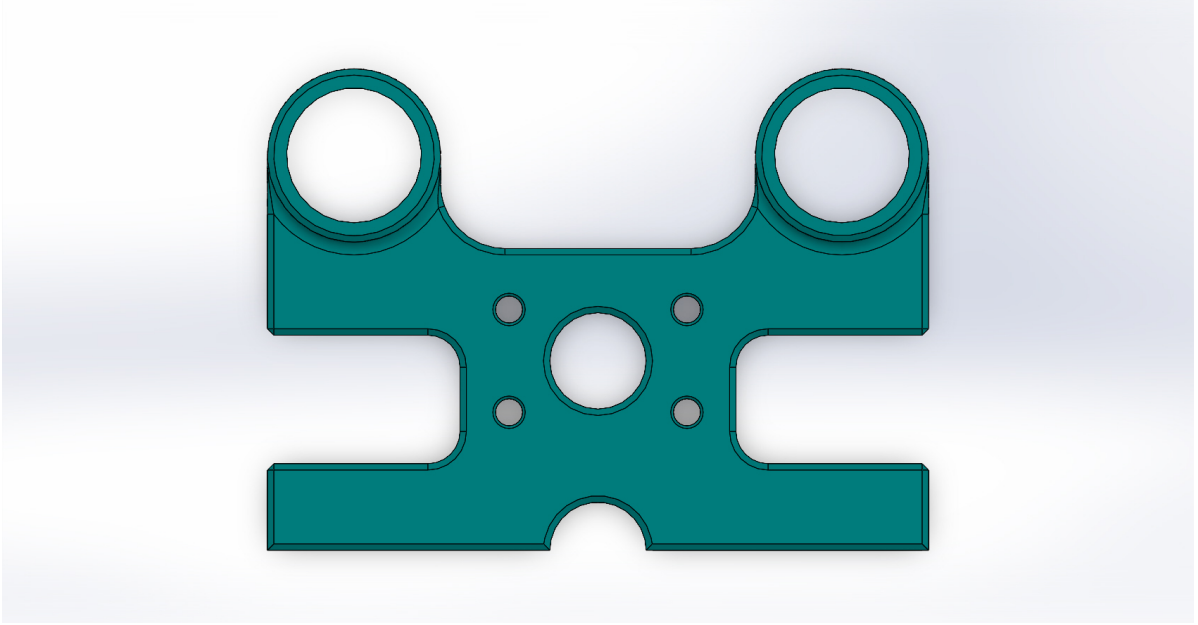


**Figure 3.18:** ASB bar

The ASB bar (Figure 3.18) is a component that allows to transmit the force generated by the ASB from the ball screw nut to the master cylinders. The connection between ASB bar and master cylinders has to be not permanent so that when the EBS is activated the inertia of the ASB does not resist the braking actuation. In order to guarantee an optimal contact also in condition of misalignment of the master cylinders an Hertzian contact between the ASB bar and the pneumatic cylinder fork has been designed as shown in Figure 3.19.

The ASB bar has been sized considering its normal operation, with equal force acting in both master cylinders. The ASB bar is symmetrical with regards to the XZ plane but not to the YZ plane, therefore the force distribution is evaluated with the free body diagram in Figure 3.20 and Figure 3.21. The forces acting between ASB bar and pneumatic cylinder fork are calculated with equations 3.29 and, where  $F_{ASB} = 2304 \text{ N}$ ,  $l_1 = 22.75 \text{ mm}$  and  $l_2 = 10.75 \text{ mm}$ .

$$F_1 = F_{ASB} \frac{l_1}{l_1 + l_2} = 782 \text{ N} \quad (3.29)$$

$$F_2 = F_{ASB} \frac{l_2}{l_1 + l_2} = 370 \text{ N} \quad (3.30)$$

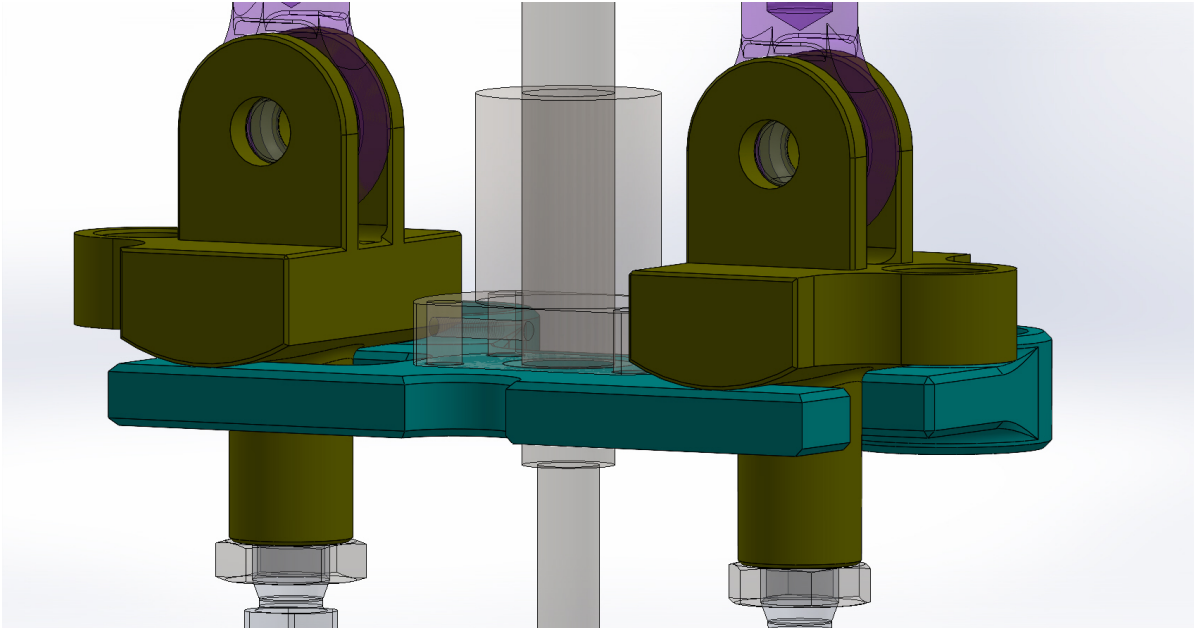


**Figure 3.19:** Hertzian contact between the ASB bar and the two master cylinders

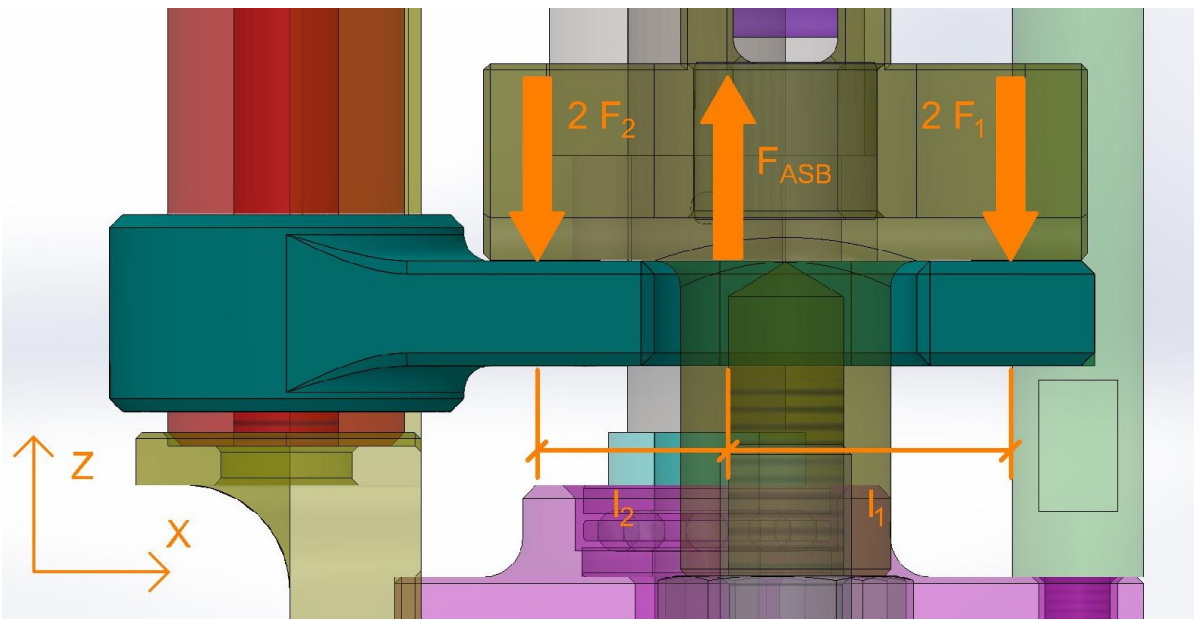


**Figure 3.20:** ASB bar free body diagram (XZ plane)

In order to be conservative the Hertzian contact has been sized on the higher force  $F_1$ . The ASB bar and the pneumatic cylinder fork have to be rigid in order not to bend too much and therefore an high strength steel has been chosen, in particular 25CrMo4 tempering steel, with a yield stress  $R_{p0.2}$  of 700 MPa, a Young Modulus  $E$  of 210 GPa and a good toughness[37].

The bar is sized in order to withstand the flexure stress caused by the contact.

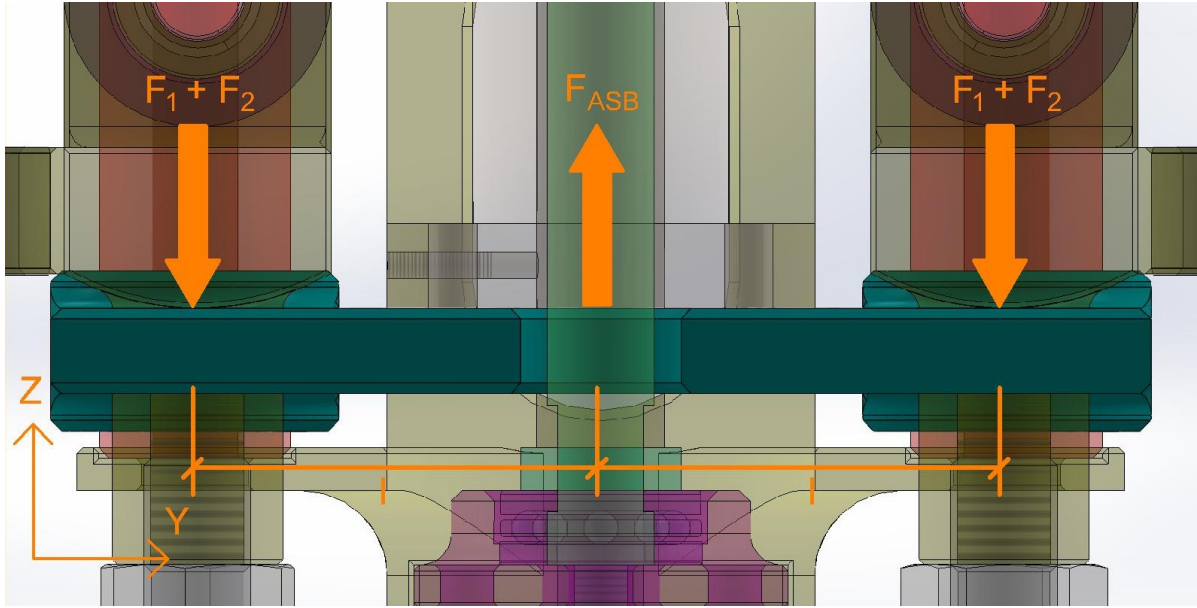


**Figure 3.21:** ASB bar free body diagram (YZ plane)

Considering a safety factor  $SF$  of 2.5 (high enough to let the ASB bar withstand loads also in case of hydraulic fail), the minimum thickness of the ASB bar is calculated with equation 3.31[34], where  $l = 37.25$  mm and  $L = 23$  mm is the total length of the contact. The thickness chosen for the ASB bar is of 6 mm, higher than the minimum calculated so that if a brake line failure occurs and the whole force generated by the ASB  $F_{ASB}$  is applied to only one master cylinder the bar will not yield.

$$s = \sqrt{\frac{6 F_1 l SF}{R_{p0.2} L}} = 5.21 \text{ mm} \quad (3.31)$$

### Linear guide

In order not to stress the ball screw with radial forces, a linear guide for the ASB bar is needed. The linear guide is sized in order to maintain the ASB bar horizontal in every case, with worst case being the hydraulic fail on one brake line: in this situation all the force generated by the ASB is transmitted only to one master cylinder and therefore the radial force on the ball screw will reach its peak. Different solutions have been evaluated:

- linear rail;
- linear bearings;
- bushings.

The linear rail guarantees a high load factor, but the volume occupied by the device is too high; on the other hand, the linear bearings is a compact device but with a low load factor. Therefore the best solution turned out to be the SKF bushings[43];

the material chosen is wrapped bronze since the following calculations proved that its strength is enough to withstand the stress. To proceed with the sizing it is first necessary to represent the free body diagrams of the bushing and of the ASB bar in hydraulic fail condition for one brake line (Figure 3.22).

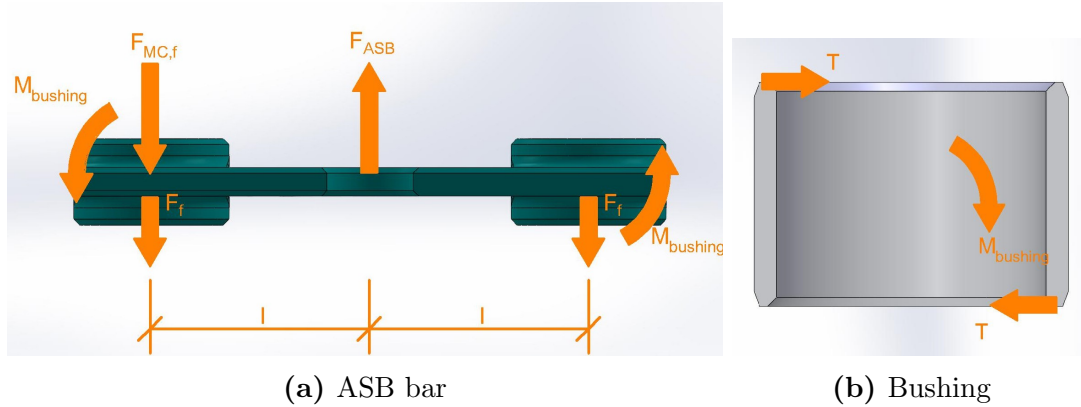


**Figure 3.22:** Free body diagrams in brake line fail condition (vertical forces on the bushing free body diagram are omitted)

From the free diagrams of Figure 3.22 it is possible to obtain equations 3.32, 3.33 and 3.34.

$$F_f = 2 \mu T \quad (3.32)$$

$$F_{ASB} l - 2 F_f l = 2 M_{bushing} \quad (3.33)$$

$$M_{bushing} = T h \quad (3.34)$$

The parameters reported in equations 3.32, 3.33 and 3.34 are the following:

- $F_f$ : friction force caused by the contact of the bushings and their shafts;
- $T$ : tangential force on the bushing, for sake of simplicity the force is considered to be applied at both ends of the bushings instead of being distributed on the whole height of the bushing;
- $M_{bushing}$ : reaction torque on the bushings;
- $F_{ASB} = 2304$  N: maximum force generated by the ASB;
- $\mu = 0.105$ : medium friction coefficient of the bushings;
- $h = 15$  mm: height of the bushing.

The calculations led to the following results:

- $T = 1400$  N
- $M_{bushing} = 21$  Nm

Form the reaction torque of the bushings  $M_{bushing}$  it is possible to evaluate the maximum stress on the single bushing using equation 3.35[34], where  $d = 18$  mm is the inner diameter of the bushing and  $D = 21$  mm is the outer diameter.

$$\sigma_{bushing} = \frac{32 M_{bushing} D}{\pi (D^4 - d^4)} = 50.20 \text{ MPa} \quad (3.35)$$

The SKF wrapped bronze bushings have a permissible load  $C_0 = 120$  MPa, therefore the safety factor is evaluated with equation 3.36.

$$SF = \frac{C_0}{\sigma_{bushing}} = 2.39 \quad (3.36)$$

The wrapped bronze bushing is suitable for the application. However it is important to underline that it does not have self-lubricating performance, unlike other type of bushings, but it is suitable for dirty environments in presence of vibrations.

It is necessary also to evaluate the mechanical characteristics of the material needed for the bushing shaft. Considering a hollow shaft with outer diameter  $d = 18$  mm and an inner diameter  $d_{in}$  of 8 mm it is possible to evaluate the minimum yield resistance required with equation 3.37. The safety factor  $SF_{shaft}$  used is equal to 1.5.

$$R_{p0.2,min} = \frac{32 M_{bushing} d SF_{shaft}}{\pi (d^4 - d_{in}^4)} = 57 \text{ MPa} \quad (3.37)$$

## FEM structural analysis

In order to verify the calculations and to evaluate the stress distribution inside the ASB bar FEM structural analysis have been carried out. The ASB bar has been tested with the maximum force applied by the ball screw nut in normal operation and in hydraulic fail condition. The software used for the analysis is SolidWorks Simulation. At first the material (25CrMo4) has been defined. Then it is necessary to define the boundary conditions:

- in both the contact line between ASB bar and pneumatic cylinder fork a constraint in the ball screw motion direction has been imposed;
- in the inner surface of the bushings' housing there is a constraint in radial direction;
- in the M5 holes that attach the ASB bar to the ball screw nut the force  $F_{ASB} = 2304$  N has been imposed.

The results of the analysis are reported in Figure 3.23, where it is possible to verify that the ASB bar withstand the loads imposed. Furthermore the maximum stress of 150 MPa is located in a concentrated zone and it is caused by a geometry variation. The stress calculated is less than the one imposed on the sizing ( $\sigma = R_{p0.2}/SF$ ) but this is potentially caused by the fact that the sizing has been made on the maximum force between  $F_1$  and  $F_2$  and not the real force and because the resistance due to the material of the cylindrical housing of the bushings has not been taken into account previously.

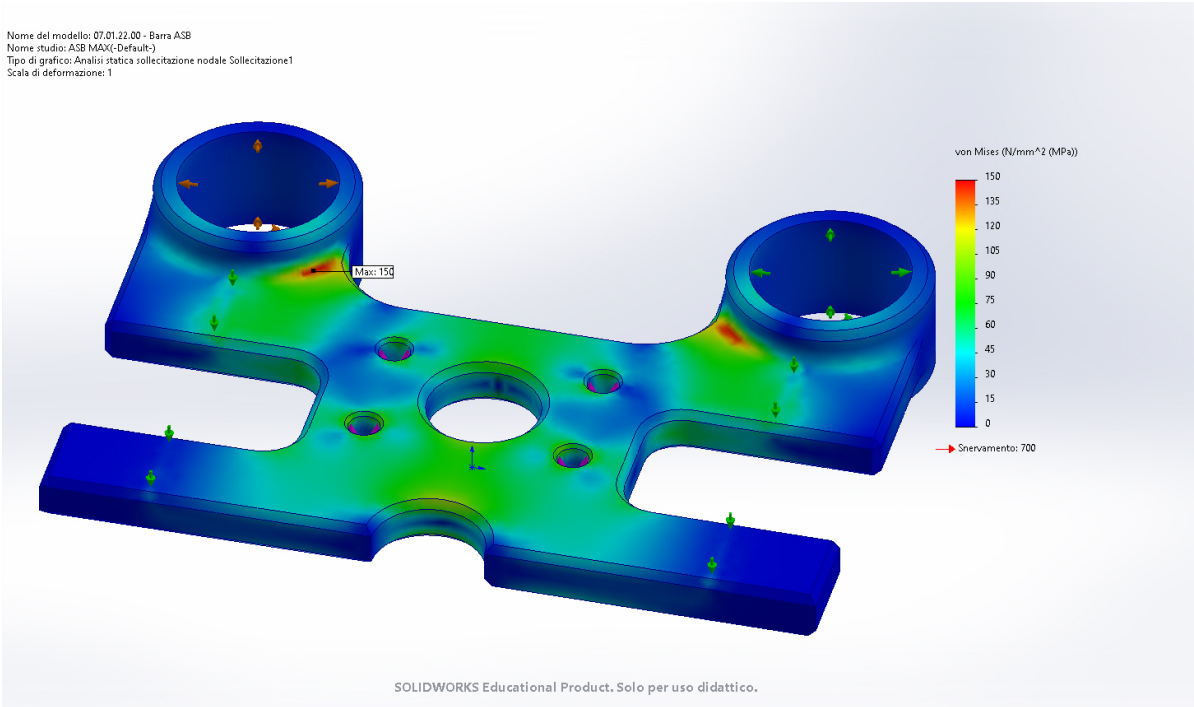


**Figure 3.23:** ASB bar stress distribution when the maximum force is generated by the ASB

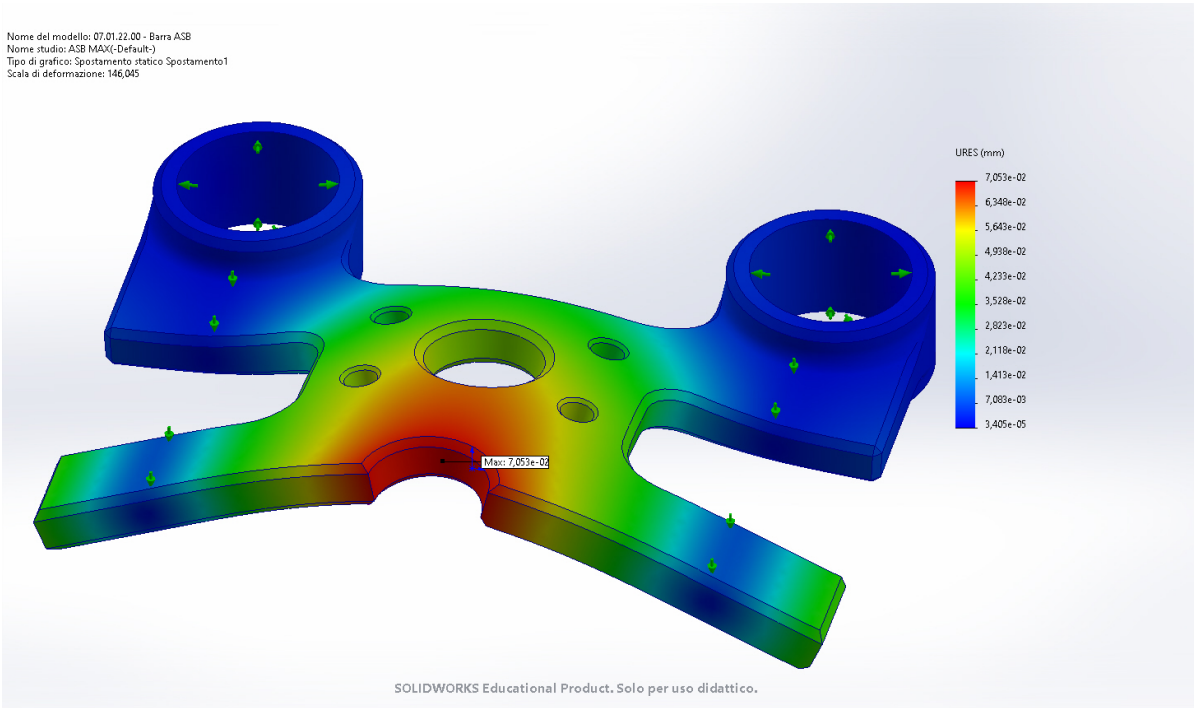


**Figure 3.24:** ASB bar displacement when the maximum force is generated by the ASB

As it is possible to see in Figure 3.24 the maximum displacement obtained in during operation at maximum performance is of  $71 \mu\text{m}$ .

The ASB bar has been also verified in condition of hydraulic fail. In this case one of the master cylinders does not react to the ASB force and the whole force is applied only to one master cylinder. For the simulation the boundary condition between ASB bar and one of the pneumatic cylinder fork has been deleted. The results are reported in Figure 3.25, where it is possible to see a stress concentration zone in proximity of a geometric variation. The maximum stress obtained is still lower than the yield stress of the material. The safety factor is 1.07 which is only a little higher than 1 but, since the analysis condition is a fail case, the component is verified.

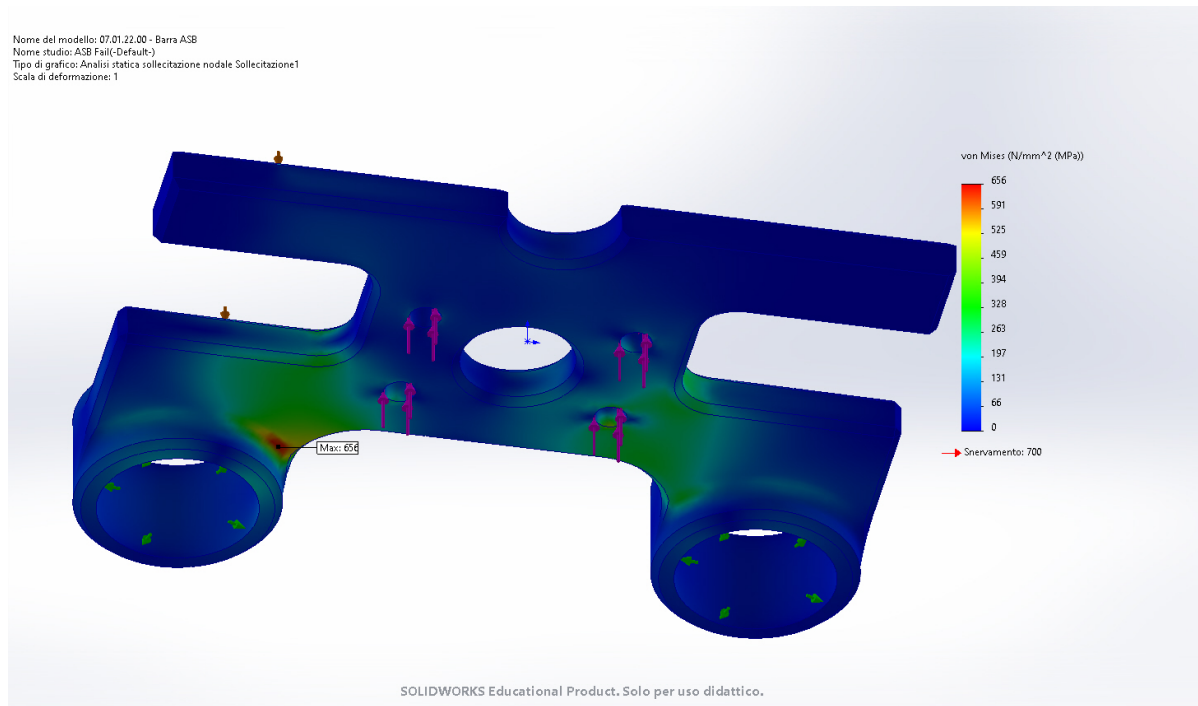


**Figure 3.25:** ASB bar stress distribution in case of hydraulic fail in one brake line and maximum force generated by the ASB

### 3.2.6 Pneumatic cylinder fork

The pneumatic cylinder fork (Figure 3.26) is the component that guarantee the permanent connection between the pneumatic cylinder and the master cylinder and the temporary connection between the ASB bar and the master cylinder by means of an Hertzian contact. The contact will be between a cylindrical surface (pneumatic cylinder fork) and a planar surface (ASB bar), therefore the deformation will cause a rectangular contact surface[41]. From experimental data it is possible to see that in a cylinder to plane contact structural failure occurs when the maximum pressure is equal to  $1.67 R_{p0.2}$ , where  $R_{p0.2} = 700 \text{ MPa}$  is the yield stress of 25CrMo4 steel[37]. At first the half

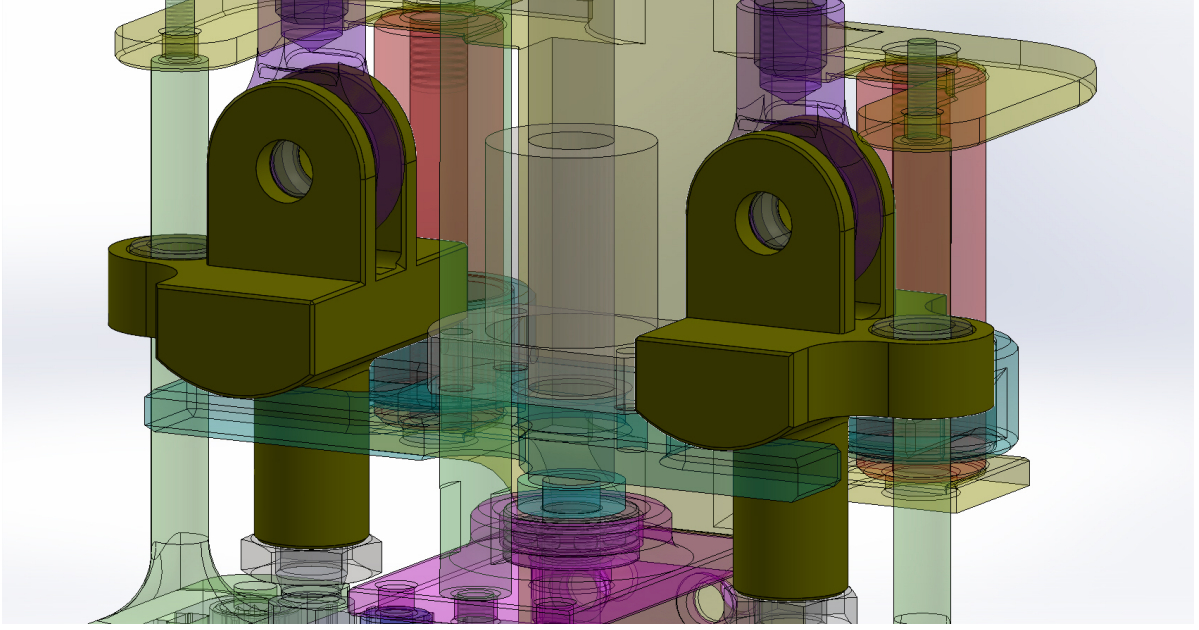


**Figure 3.26:** Pneumatic cylinder forks

width  $b$  of the rectangular contact area generated has been calculated with equation 3.38. Since the contact between ASB bar and pneumatic cylinder fork is divided into two parts  $F_1 = 782$  N is the force acting in half of the contact calculated with equation 3.29 in Section 3.2.5, while  $a = L/2 = 11.5$  mm is half of the total contact length.

$$b_{min} = \frac{2 F_1}{1.67 \pi a} = 83 \mu\text{m} \quad (3.38)$$

It is possible to calculate the maximum curvature  $\alpha_{MAX}$  with equation 3.39 and then the minimum radius of curvature  $r_{min}$  with equation 3.40.  $\nu = 0.3$  is the Poisson coefficient and  $E = 210$  GPa is the Young Modulus of the steel. The radius of curvature  $r$  chosen is of 20 mm.

$$\alpha_{MAX} = \frac{4 F_1}{\pi a b_{min}^2} \cdot \frac{1 - \nu^2}{E} = 0.054 \text{ mm}^{-1} \quad (3.39)$$

$$r_{min} = \frac{1}{\alpha_{MAX}} = 18.51 \text{ mm} \quad (3.40)$$

In order not to stress the pneumatic cylinder rod with radial loads a bushing has been connected to the pneumatic cylinder fork. Details on the bushing are reported in Section 3.2.8.

### 3.2.7 Master cylinder rod end

In order to connect the pneumatic cylinder fork to the master cylinder the master cylinder rod end has been designed (Figure 3.27). This component present a Uniball housing

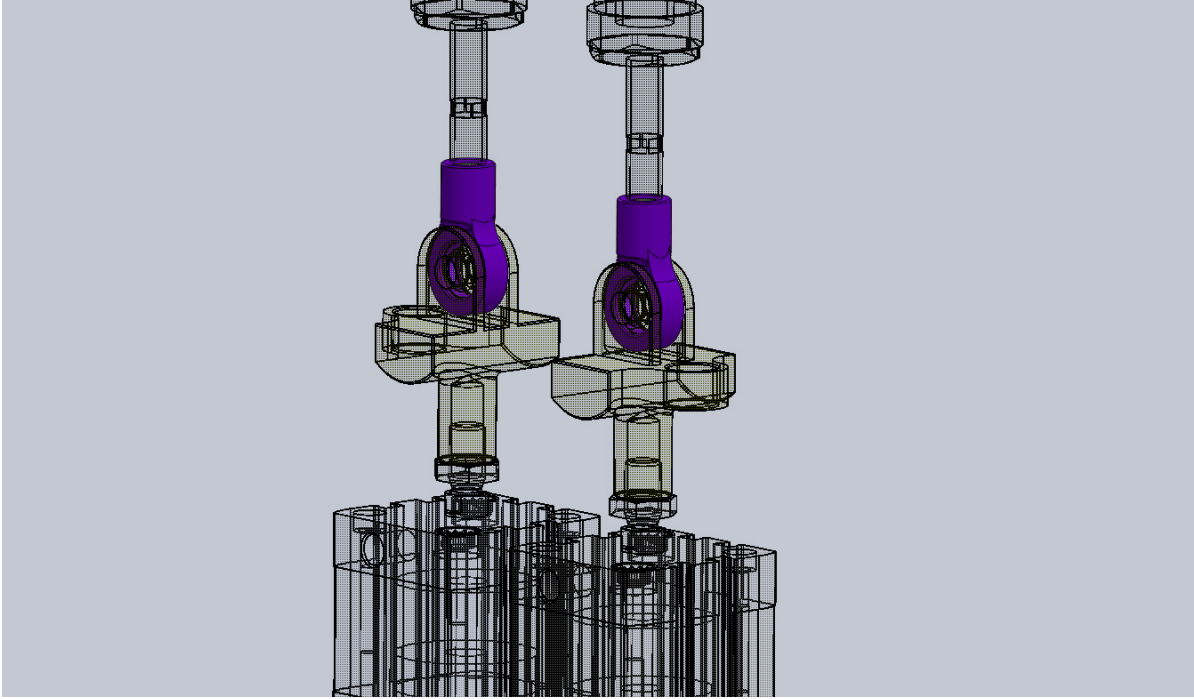


**Figure 3.27:** Master cylinders' rod ends

for the connection with the pneumatic cylinder fork and it has a threaded hole for the connection with the master cylinder. A locknut prevents the rod end to move from its position, allowing the optimal operation of the Uniball.

### 3.2.8 Balance bar

The two master cylinders connected to the ASB bar could be schematised with two springs acting in parallel since the displacement is the same[26]. The equivalent stiffness of the master cylinders depends on the volume of hydraulic fluid and on the area of the master cylinder piston[44]. Since these two parameters are different between front and rear line the stiffness of the brake lines is different and with an equal displacement different forces are applied to the master cylinders. To overcome this issue a balance bar has been designed.

The balance bar is a device that allows the repartition of the force between the two master cylinders[45]. Its operating principle is based on the torque equilibrium at each side of the balance bar that guarantee a correct force repartition. The free body diagram of the system is reported in Figure 3.28, from which equation 3.41 can be obtained.

$$F_{MC,f} = \frac{b}{a} F_{MC,r} \quad (3.41)$$

From equation 3.41 it is possible to see that the brake repartition depends on the ratio  $b/a$ . For the ASB application a 50:50 repartition has been chosen, therefore  $a = b$ ,

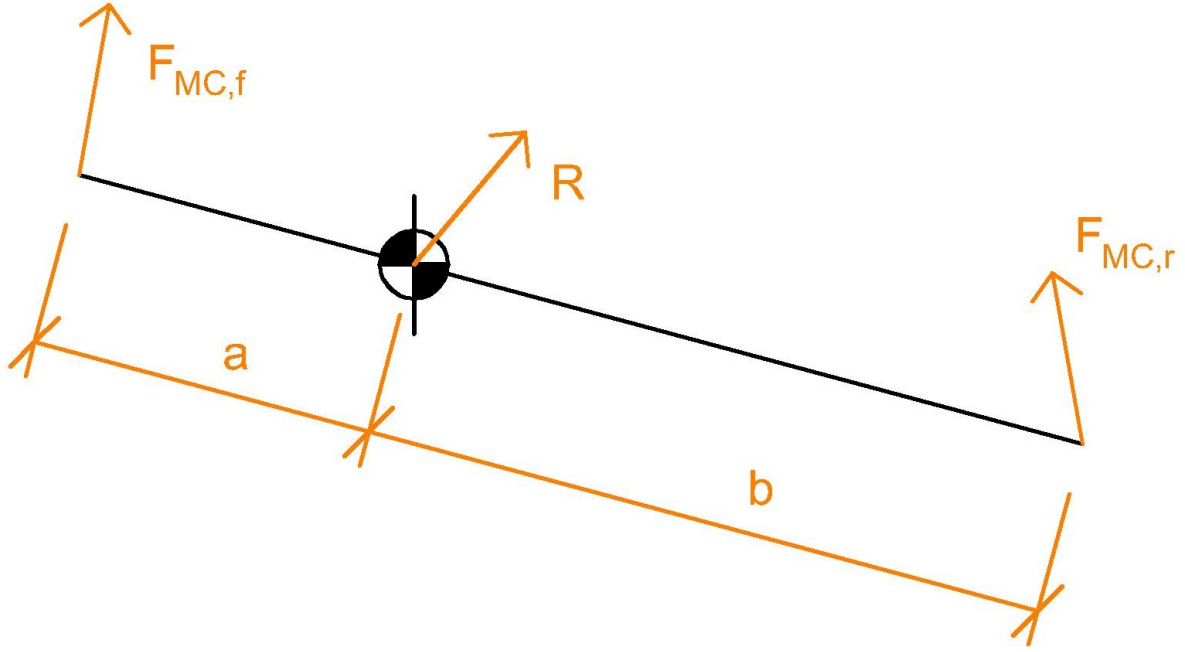


**Figure 3.28:** Balance bar free body diagram

but changing the length of the balance bar arms it is possible to change the brake repartition.

The balance bar is assembled both on front and rear column by means of SKF Uniballs[28], leaving enough space for the electric motor at the center of the assembly. Two calibrated screws allow the assembly of the two parts that make up the balance bar. The component needs to be sized, therefore it is important to evaluate the mechanical stress. The component is evaluated in its horizontal position, when all the forces are parallel to the Z axis. At first it is necessary to represent the forces acting on the balance bar with a free body diagram reported in Figure 3.29 and, considering that  $F_{MC,f} = F_{MC,r} = F_{ASB}/2$  thanks to the balance bar itself, it is possible to obtain equations 3.42 and 3.43.

$$Z_R = 2 F_{MC} \frac{a}{a+b} \quad (3.42)$$

$$Z_F = 2 F_{MC} \frac{b}{a+b} \quad (3.43)$$

Each side of the balance bar is under bending stress, evaluated with equation 3.44, where  $d = 10$  mm is the diameter of the balance bar link.

$$\sigma = \frac{32 F_{MC} l}{2 \pi d^3} = 221 \text{ MPa} \quad (3.44)$$

The minimum yield stress required is 221 MPa, therefore the 25CrMo4 tempering steel with a yield stress  $R_{p0.2} = 700$  MPa has been chosen, so that the safety factor has a value of 3.32.

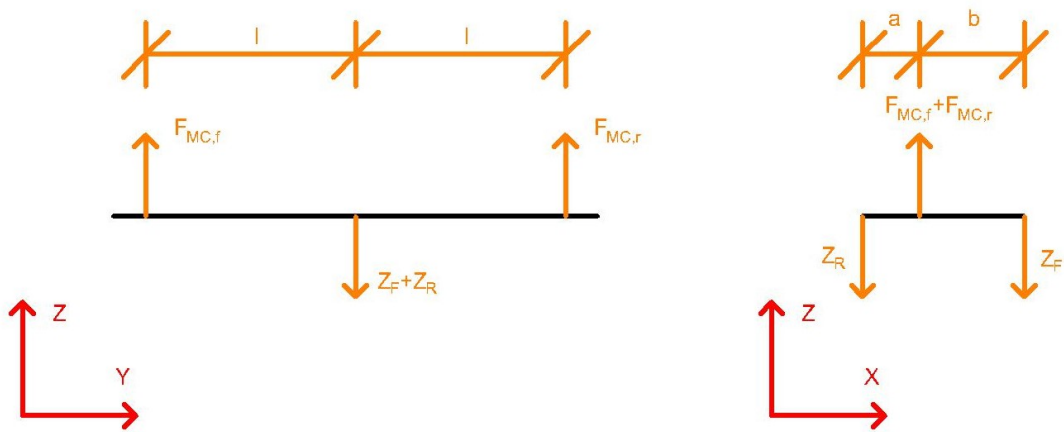


**Figure 3.29:** Balance bar free body diagram in horizontal position

The balance bar is fundamental for the ASB but it is an issue for the EBS because, in case of failure in one brake line, the pneumatic cylinder will reach its end stroke before the master cylinder is compressed enough to generate pressure in the brake line. Therefore cylindrical end strokes have been designed in order to stop the balance bar from rotating at  $8^\circ$  from the horizontal line, guaranteeing enough stroke to generate pressure inside the brake line.

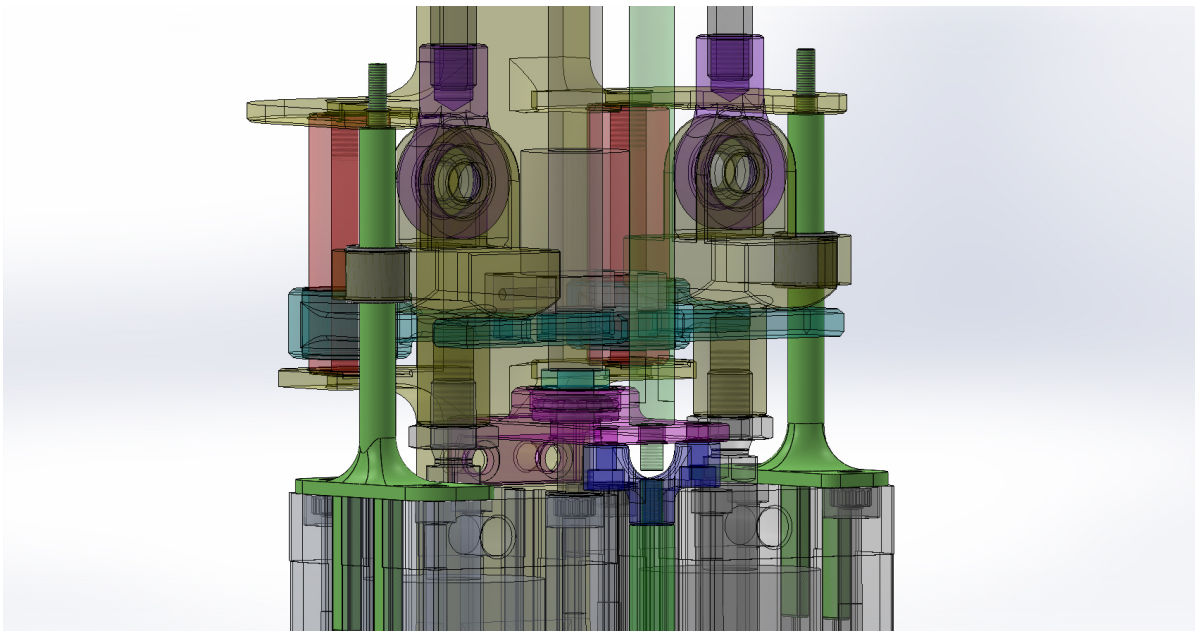


**Figure 3.30:** The two linear guides for the pneumatic cylinder forks, each one composed by a bushing and a shaft

Another issue for the EBS is the fact that if the master cylinder rotates because of the balance bar the force on the pneumatic cylinder rod will not be perfectly axial. For this reason a SKF bushing[43] has been added to each pneumatic cylinder fork, in order to discharge the radial force on the bushing shaft and not on the pneumatic cylinder rod (Figure 3.30). The bushing shaft is connected with two M6 screws to the pneumatic cylinder head and it has a M5 thread for the connection with a flange on the rear column; two prismatic pins guarantee the alignment of the bushing shaft with the pneumatic cylinder.

### 3.2.9 Kinematic analysis

To better understand how the ASB/EBS works a kinematic analysis has been carried out. Three conditions have been evaluated:

- simultaneous activation;
- non simultaneous activation;
- fail in one brake line.

In each case the inputs are the displacement of the pneumatic cylinders' rod.

At first it was necessary to evaluate the degrees of freedom of the system using Grübler Formula[46] (equation 3.45). Referring to the scheme in Figure 3.31  $i = 8$  is the number of links in the mechanism (including the fixed link),  $j = 9$  is the number of kinematic pairs and  $f_i$  is the number of degree of freedom constrained by the  $i$ -th kinematic pair; since all the kinematic pairs are either hinges or carriages  $f_i = 1$ .

$$F = 3(l - 1) - \sum_{i=1}^j (3 - f_i) = 3 \quad (3.45)$$

The system as schematized in Figure 3.31 has three degrees of freedom. However, since the master cylinders are not simple sliders but they transmit a force on the two links that compose them, using equation 3.46 derived from the rotation balance of the balance bar it is possible to subtract one degree of freedom.  $l = 37.75$  mm is half the length of the balance bar.

$$\alpha = \frac{k_{OIL}(z_r - z_f)}{2lk_{OIL}} \quad (3.46)$$

For the analysis a simplified model has been used. In particular the master cylinders have been modelled has two springs with stiffness  $k_{OIL} = 1.3788 \cdot 10^5$  N/m as evaluated during experimental tests[22]. It is important to underline that the stiffness calculated takes into account also the effect of the force distribution given by the balance bar. The actual stiffness of the brake lines will be slightly different from each other due to different volumes and actuators' areas.

Since the horizontal displacement is very low compared to the vertical displacement, horizontal forces from the master cylinders are omitted. The scheme of the balance bar is reported in Figure 3.32.

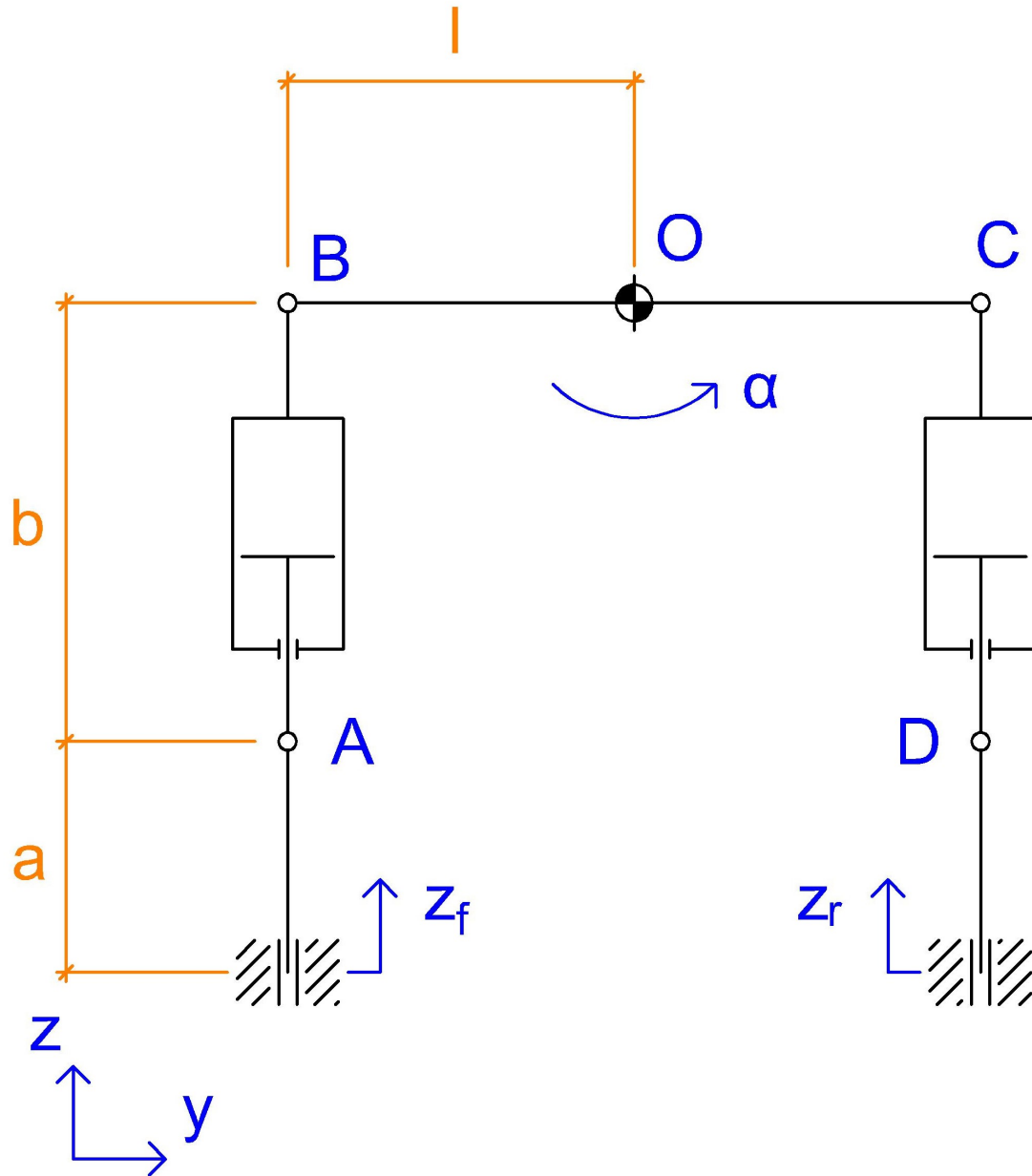


**Figure 3.31:** ASB kinematic analysis scheme

Thanks to equation 3.46 the degrees of freedom of the mechanism are reduced to two, therefore the system will be controlled only with the positions  $z_f$  and  $z_r$ . Following the scheme of Figure 3.31 the other points' position are calculated with the following equations 3.47, 3.48, 3.49 and 3.50.

$$\begin{cases} z_A = z_f + a \\ y_A = -l \end{cases} \quad (3.47)$$

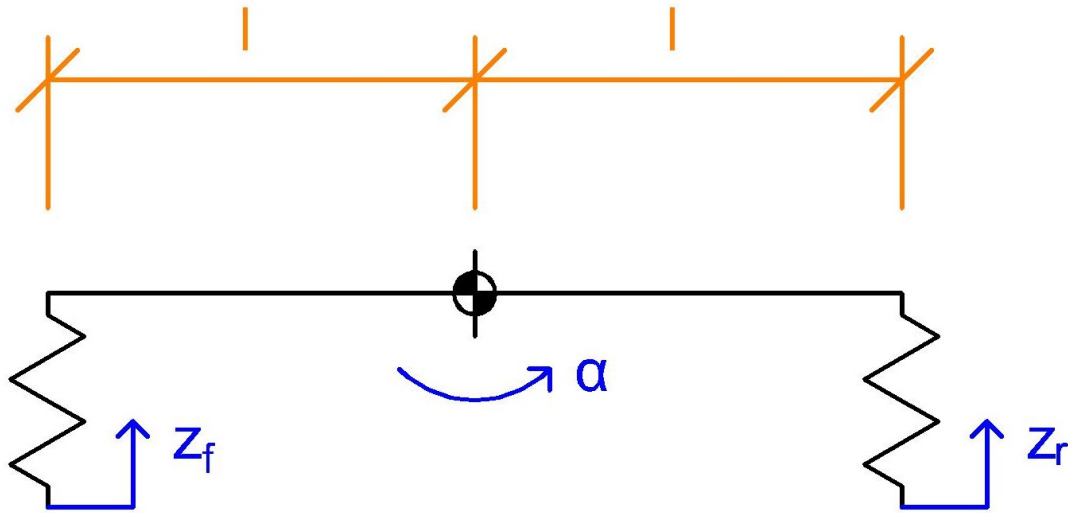


**Figure 3.32:** Simplified model for balance bar and master cylinders

$$\begin{cases} z_B = a + b - l \sin \alpha \\ y_B = -l \cos \alpha \end{cases} \quad (3.48)$$

$$\begin{cases} z_C = a + b + l \sin \alpha \\ y_C = l \cos \alpha \end{cases} \quad (3.49)$$

$$\begin{cases} z_D = z_r + a \\ y_D = l \end{cases} \quad (3.50)$$

### Simultaneous activation

In Figure 3.33 it is possible to see the results of a simultaneous activation. In blue are reported the pneumatic cylinders, in red the master cylinders while in green the balance bar. It is possible to see that with a simultaneous activation and with the stiffness of the master cylinders' equivalent springs equal for front and rear brake lines the balance bar remains horizontal during the whole actuation.

### Non simultaneous activation

In this case the right brake line actuation is delayed compared to the left line. The results are reported in Figure 3.34 where it is possible to see that the non simultaneous actuation causes the inclination of the balance bar in order to maintain equal forces on both the master cylinders. However the incline of the master cylinder is very low.

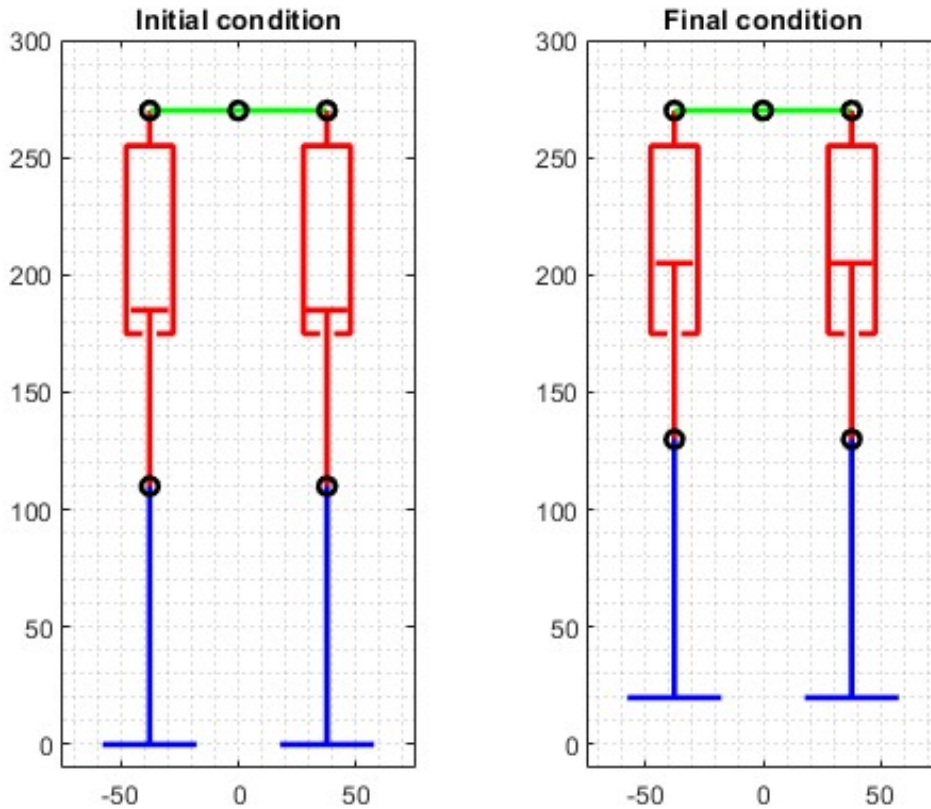


**Figure 3.33:** Kinematic analysis with simultaneous activation of the brake lines

### Fail in one brake line

In this case a fail occurred in the right brake line and therefore the equivalent stiffness of the line in failure condition drops to zero. The results are reported in Figure 3.35. At first the actuation of the left line causes the balance bar to incline while no force is converted in brake pressure. As soon as the balance bar comes into contact with the end stops the master cylinder begins its compression and the force on the master cylinder begins to rise: the actuation of the brake line not in fault is still possible. Also in this case the incline of the master cylinders is very low.

## 3.3 Case design

The last subassembly to be designed is the case able to integrate the EBS with the ASB and to withstand the loads generated by the autonomous actuators.

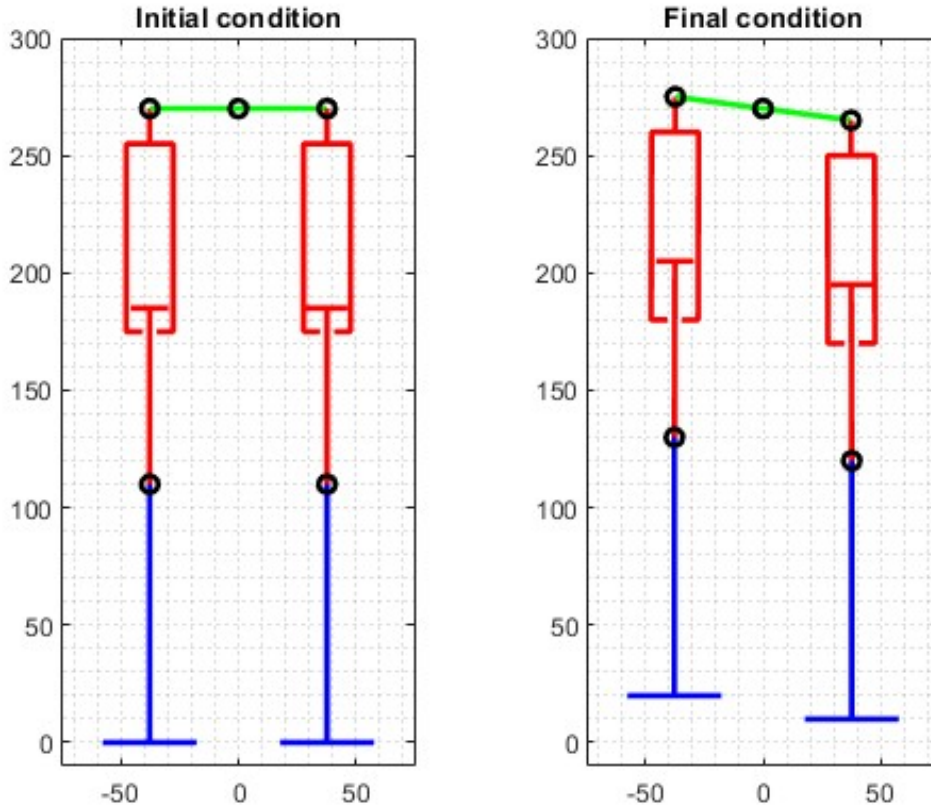


**Figure 3.34:** Kinematic analysis with right brake line activated with a delay

### 3.3.1 Base

The base (Figure 3.36) has been designed to be made out of a sheet of steel 3 mm thick. It connects the assembly to the vehicle using four M5 bolts. On the top of the base there are holes for the connection of rear and front columns and pneumatic cylinders. The base has to be strong enough to withstand the loads generated by the EBS and it has to provide a good dimensional stability in order to not bend when the braking actuators are operating.

The material chosen for this application is a low alloy steel, in order to be easy to manufacture and to weld[37]. Reinforcement plates at the front and at the rear of the base guarantee an optimal stress distribution and a low deformation of the component. A hole on the front allows the front column nut to be screwed up.

### 3.3.2 Rear column

The rear column (Figure 3.37) is made out of Ergal (Al 7075-T6) and it provides the connection between different components and the base. Like the base it has to provide enough resistance and low deformation under stress. On the column there are holes

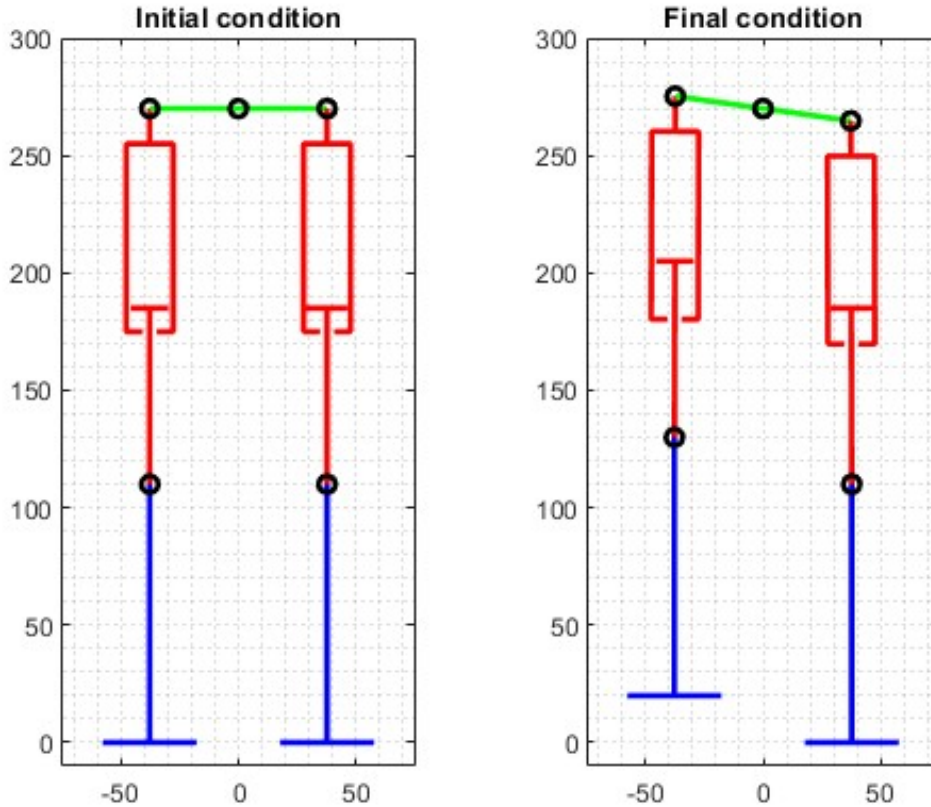


**Figure 3.35:** Kinematic analysis with right brake line in fail

for the attachment of the bearing supports and of the gear train support (Figure 3.38); pockets have been realized in order to have an optimal positioning of the supports.

Horizontal flanges are required to position the bushings' shafts (Figure 3.39). These flanges can be made out of the same piece of the rear column but could also be manufactured separately and then attached with bolts.

At the top of the rear column the balance bar Uniball housing has been designed (Figure 3.40). On the sides of it two cylindrical extrusions operate as end stops as specified in Section 3.2.8.

### 3.3.3 Front column

The rear column can guarantee enough resistance to withstand alone all the loads generated by the EBS and the ASB, but its deformation will be too high. Therefore a front column has been designed in order to reduce the displacement of the components, in particular of the ball screw bearings since the ball screw has to operate with a low degree of misalignment[32].

The front column is divided into three parts:

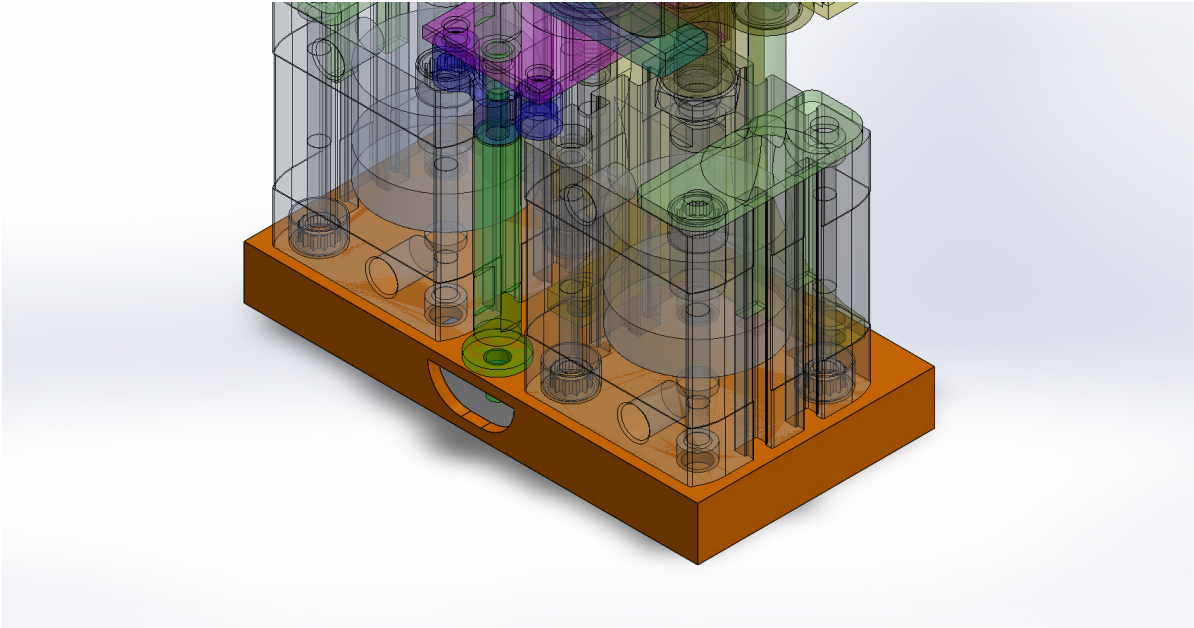


**Figure 3.36:** Base 3D model

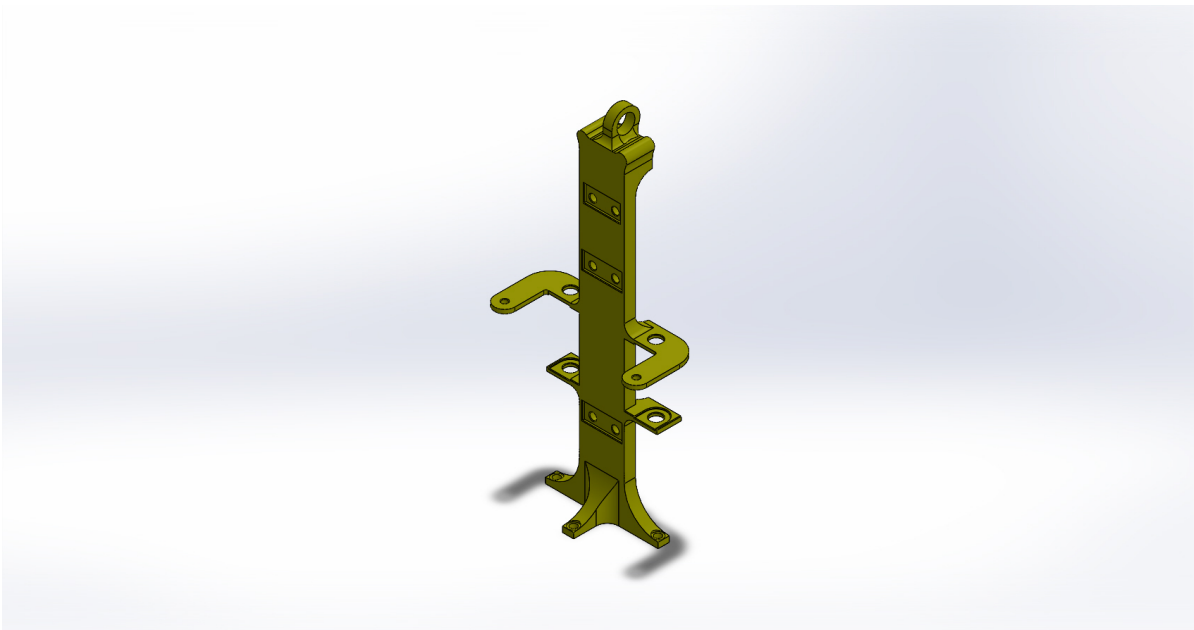


**Figure 3.37:** Rear column

- lower front column (Figure 3.41a);
- medium front column (Figure 3.41b);
- upper front column (Figure 3.41c).

Each of the part of the front column is an aluminium (Al 7075-T6) cylindrical com-

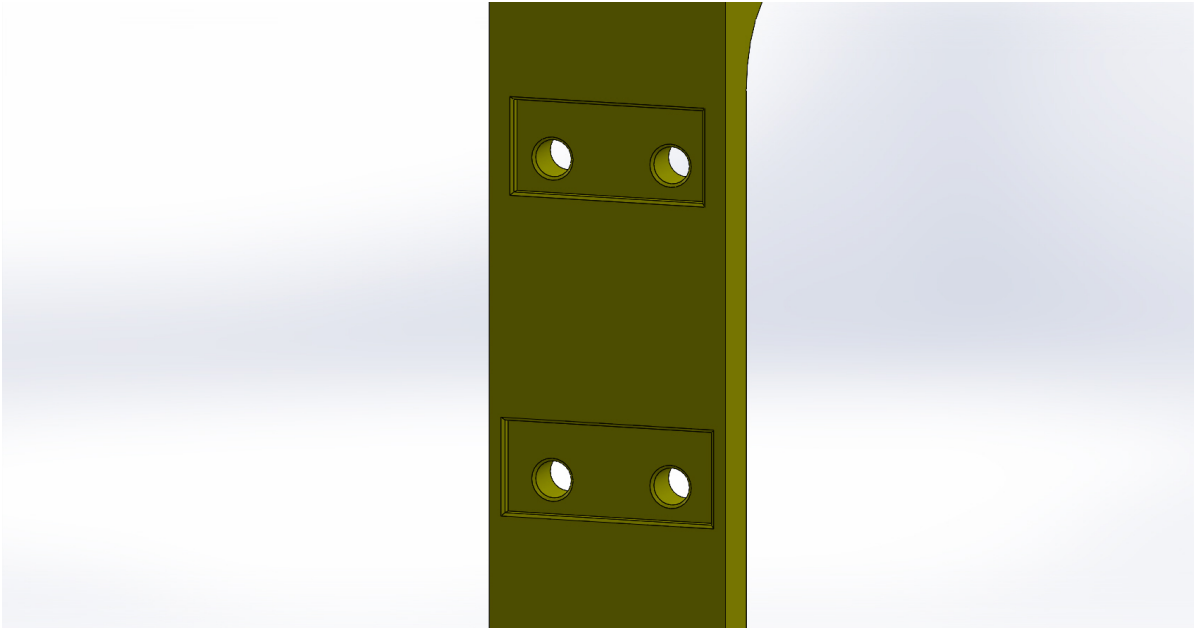


**Figure 3.38:** Rear column holes for the bearing supports and the gear train support

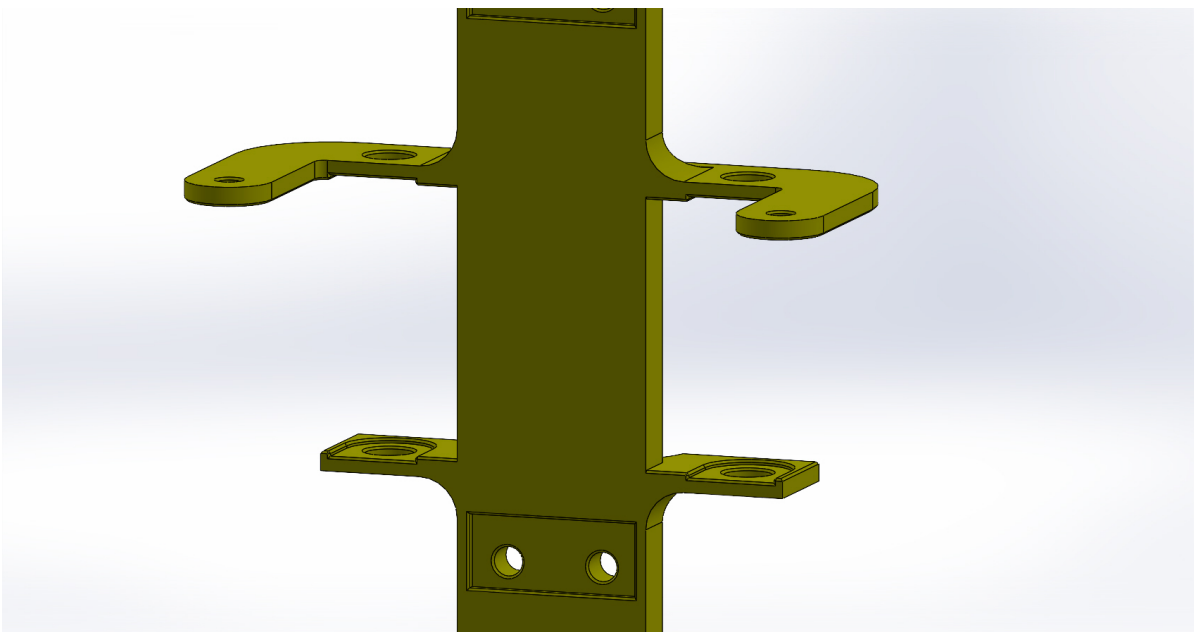


**Figure 3.39:** Rear column flanges for the bushings' shafts

ponent with a diameter of 10 mm. The main common characteristics are:

- each rod end threaded with a M5x10 mm thread;
- a flattening in order to allow the use of a 8 mm wrench during assemble and disassemble operations.

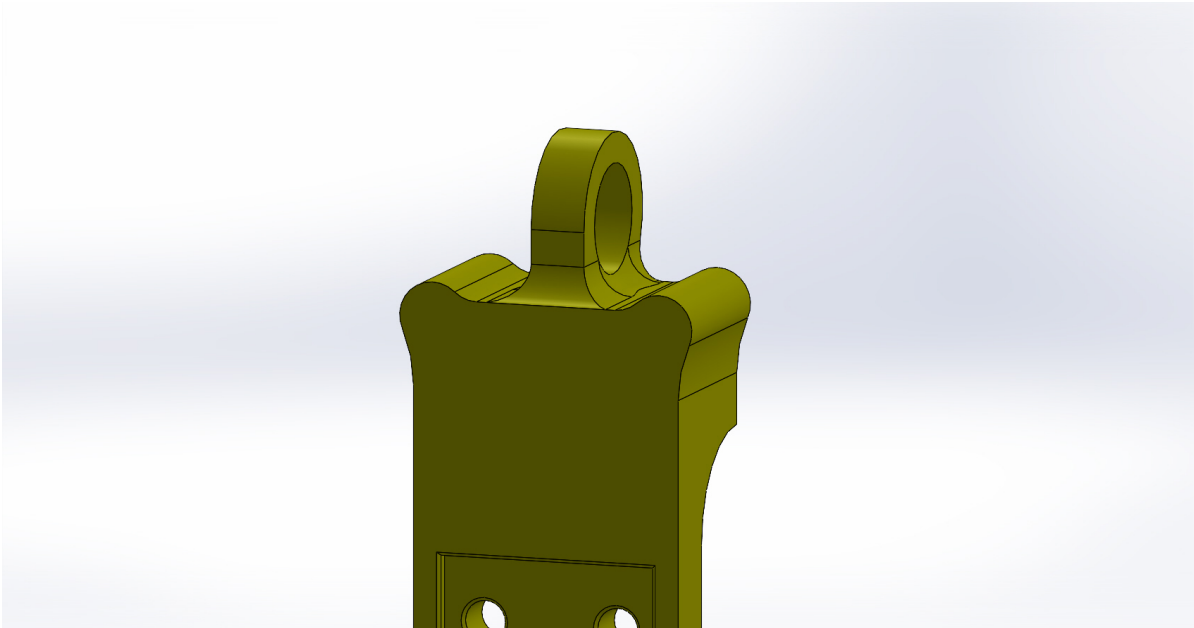
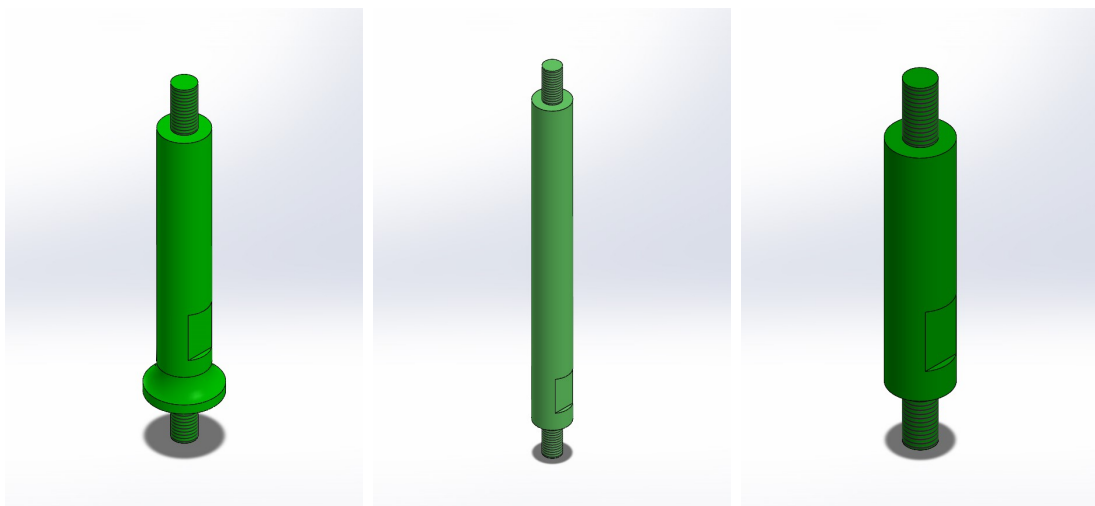


**Figure 3.40:** Balance bar's Uniball housing on the rear column



(a) Lower front column      (b) Medium front column      (c) Upper front column

**Figure 3.41:** Front column

The main difference is in the height of the three parts. Furthermore the lower front column has a lower shoulder of 15 mm instead of 10 mm in order to guarantee a better stress distribution as it is possible to see in FEM analysis (Section 3.3.7).

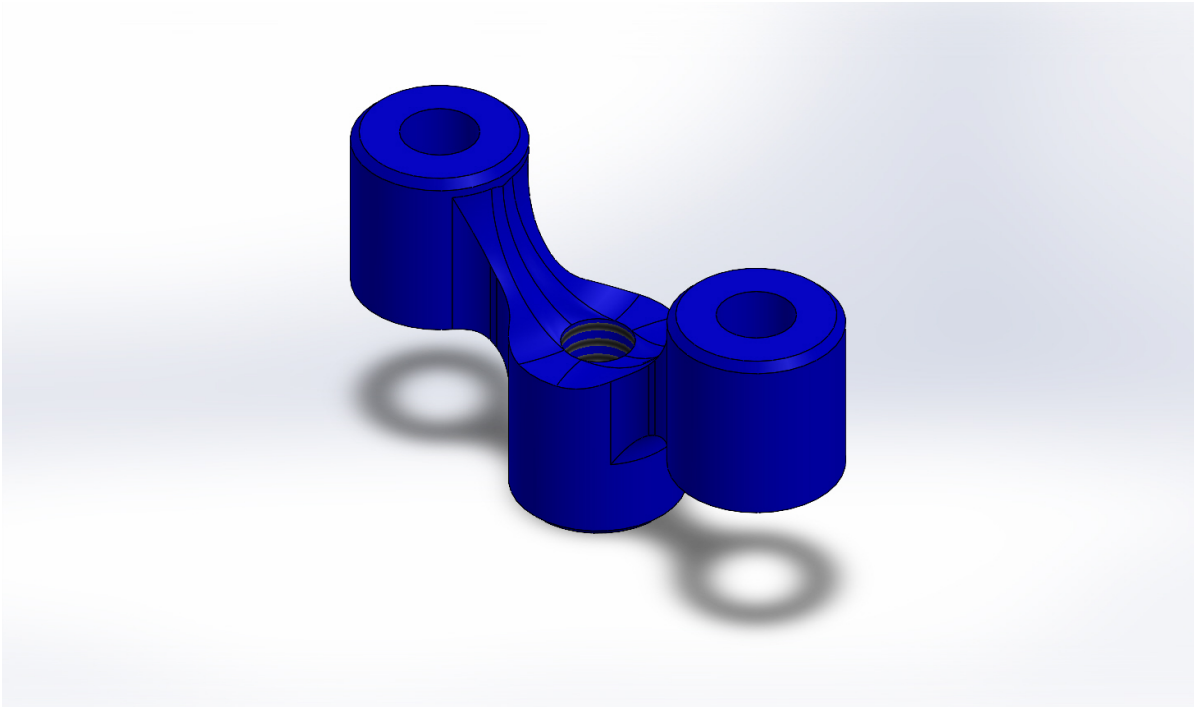


**Figure 3.42:** Front column connections

### 3.3.4 Front column connections

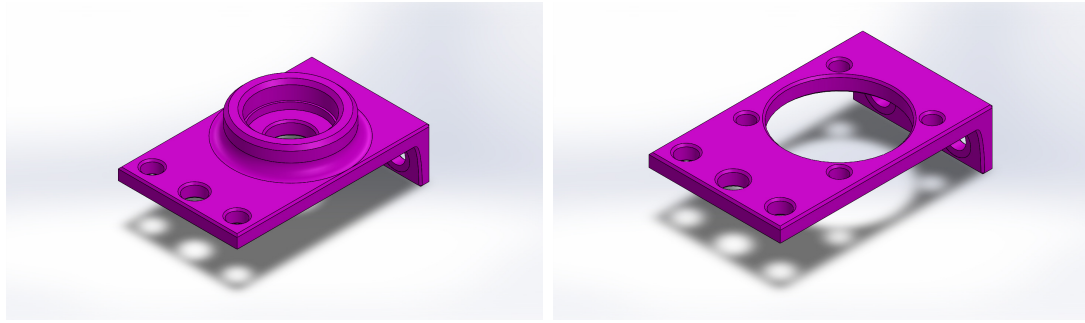
To connect all the components in which the front column is divided front column connections have been designed (Figure 3.42). The lower part of the connection is an M5 nut screw in order to be attached to the thread of the front column. On the upper part two counterbore holes for M5 bolts are designed in order to guarantee the connection to the bearing supports. Between the bosses where the holes are placed enough space is granted to allow the placement of an M5 nut that allows the connection of one component of the front column to the bearing support.

The front column connections will be realized with CNC milling machine and with AL 7075-T6. FEM analysis showed that this component is the most stressed in most of the cases (Section 3.3.7). However the safety factor is always higher than 2 therefore the geometry has been confirmed.

### 3.3.5 Bearing supports

The bearing supports (Figure 3.43) are the components that connect the ball screw bearings to the columns of the ASB. Since the bearings used are different also the ball screw supports are not the same. Anyway both the supports are L shaped and attached to the rear column with two M5 bolts. They are also attached to the front column connection with two M5 bolts and to the front column with one M5 bolt.

Since the lower bearing is a thrust bearing (Section 3.2.1) the lower bearing support has a cylindrical housing that guarantees the positioning of the bearing (Figure 3.43a).



(a) Lower bearing support

(b) Upper bearing support

**Figure 3.43:** Bearing supports

On the other hand the upper bearing is a floating bearing manufactured with a flanged case, therefore the upper bearing support has four holes for M3 screws to connect the flange to the support (Figure 3.43b).

The supports are going to be realized in Al 7075-T6 CNC milled.

### 3.3.6 Gear train support

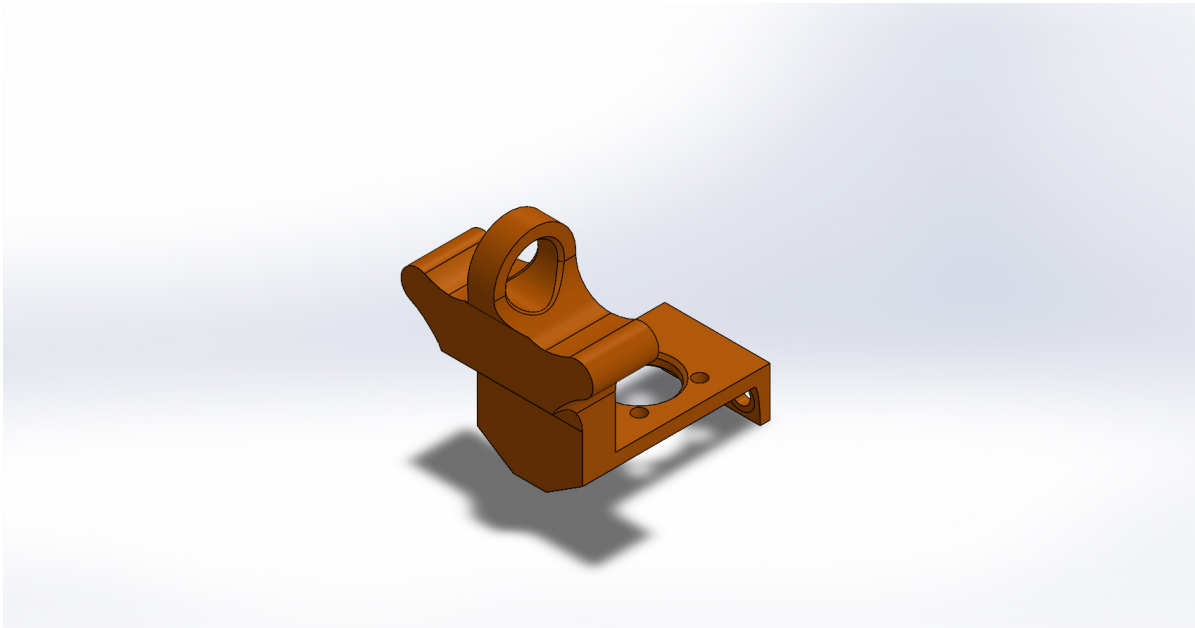


**Figure 3.44:** gear train support

The gear train support (Figure 3.44) is divided into two main parts that fulfill different tasks:

- the lower part is the real gear train support, and it is necessary to connect the gear train and electric motor system to the ASB columns;

- the upper part is composed by the balance bar's Uniball housing and the balance bar end stroke.

The gear train support is connected to the rear column similarly to the bearing supports (Section 3.3.5), while it presents an M5 nut screw for the connection to the front column. The component is going to be realized in Al 7075-T6.

### 3.3.7 Case assembly structural analysis

The case assembly has been analysed with finite element method analysis performed with Solidworks Simulation[47]. The main purpose of the analysis is to verify that an aluminium structure guarantees enough resistance and does not deform too much compared to a steel structure. Furthermore the effective benefit of the weight reducing holes has been evaluated. Therefore four different structures have been analysed:

- steel structure, no weight reducing holes;
- steel structure, weight reducing holes;
- aluminium structure, no weight reducing holes;
- aluminium structure, weight reducing holes.

The steel used for the analysis is the 25CrMo4 tempering steel, while the aluminium is Ergal (Al 7075-T6). The case assembly is attached to the vehicle with four M5 bolts, therefore a translation constraint has been applied on the base of the case assembly.

The case assembly has been analysed in different conditions:

- ASB operation: the ASB generates a force  $F_{ASB} = 2304$  N;
- ASB maximum operation: the ASB generates a force  $F_{ASB} = 4000$  N;
- ASB with one brake line fail: the ASB generates a force  $F_{ASB} = 1152$  N but only one master cylinder absorb the energy;
- EBS operation: the EBS generates a force  $F_{EBS} = 1273$  N on each brake line;
- EBS with one brake line fail: the EBS generates a force  $F_{EBS} = 1273$  N only on one brake line.

In ASB operation the balance bar is considered to be horizontal. Due to the different arm of the force applied to the master cylinders with regards to the Uniballs, the force on the front Uniball is different to the one applied to the rear Uniball. In particular at the front 40 % of the total force on the master cylinders is applied, while on the rear 60 % of the total force on the master cylinders is applied. On the lower bearing support is applied a downward force equal to the total force applied to the master cylinder. Furthermore on the gear train support is applied the reaction torque needed for the ASB actuation.

In case of ASB with one brake line fail a torque is applied to the bushing shafts. This torque is the reaction generated by the shafts in order to maintain the ASB bar horizontal. Furthermore the brake line fail causes the balance bar to not be horizontal anymore and it comes into contact with the end stops: a force is generated on the end stops in order to balance the torque due to the force on the working master cylinder. The reaction force on the gear train support is 1.56 times the force on the gear train's Uniball while the reaction force on the rear column is 2.70 times the force on the rear column's Uniball.

In EBS operation the force of the actuation is not applied to the lower bearing support but to the base on a surface equal to the pneumatic cylinders surface. The torque applied to the gear train support is null. In case of failure no torque is applied to the bushing shafts since the ASB bar is decoupled from the master cylinders. With regards to the master cylinders' forces no changes are applied compared to the ASB case.

The parameters taken into account for the comparison are the maximum stress, the safety factor, the maximum displacement and the displacement of the upper bearing support compared to the lower one. The latter value is important to evaluate the misalignment on the ball screw that can cause a reduction of the component life. However it is important to underline that the displacements obtained are overestimated because of the absence of the ball screw that increases the case stiffness.

### **Aluminium case with weight reducing holes**

The results of the analysis are reported in Table 3.11.

As it is possible to see the case assembly is validated also in fail conditions, since the safety factor is always higher than 1. The total weight of the case assembly is of 1.056 kg.

### **Aluminium case without weight reducing holes**

The results of the analysis are reported in Table 3.12. Graphics for the ASB operation condition are reported in Figure 3.45 and Figure 3.46.

As it is possible to see the case assembly is validated also in fail conditions, since the safety factor is always higher than 1. The total weight of the assembly is of 1.155 kg. The weight is obviously higher than the previous case, but the displacements and the stresses obtained in this configuration are considerably lower, therefore the weight reduction is not justified and the solution without weight reducing holes is preferred.

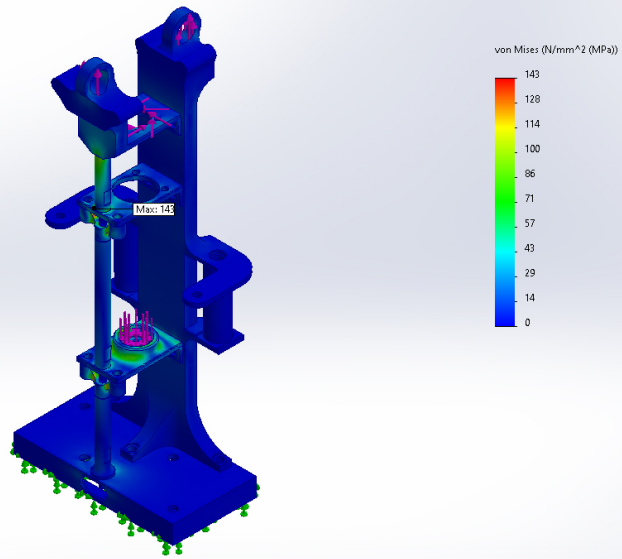
Analysis condition	Maximum stress	Safety factor	Maximum displacement	Displacement between bearings
ASB operation	166 MPa	3.04	495 $\mu\text{m}$	57 $\mu\text{m}$
ASB maximum operation	289 MPa	1.75	859 $\mu\text{m}$	104 $\mu\text{m}$
ASB fail	207 MPa	1.90	505 $\mu\text{m}$	238 $\mu\text{m}$
EBS operation	203 MPa	1.39	853 $\mu\text{m}$	149 $\mu\text{m}$
EBS fail	270 MPa	1.67	1250 $\mu\text{m}$	337 $\mu\text{m}$

**Table 3.11:** Aluminium case with weight reducing holes FEM analysis

Analysis condition	Maximum stress	Safety factor	Maximum displacement	Displacement between bearings
ASB operation	143 MPa	3.54	261 $\mu\text{m}$	54 $\mu\text{m}$
ASB maximum operation	247 MPa	2.04	453 $\mu\text{m}$	101 $\mu\text{m}$
ASB fail	194 MPa	1.94	412 $\mu\text{m}$	249 $\mu\text{m}$
EBS operation	203 MPa	1.39	554 $\mu\text{m}$	130 $\mu\text{m}$
EBS fail	260 MPa	1.73	1102 $\mu\text{m}$	321 $\mu\text{m}$

**Table 3.12:** Aluminium case without weight reducing holes FEM analysis

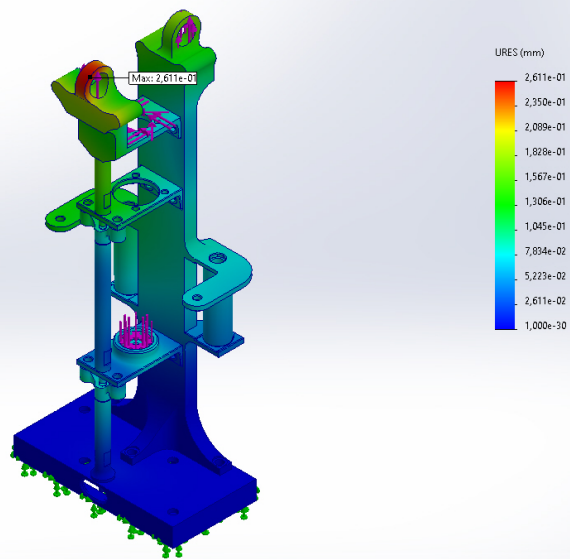
Nome del modello: Basamento\_alluminio\_noh  
Nome studio: ASB(-Default-)  
Tipo di grafico: Analisi statica sollecitazione nodale Sollecitazione1  
Scala di deformazione: 1



SOLIDWORKS Educational Product. Solo per uso didattico.

Figure 3.45: ASB operation: stress distribution

Nome del modello: Basamento\_alluminio\_noh  
Nome studio: ASB(-Default-)  
Tipo di grafico: Spostamento statico Spostamento1  
Scala di deformazione: 1



SOLIDWORKS Educational Product. Solo per uso didattico.

Figure 3.46: ASB operation: displacement

### Steel case with weight reducing holes

The results of the analysis are reported in Table 3.13.

Analysis condition	Maximum stress	Safety factor	Maximum displacement	Displacement between bearings
ASB operation	166 MPa	3.74	174 $\mu\text{m}$	21 $\mu\text{m}$
ASB maximum operation	288 MPa	2.16	301 $\mu\text{m}$	40 $\mu\text{m}$
ASB fail	212 MPa	2.04	182 $\mu\text{m}$	113 $\mu\text{m}$
EBS operation	183 MPa	1.55	309 $\mu\text{m}$	54 $\mu\text{m}$
EBS fail	233 MPa	2.66	164 $\mu\text{m}$	101 $\mu\text{m}$

**Table 3.13:** Steel case with weight reducing holes FEM analysis

As it is possible to see the case assembly is validated also in fail conditions, since the safety factor is always higher than 1. The total weight of the assembly is of 2.102 kg. It is possible to see that the steel guarantees a big reduction in displacement, however the almost doubled mass is not suitable for a motorsport application.

### Steel case without weight reducing holes

The results of the analysis are reported in Table 3.14.

Analysis condition	Maximum stress	Safety factor	Maximum displacement	Displacement between bearings
ASB operation	146 MPa	4.26	93 $\mu\text{m}$	20 $\mu\text{m}$
ASB maximum operation	253 MPa	2.45	162 $\mu\text{m}$	35 $\mu\text{m}$
ASB fail	199 MPa	2.09	151 $\mu\text{m}$	89 $\mu\text{m}$
EBS operation	182 MPa	1.55	205 $\mu\text{m}$	48 $\mu\text{m}$
EBS fail	222 MPa	2.80	140 $\mu\text{m}$	84 $\mu\text{m}$

**Table 3.14:** Steel case with weight reducing holes FEM analysis

As it is possible to see the case assembly is validated also in fail conditions, since the safety factor is always higher than 1. The total weight of the assembly is of 2.375 kg. The displacement is lower than the previous case, however it weights 0.273 kg more.

Thanks to the FEM analysis it has been possible to choose the optimal solution for the ASB. The Aluminium case without weight reducing holes has been chosen because it resulted to be the best compromise between low mass and low displacement.

### 3.4 Assembly pictures

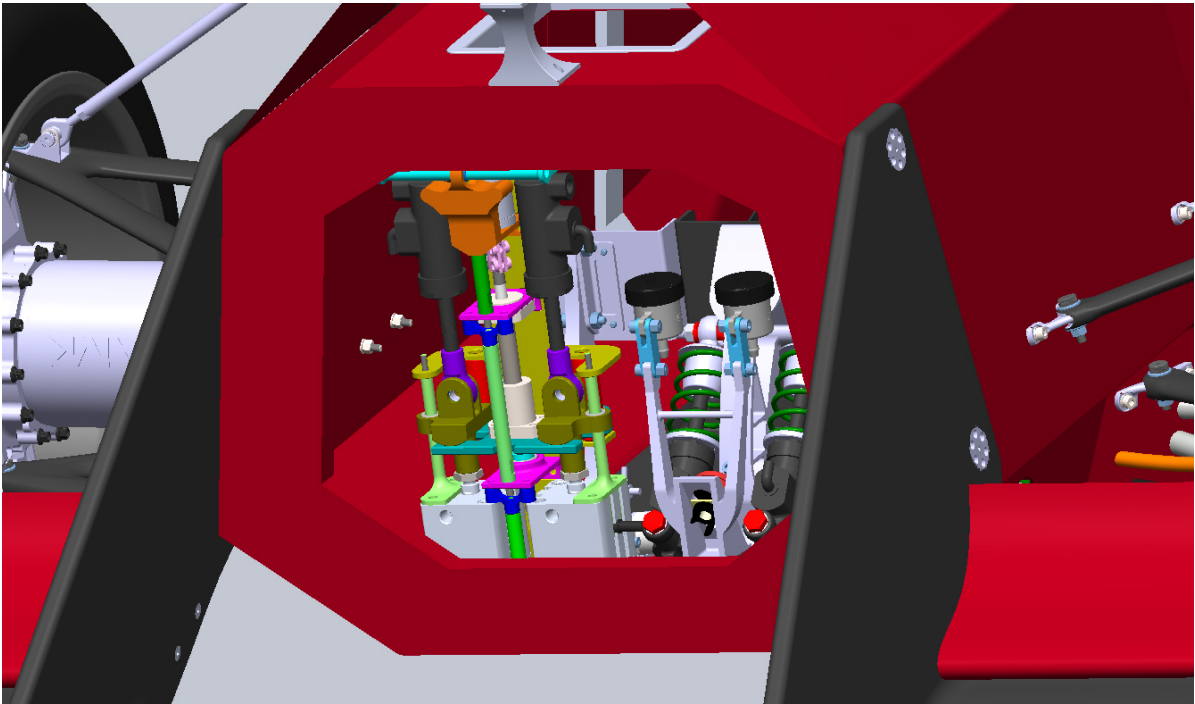
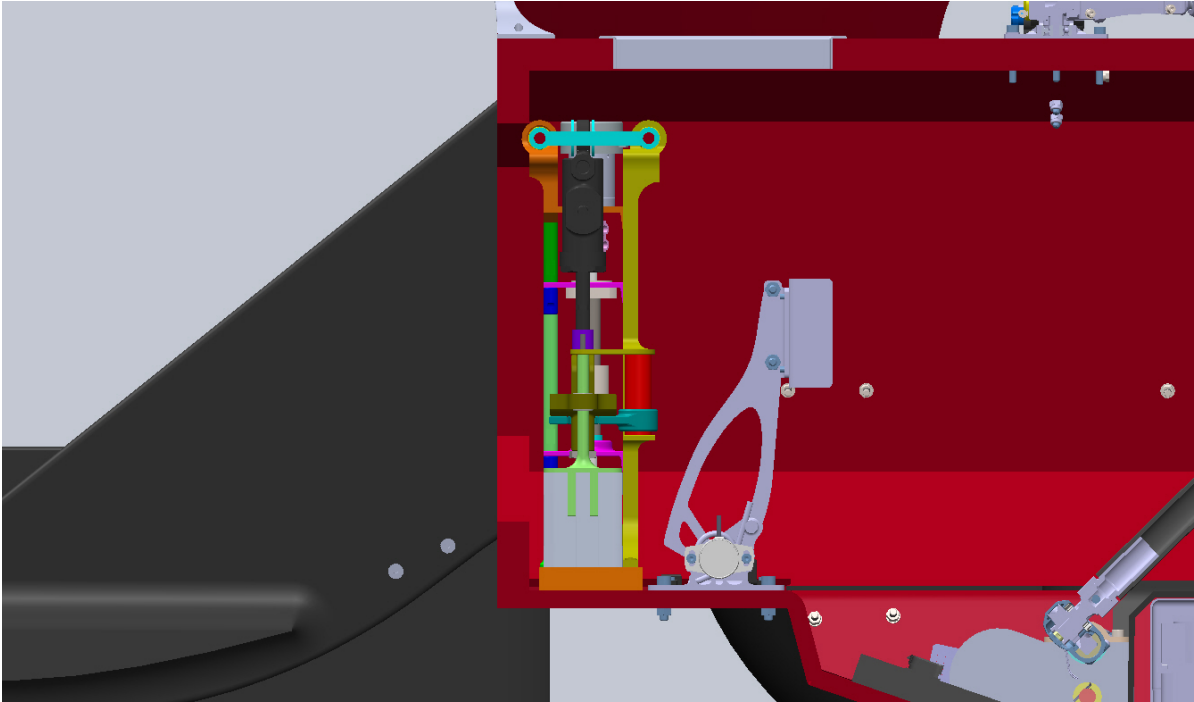
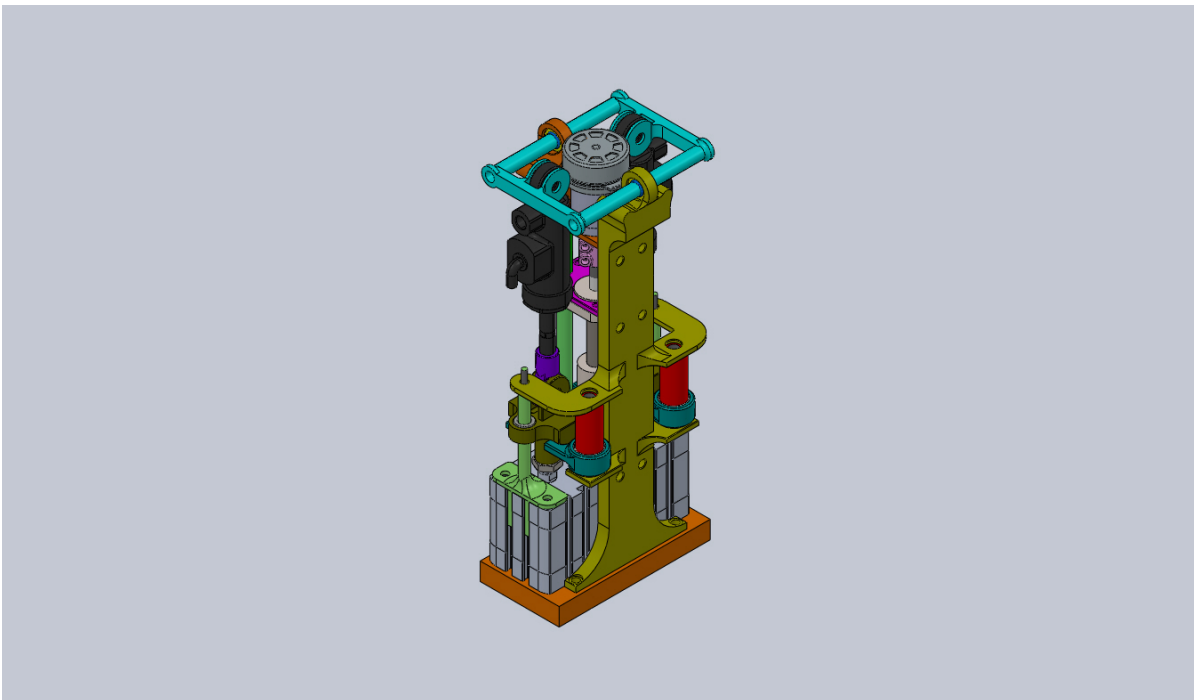


Figure 3.47: ASB/EBS assembly seen from the front bulkhead of the vehicle



**Figure 3.48:** ASB/EBS assembly mounted on the vehicle



**Figure 3.49:** Rear of the ASB/EBS assembly

# Chapter 4

## Modelling

In order to evaluate the performance the Autonomous System Brake has been simulated thanks to a Simulink script reported in Appendix B. The script has been divided in several subsystems:

- electric motor;
- gear train;
- ball screw;
- ASB bar and master cylinders;
- controller.

The block diagram of the ASB model is reported in Figure 4.1.

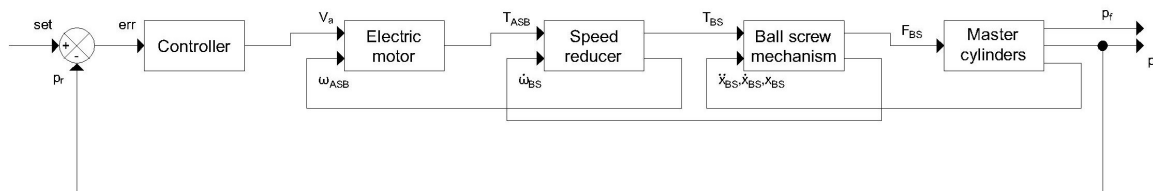


**Figure 4.1:** ASB model block diagram

Thanks to the Simulink script it was possible to understand the performance of the system designed. The first tests concerned the step response, in order to understand the promptness of the system, its precision and its capability to reach the targets required. A frequency response analysis was then conducted in order to evaluate the bandwidth of the ASB.

## 4.1 Electric motor

The electric motor used for the ASB actuation is an electric brushless motor. Details of the motor can be found in Section 3.2.2. The electric motor can be divided into three subsystems[44]: electric subsystem, magnetic subsystem and mechanical subsystem. For the electric subsystem the motor can be analysed with the equivalent electrical circuit reported in Figure 4.2[36]. Considering  $e_{in} = K_e \omega$ , from the equivalent electrical circuit it is possible to obtain equation 4.1.

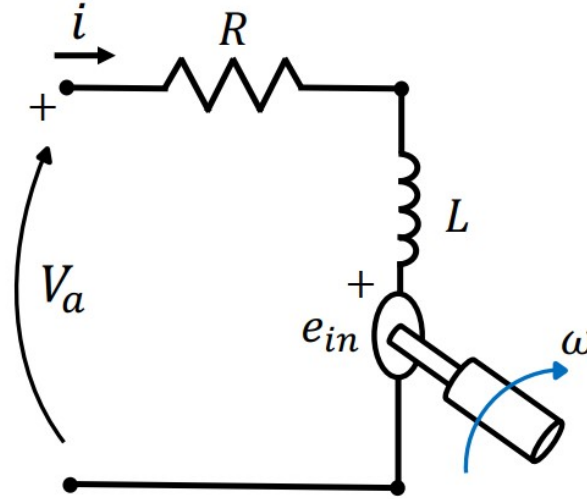


**Figure 4.2:** Electric motor equivalent circuit[44]

$$\frac{di}{dt} = \frac{1}{L}(V_a - Ri - K_e \omega_{ASB}) \quad (4.1)$$

Parameters in equation 4.1 are the following:

- $i$ : current absorbed by the motor;
- $L = 0.363$  mH: terminal inductance;
- $R = 0.942$   $\Omega$ : terminal resistance;
- $V_a$ : supply voltage ( $V_a = 24$  V is the maximum voltage);
- $K_e = 36$  mV/(rad/s): voltage constant;
- $\omega_{ASB}$ : electric motor's angular speed.

Thanks to the magnetic subsystem the current is transformed into torque (equation 4.2).  $K_t = 36$  mNm/A is the torque constant of the electric motor.

$$T_{motor} = K_t i \quad (4.2)$$

The mechanical subsystem consists in the torque equilibrium at the shaft of the electric motor and it allows to calculate the force which is output to the electric motor and input to the gear train. As it is possible to see in equation 4.3 the torque  $T_{ASB}$ , output of the electric motor, is equal to the torque  $T_{motor}$  generated by the motor minus the inertia of the rotor.

$$T_{ASB} = T_{motor} - I \frac{d\omega_{ASB}}{dt} \quad (4.3)$$

The parameters in equation 4.3 are the following:

- $T_{ASB}$ : torque output of the motor;
- $T_{motor}$  = total torque generated by the motor;
- $I = 137 \cdot 10^{-7}$  kg m<sup>2</sup> moment of inertia of the rotor;
- $\omega_{ASB}$ : electric motor angular speed.

The Simulink subsystem of the electric motor is reported in Figure B.4

## 4.2 Gear train

The gear train has effects on the kinematic of the ASB (equations 4.4, 4.5 and 4.6) and on its dynamic (equation 4.7)[26]. The output torque will be higher than the input torque, however the displacement, the speed and the acceleration will be reduced. Details on the gear train are reported in Section 3.2.3.

$$\theta_{GT} = \frac{1}{u} \theta_{ASB} \quad (4.4)$$

$$\omega_{GT} = \frac{1}{u} \omega_{ASB} \quad (4.5)$$

$$\dot{\omega}_{GT} = \frac{1}{u} \dot{\omega}_{ASB} \quad (4.6)$$

$$T_{GT} = u \eta_{SR} (T_{ASB} - I_{SR} \dot{\omega}_{ASB}) \quad (4.7)$$

The parameters in equations 4.4, 4.5, 4.6 and 4.7 are the following:

- $\theta_{GT}$ : angular displacement of the ball screw;
- $\theta_{ASB}$ : angular displacement of the electric motor;
- $\omega_{GT}$ : angular speed of the ball screw;
- $\omega_{ASB}$ : angular speed of the electric motor;
- $\dot{\omega}_{GT}$ : angular acceleration of the ball screw;
- $\dot{\omega}_{ASB}$ : angular acceleration of the electric motor;

- $T_{GT}$ : torque applied to the ball screw;
- $T_{ASB}$ : torque generated by the electric motor;
- $u = 18$ : transmission ratio;
- $\eta_{SR} = 0.75$ : efficiency of the gear train;
- $I_{SR} = 162 \cdot 10^{-7} \text{ kg m}^2$ : moment of inertia of the gear train.

The Simulink script of the gear train subsystem is reported in Figure B.5

### 4.3 Ball screw

The ball screw converts the rotary motion of the gear train to the linear motion of the ball screw nut (equations 4.8, 4.9 and 4.10). It also converts the torque in output from the gear train to a force applied to the ball screw nut (equation 4.11). Details of the ball screw are reported in Section 3.2.1.

$$x_{GT} = \frac{p}{2\pi} \theta_{GT} \quad (4.8)$$

$$\dot{x}_{GT} = \frac{p}{2\pi} \omega_{GT} \quad (4.9)$$

$$\ddot{x}_{GT} = \frac{p}{2\pi} \dot{\omega}_{GT} \quad (4.10)$$

$$F_{GT} = \frac{2\pi \eta_{GT}}{p} T_{GT} \quad (4.11)$$

The parameters in equations 4.8, 4.9, 4.10 and 4.11 are the following:

- $x_{GT}$ : ball screw nut displacement;
- $\theta_{GT}$ : ball screw shaft angular displacement;
- $\dot{x}_{GT}$ : ball screw nut speed;
- $\omega_{GT}$ : ball screw shaft angular speed;
- $\ddot{x}_{GT}$ : ball screw nut acceleration;
- $\dot{\omega}_{GT}$ : ball screw shaft angular speed;
- $F_{GT}$ : force applied to the ball screw nut;
- $T_{GT}$ : torque applied to the ball screw shaft;
- $p = 5 \text{ mm}$ : ball screw pitch;
- $\eta_{GT} = 0.96$ : ball screw efficiency.

In equation 4.11 the mass of the nut has been omitted since it will be considered in equation 4.12.

The Simulink script of the ball screw is reported in Figure B.6.

## 4.4 ASB bar and master cylinders

The ball screw nut, the ASB bar and the master cylinders are modelled in this section. As reported in Section 3.2.5 the nut and the ASB bar have a permanent connection, while the ASB bar and the master cylinders have a Hertzian contact connection which is detachable. For the analysis all the connections have been considered permanent, since the EBS activation has not been modelled.

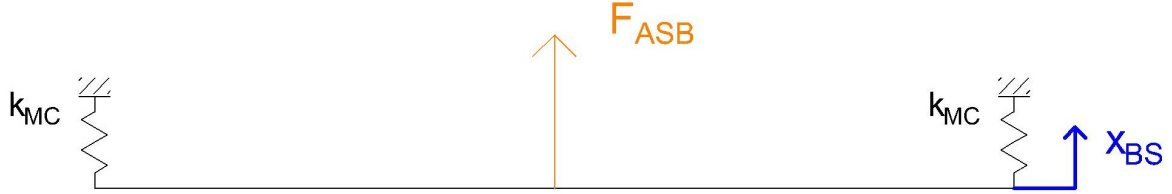


**Figure 4.3:** ASB bar model

Each master cylinder has been modelled as a spring (Figure 4.3) with equivalent stiffness  $k_{OIL} = 1.38 \cdot 10^5$  N/m, evaluated experimentally[22]. In this calculations the balance bar has not been taken into account since the value of  $k_{OIL}$  has been yet calculated with the presence of the balance bar, therefore it represents an equivalent stiffness that takes into account the stiffness of both the brake lines and of the balance bar.

Equation 4.12 represents the motion equation of the subsystem, from which it is possible to calculate the deceleration and, thanks to integrations, speed and displacement.

$$\ddot{x}_{GT} = \frac{F_{GT} - 2k_{OIL}x_{MC}}{m_{ASB} + 2m_{MC}} \quad (4.12)$$

Parameters in equation 4.8 are the following:

- $\ddot{x}_{GT}$ : acceleration of the subassembly;
- $x_{GT}$ : displacement of the subassembly;
- $F_{GT}$ : force applied to the ball screw nut;
- $m_{ASB} = 345$  g: mass of the ASB bar;
- $m_{MC} = 322$  g: mass of the moving part of the master cylinder.

The displacement of the master cylinders is saturated at 0 mm and at 20 mm, values corresponding to the end strokes of the ASB.

The force acting on the equivalent springs of the hydraulic pressure directly depends on the displacement of the master cylinder. From this force it is possible to evaluate the hydraulic pressure with equations 4.13 and 4.14, where  $A_{MC,f} = 2.41 \cdot 10^{-4} \text{m}^2$  is

the area of the front master cylinder and  $A_{MC,r} = 2.01 \cdot 10^{-4} \text{m}^2$  is the area of the rear master cylinder.

$$p_f = \frac{k_{OIL} x_{GT}}{A_{MC,f}} \quad (4.13)$$

$$p_r = \frac{k_{OIL} x_{GT}}{A_{MC,r}} \quad (4.14)$$

The Simulink script of the ASB bar and master cylinders subsystem is reported in Figure B.7.

## 4.5 Controller

For the ASB a closed loop system has been chosen, in order to compensate errors due to friction and external disturbances not predictable during the design process[44] (for example a State of Charge drop on the low voltage battery that supplies the electric motor). In order to ensure a good static and dynamic behaviour a Proportional Integrative controller has been chosen, tuned with Simulink PID Tuner toolbox. The PI controller has been preferred to the PID controller because of the oscillations that a derivative action could cause on the system. Values of the PI gains used are the following:

- proportional gain:  $K_P = 29.33$ ;
- integrative gain:  $K_I = 56.06$ .

The inputs to the controller subsystem are the set of pressure and the feedback of pressure on the rear line. The pressure on the front line is not directly controlled but, since the two master cylinders are connected with the balance bar, the force on the two master cylinders is the same and the pressures on front and rear lines differs only due to the different areas of the master cylinder pistons. The rear pressure has been preferred to the front pressure because it has higher values, since the area of the rear master cylinder pistons is lower, and therefore the sensitivity of the control will be higher.

The output of the controller subsystem is the voltage input to the electric motor subsystem. The maximum voltage allowed by the low voltage battery of the vehicle is 24 V, therefore the output of the PI controller is saturated to  $\pm 24$  V. In order to avoid the wind-up of the integrative action, an anti wind-up algorithm has been used.

The controller used is basic and does not take into account some characteristics of the ASB. For example the PI does not limit the current on the motor, and therefore its torque. This means that the current can be higher than the maximum current expected by datasheet and moreover the performance obtained will be slightly overestimated. Furthermore the ASB system has to be inserted in a more complete system that can control the dynamic of the whole vehicle.

The Simulink script of the controller is reported in Figure B.2.

## 4.6 Step response analysis

At first the system's step response behaviour has been analysed. The results are reported in Figure 4.4.

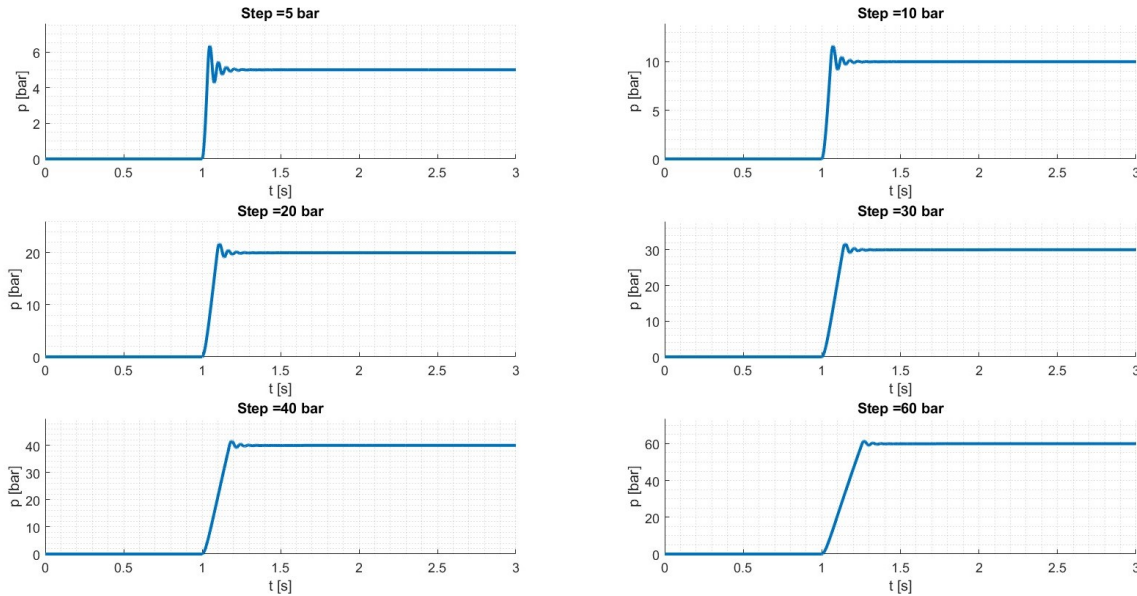


**Figure 4.4:** ASB step response at different sets of pressure

Figure 4.5 shows the main characteristics derived from the step response analysis. The parameters calculated are the following:

- rising time: time needed by the system to reach 95 % of the steady state value after the input change;
- settling time: time needed by the system to reach and remain between 95 % and 105 % of the steady state value after the input change;
- overshoot: maximum amount by which the pressure exceed its steady state value.

Because of the non linearity of the system (saturation) the system behaves differently at different values of input pressure. The readiness of the system (slope of the curve after  $t = 1$  s) does not change between the different sets, therefore the rising time has a linear dependency on the amplitude of the step, as it is possible to see in the first graphic of Figure 4.5.

The worst case between the ones analysed is the set at 60 bar of pressure on the hydraulic line. In this case the rising time obtained is of 191 ms, far less than the medium driver response time of 435 ms[29] that was the reaction target for the ASB.

The oscillations of the system are inversely proportional to the pressure set and the system is more damped because it approaches its dynamic limits. In fact, the saturation

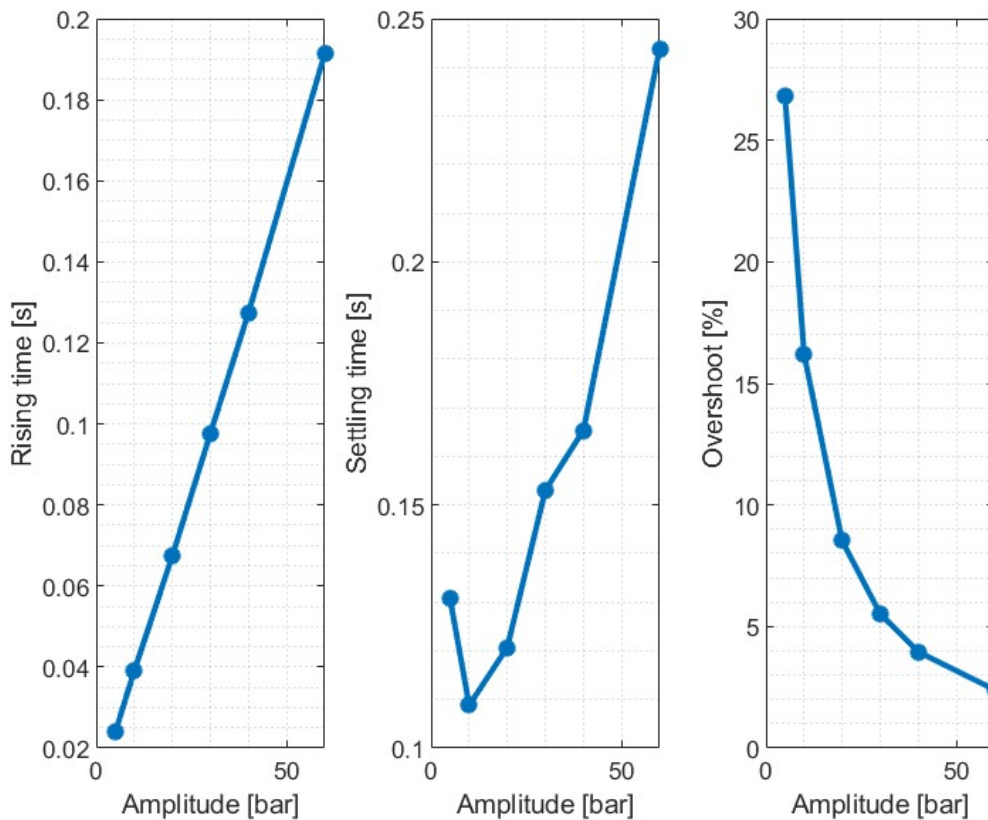


**Figure 4.5:** ASB step response analysis

of the supply voltage at 24 V imposes a limit on the torque generated by the electric motor. The oscillations around the steady state value are caused by excess of torque at the approaching of the feedback to the set; if the margin between the torque needed to reach the set and the maximum torque available decreases the excess of torque will reduce and, therefore, also the oscillations of the system. Due to the same principle also the overshoot of the feedback will reduce with higher sets. On the last graphic of Figure 4.5 it is possible to see that the reduction follows an hyperbolic trend.

The maximum overshoot obtained is of 26.8 %, which is a value higher than optimal[44]. However, for a medium-high demanding brake manoeuvre that will require 30 bar of pressure the overshoot will be only 5.5 %.

On the second graphic of Figure 4.5 it is possible to see both trends previously underlined:

- for low pressure sets the settling time decreases since the oscillations decrease;
- for medium-high pressure sets the settling time increases since the rising time increases.

The settling times obtained differ from the rising times by few hundredths of a second

(the mean difference is of 63 ms). This means that the oscillations does not affect too much the behaviour of the ASB.

Comparing with the step response of the ASB mounted on the SCD23 shown in Figure 2.8a it is possible to see that the electromechanical system has much less oscillations compared to the pneumatic system and therefore it is a much precise system. The rising time is lower on the SCD23's system, but the difference is negligible considering the lower oscillations that causes the system object of this thesis.

## 4.7 Frequency response analysis

A frequency response analysis has been performed on the ASB. Because of the model used, the brake fluid pressure can only be positive and therefore the ASB is a positive system, that is a system in which the state variables are always positive (or at least non-negative) in value[48]. Therefore the pressure set used to perform the frequency response analysis is a sine wave with a bias equal to its amplitude, so that the minimum of the input is 0 and the maximum of the input is two times the amplitude.

The resulting Bode diagram is reported in Figure 4.6. Since the system is non-linear the curve of the Bode plot depends on the amplitude of the signal.

As it was possible to imagine the bandwidth of the system, defined as the frequency at which the magnitude has a value of -3 dB[44], is inversely proportional to the amplitude of the input signal. From Figure 4.7 it is possible to see that the bandwidth curve as a function of the amplitude follows an hyperbolic trend.

From Figure 4.7 it is possible to observe a bandwidth up to 14 Hz for low demanding brake manoeuvre, while to obtain 60 bar on the line (amplitude = 30 bar) the bandwidth decrease up to 2 Hz. The results are promising compared to the SCD23 pneumatic architecture (Section 2.1.3) that can guarantee a maximum bandwidth of only 6.6 Hz (Figure 2.8b).

From Figure 4.7 it is possible to see also a small resonance around 10 Hz. The phenomenon reduces with higher amplitude since the non-linearities of the system move the bandwidth below the natural frequency of the system.

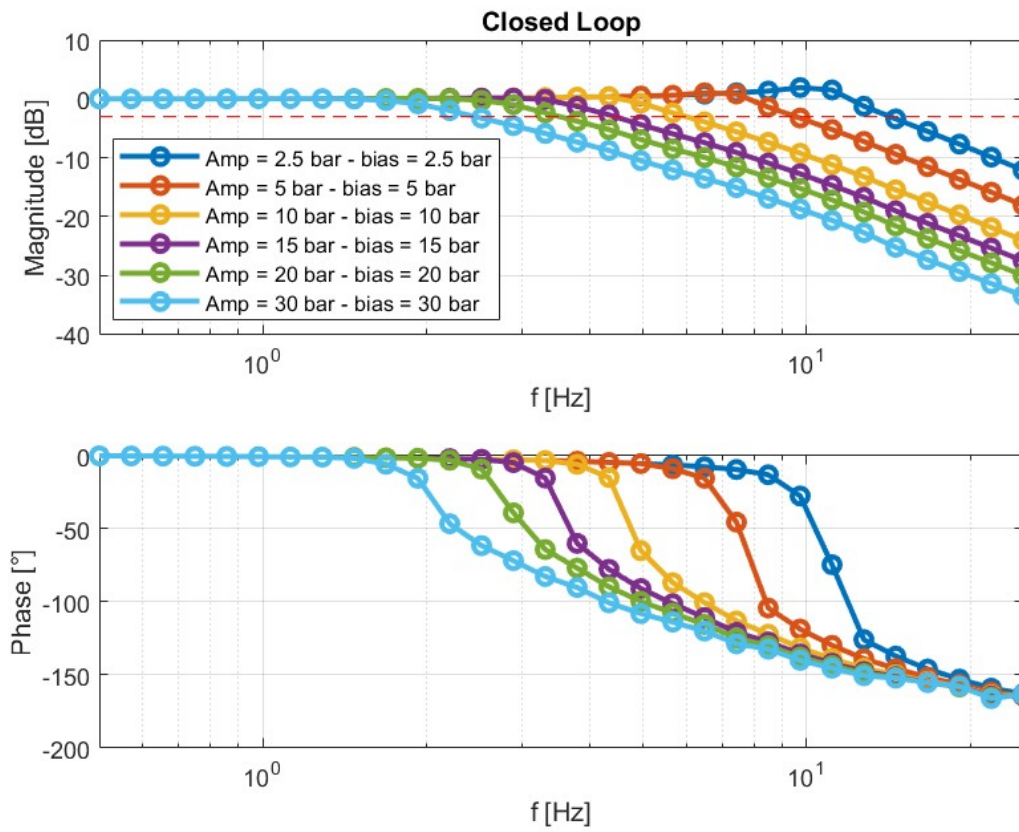
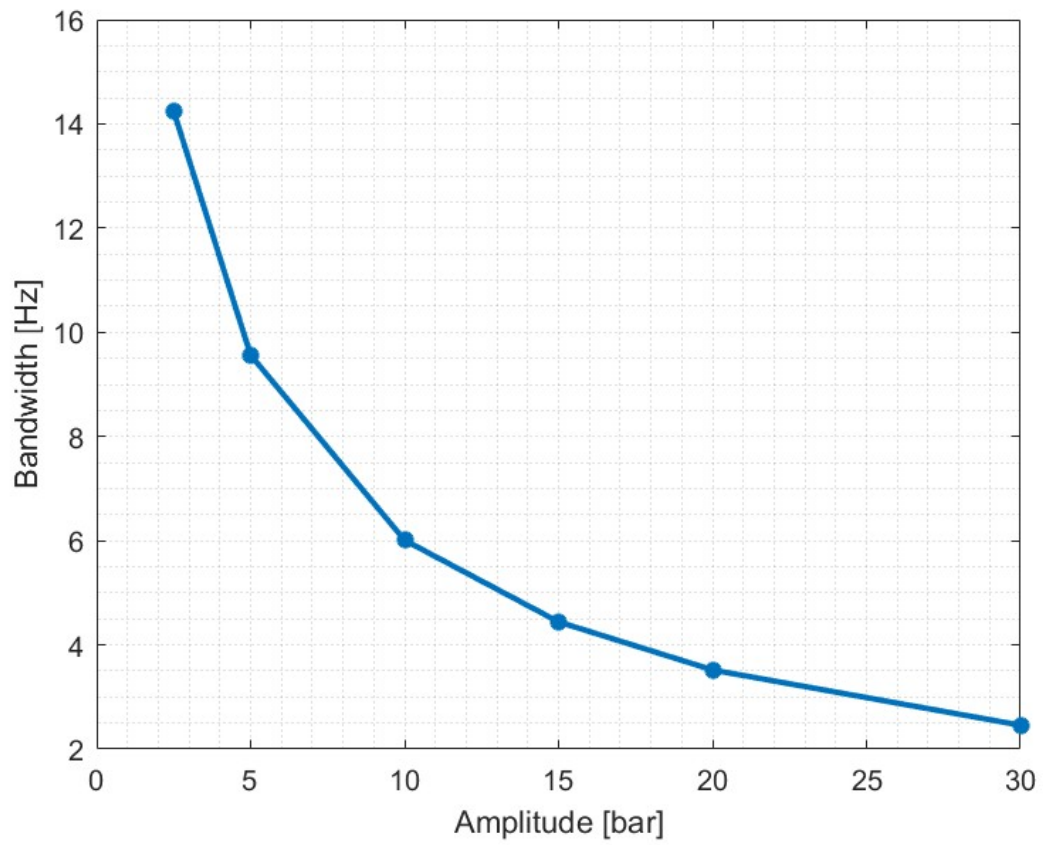


Figure 4.6: ASB Bode diagram



**Figure 4.7:** Bandwidth as a function of the signal amplitude

## Chapter 5

### EBS experimental campaign



**Figure 5.1:** SCD23 EBS mounted on the vehicle

Thanks to the low budget needed for the production of the Emergency Brake System, compared to the one needed for the ASB, it was possible to realize the new EBS architecture and to implement it on the 2023 prototype. In Figure 5.1 it is possible to see the ESB mounted on the vehicle. The case for the EBS is not the one designed in Section 3.3 but it is a simpler solution, therefore components like the balance bar and the bushing on the pneumatic cylinder fork are not present.

## 5.1 Test setup

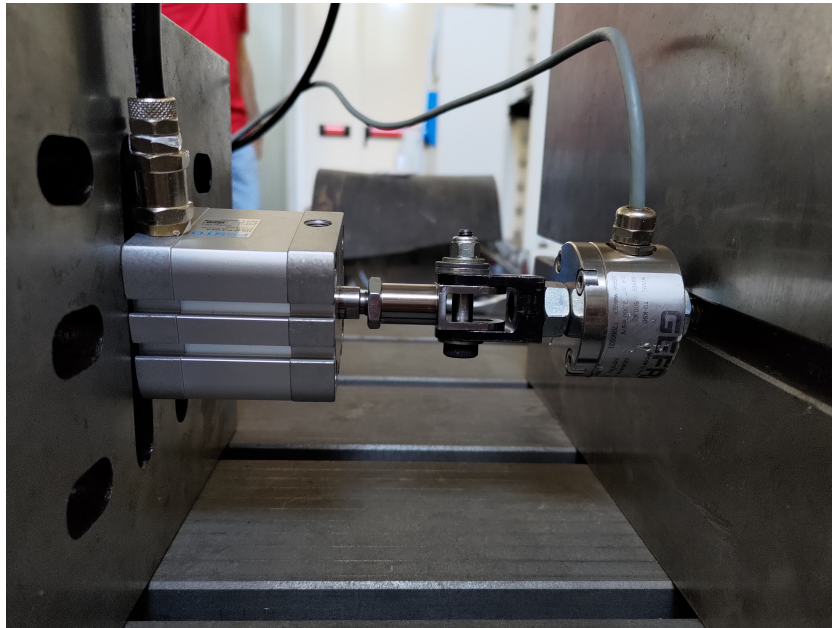


**Figure 5.2:** EBS actuator test setup

To perform the tests a test bench has been used. The pneumatic actuator has been mounted on a seismic mass in order to perform dynamic tests. The pneumatic cylinder rod has been jointed with a load cell able to evaluate the force developed by the actuator; the load cell is also connected to the seismic mass. In Figure 5.2 it is possible to see the test setup.

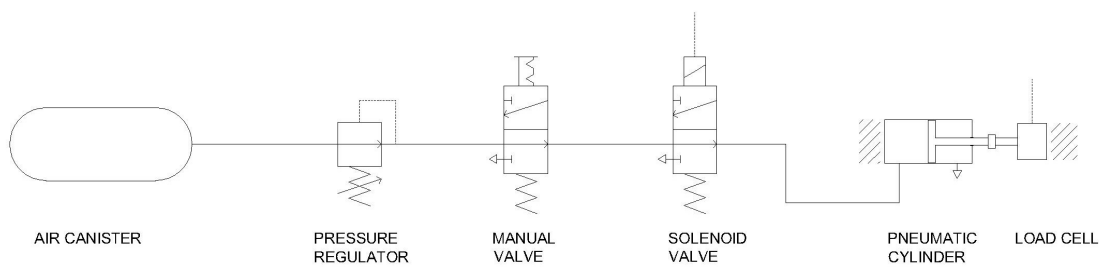


**Figure 5.3:** EBS actuator test bench pneumatic circuit

For the testing only one pneumatic cylinder has been used. The pneumatic line is the same as the one used on the vehicle and therefore it follows the scheme in Figure 5.3. The air supply is a canister loaded with compressed air at 140 bar. A pressure regulator is attached to the canister in order to reduce the pressure at 10 bar, maximum pressure allowed by rule T9.1.1. A manual valve allows the pressure to rise into the EBS

pneumatic line and it operates also as brake release (T15.1.7) after an emergency braking since it can connect the pneumatic cylinder to ambient pressure. The EBS actuator is eventually controlled by a normally open solenoid valve. The presence of the valves as well as the tubes of identical length to the one used in the vehicle guarantees the air to have the same fluid resistance that is possible to find once the system is assembled on the prototype.

Two pressure sensors are connected before and after the solenoid valve. The pressure measured before the valve will be called  $p_{supply}$  while for the pressure measured after the valve it will be referred as  $p_{EBS}$ .

Unfortunately it was not possible to evaluate the pressure that the EBS actuator will generate inside the brake lines since it was not possible to recreate the hydraulic lines outside the vehicle. Because of this the pneumatic actuator cylinder was not able to move and its stroke was null (excluding deformations of the material).

## 5.2 Data analysis

The tests performed had two main targets:

- evaluation of the maximum force developed;
- evaluation of rising time and decreasing time.

To evaluate the maximum force developed the system has been controlled with only the manual valve, leaving the solenoid valve open. The results of the tests are reported in Figure 5.4. The maximum force developed is  $F = 1445$  N. The value obtained is higher than the theoretical value of 1273 N obtained in Section 3.1.1. Furthermore the maximum pressure obtained is higher than 10 bar and has a value of 10.56 bar: this difference is due to the regulation of the pressure regulator, whose gauge precision is too low. Therefore, considering a pressure of 10.56 bar instead of 10 bar, the maximum theoretical force is of 1345 N. The force measured is still higher than the theoretical one and this is probably due to calibration errors of the pressure sensors and the load cell. However from the test it was possible to confirm that the force generated by the actuator is enough for the EBS application.

With further analysis on the curves of Figure 5.4 it is possible to see the behaviour of the pneumatic line. After the actuation the pressure and the force rise following a linear curve: during this period the fluid is in supersonic state[24]. After a few milliseconds the curve slope start to decrease, potentially because the ratio  $p_{EBS}/p_{supply}$  rise above the sonic ratio of the system. Since for this test the system has been actuated using the manual valve and not the solenoid valve it is not possible to evaluate the rising and decreasing time of the EBS because the actuation procedure differs from the one used in the vehicle.

For the rising time and decreasing time calculations the system has been actuated by means of the solenoid valve, leaving the manual valve open. The rising time has been defined as the time needed by the system to rise to 95 % of the steady state value after

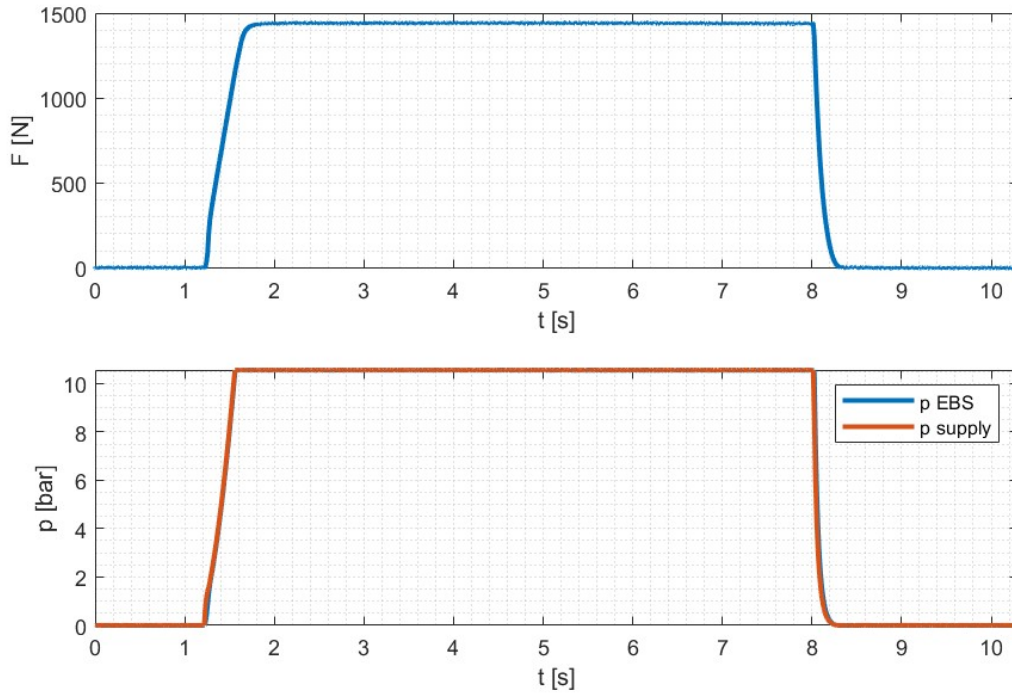


**Figure 5.4:** Experimental data of force and pressure during the test to evaluate the force developed

the input step; similarly the decreasing time has been defined as the time needed by the system to decrease to 5 % of the steady state value after the input step. Since the system does not oscillates the rising time is equal to the settling time.

At first a test has been conducted in order to understand the order of magnitude of rising time and decreasing time. Graphics are reported in Figure 5.5. Differently from the test reported in Figure 5.4 it is possible to see that the pressure  $p_{supply}$  is always at approximately 10 bar since the manual valve is in open position. During the rising of the pressure  $p_{EBS}$  inside the pneumatic cylinder chamber it is possible to see a small drop of  $p_{supply}$ : when the cylinder is actuated the flow from the canister to the cylinder causes a drop of pressure inside the part of the pneumatic line that was previously pressurized since the pressure regulator is not able to maintain a constant pressure during transient[24]; however  $p_{supply}$  rises to its steady state value as soon as the flow decreases.

From Figure 5.5 it is possible to see that the mean rising time is of 197 ms and it is higher than the decreasing time. In order to have an higher repeatability a larger number of actuations has been performed. The last test has been conducted controlling the solenoid valve with a PWM signal, using a frequency of 1 Hz and a duty cycle of 50 % which means that for every actuation/deactivation it is available a time of 500 ms, higher than both rising time and decreasing time. The results are reported in Figure 5.6.

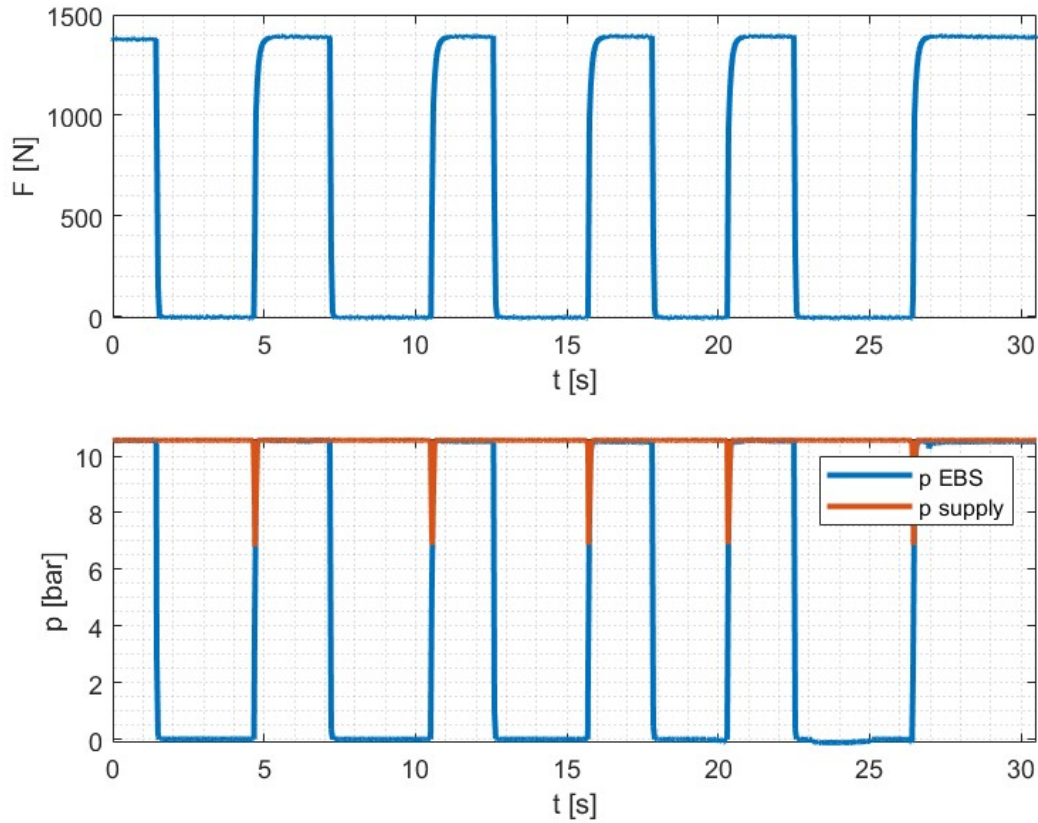


**Figure 5.5:** Graphics from test on the pneumatic actuator whose target is to define the order of magnitude of rising time and decreasing time

Data analysis graphics are reported in Figure 5.7. The mean rising time obtained has a value of 183 ms, while the mean decreasing time obtained has a value of 110 ms. The values obtained are very low and compatible with an emergency brake manoeuvre, considering that the rising time obtained is the time needed to reach the maximum braking force, while the time required to obtain the force needed by the EBS to reach the pressure targets calculated in Section 2.5 will be lower. However it is important to underline that due to lack of stroke on the test bench the value obtained are lower than the one expected on the vehicle.

Analysing the trend of the curve in Figure 5.7 it is possible to see that the rising time values follows a linear trend with positive slope. This trend is potentially due to the progressive discharge of the air canister and therefore to the decrease of flow speed. However the difference between the maximum and the minimum value for the rising time is lower than the one calculated for the decreasing time, meaning the canister discharge phenomenon does not affect the analysis on EBS performance.

At last it is possible to evaluate the characteristic time for the rising  $\tau_{rise}$  and for the decreasing  $\tau_{decrease}$  of the force. Since they are both defined as 1/3 of the rising/de-

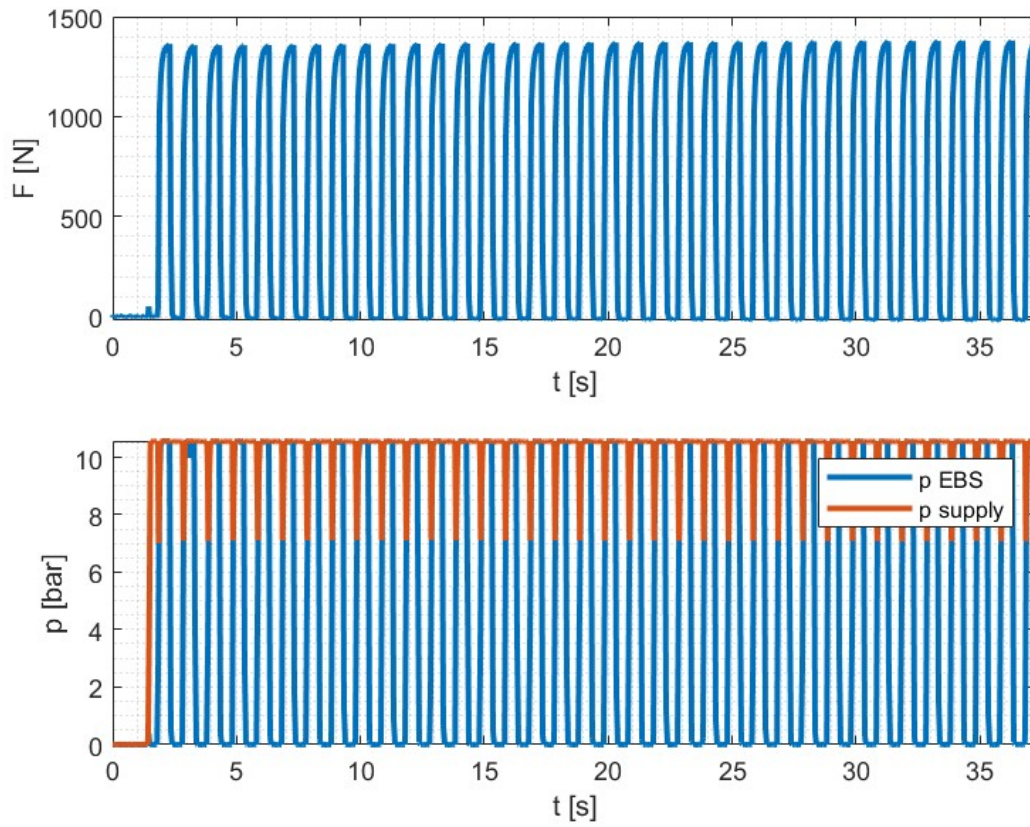


**Figure 5.6:** Graphics from test on the pneumatic actuator whose target is to define rising time and decreasing time

creasing time[44] the following mean values are obtained:

$$\tau_{rise} = 61 \text{ ms}$$

$$\tau_{decrease} = 37 \text{ ms}$$

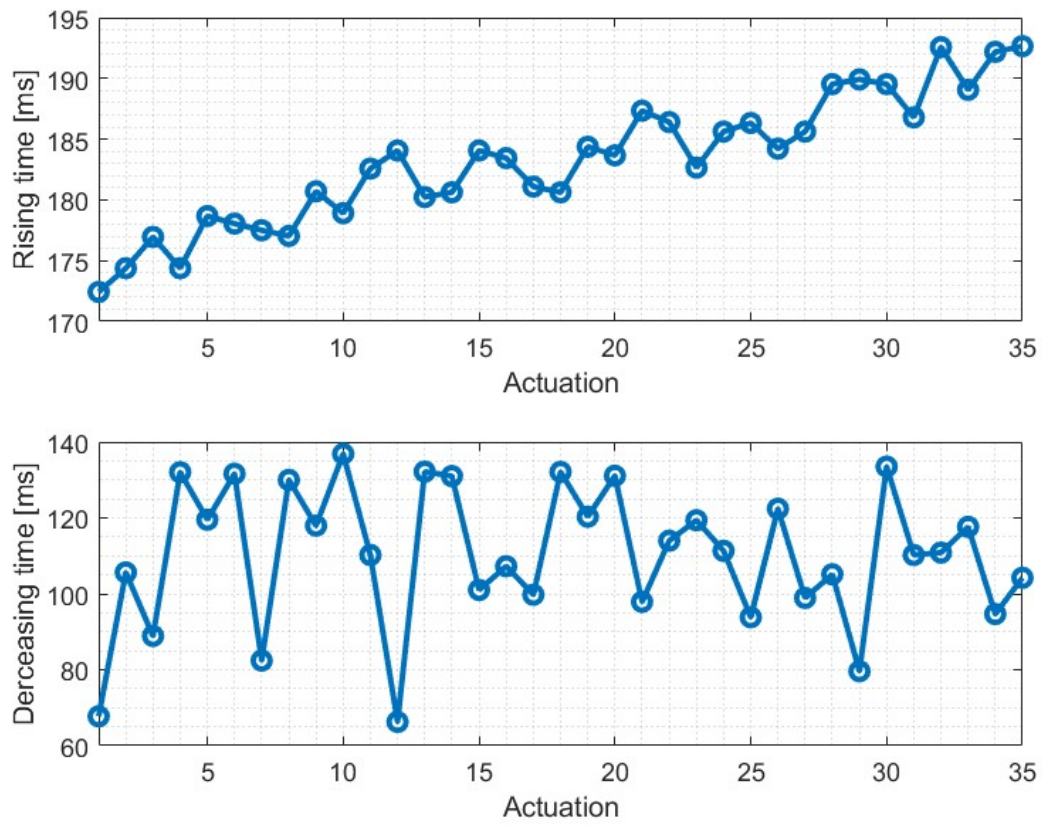


**Figure 5.7:** Rising time and decreasing time as a function of the number of actuations

# Chapter 6

## Conclusions and future steps

Since the Autonomous System Brake has been divided into ASB and EBS (Section 1.5) the conclusions will be divided for the two subsystems.

As regards to the EBS the main difference of the system designed compared to the one used in 2022 is the physical division between air and brake fluid chambers into the actuators. This characteristic together with the use of OEM components increased the reliability of the system, which was one of the drawback of the EBS mounted on the SCD22 prototype. Furthermore experimental tests show that the pneumatic cylinder used as EBS actuator develops enough force in a short time, and it is compatible with the safety function required by the EBS.

The ASB is a far more complex system, since it requires a fine control on the braking force. Like the EBS, the ASB is composed either of OEM and custom components, in order to reduce the cost and increase the reliability of the system. Due to the complexity of some custom components the ASB is planned to be manufactured only for the 2024 season. However numerical tests performed with Simulink show an excellent static and dynamic behaviour.

Compared with SCD22 ASB the system object of this thesis is expected to be more fast and able to achieve more braking force. Since the system is integrated to the EBS and not to the manual braking pedal, the complexity of the system will be higher. However no ordinary maintenance should be needed by the system, unlike the tensioning of the metal cable. The SCD23 ASB has a simpler concept than the new one, but, according to Simulink model analysis, the 2024 system is expected to have a better performance.

The complexity of the system is strictly tied to the space available inside the prototype, being the vehicle a Formula Electric car built in 2019 and not originally driverless. With the availability of enough space due to the manufacture of a new monocoque new options would be available. Using the same working principle as the system object of this thesis it would be possible to integrate the ABS and the ESB directly on the manual braking pedal. This solution would reduce the mass of the car and the complexity of the system.

Thinking outside of the Formula Student Driverless environment the same system could be used on road legal vehicles. For example the EBS could be used in cars for

emergency braking, while the ASB can be used in autonomous driving car as braking actuator. In both cases the systems have to be coupled to an Anti-lock Brake System, in order to increase brake effectiveness; however also a fine control on the ASB could decrease the possibility of wheel locking.

# Bibliography

- [1] History.com editors. *Automobile History*. 2018. URL: <https://www.history.com/topics/inventions/automobiles>.
- [2] ULRICH Lawrence. *Car History Timeline: From 3-Wheeled Buggies to Self-Driving Vehicles*. 2023. URL: <https://www.history.com/news/car-history-timeline>.
- [3] OICA. *Motorization rate 2020 – Worldwide*. 2020. URL: <https://www.oica.net/category/vehicles-in-use/>.
- [4] World Health Organization. *Global status report on road safety 2018*. Geneva, 2018. URL: <https://apps.who.int/iris/rest/bitstreams/1164010/retrieve>.
- [5] Istat. *Road accidents*. 2022. URL: [https://www.istat.it/it/files//2023/07/REPORT\\_INCIDENTI\\_STRADALI\\_2022\\_EN.pdf](https://www.istat.it/it/files//2023/07/REPORT_INCIDENTI_STRADALI_2022_EN.pdf).
- [6] RoadSafetyFacts.eu. *Passive safety systems: what are they and how do they work?* URL: <https://roadsafetyfacts.eu/passive-safety-systems-what-are-they-and-how-do-they-work/>.
- [7] RoadSafetyFacts.eu. *Active safety systems: what are they and how do they work?* URL: <https://roadsafetyfacts.eu/active-safety-systems-what-are-they-and-how-do-they-work/>.
- [8] RoadSafetyFacts.eu. *How can automated and connected vehicles improve road safety?* URL: <https://www.roadsafetyfacts.eu/how-can-automated-and-connected-vehicles-improve-road-safety/>.
- [9] Society of Automotive Engineers. *Taxonomy and Definitions for Terms Related to Driving Automation Systems for On-Road Motor Vehicles - J3016*. 2021. URL: [https://www.sae.org/standards/content/j3016\\_202104/](https://www.sae.org/standards/content/j3016_202104/).
- [10] National Highway Traffic Safety Administration. *Levels of Automation*. URL: <https://www.nhtsa.gov/sites/nhtsa.gov/files/2022-05/Level-of-Automation-052522-tag.pdf>.
- [11] European Transport Safety Council. *Europe's first cars with Level 3 automated driving go on sale in Germany*. URL: <https://etsc.eu/europes-first-cars-with-level-3-automated-driving-go-on-sale-in-germany/>.

- [12] Technical Committee on Motor Vehicles. *Guidelines on the exemption procedure for the EU approval of automated vehicles*. URL: [https://www.google.com/url?sa=t&rct=j&q=&esrc=s&source=web&cd=&ved=2ahUKEwih5b-q7mAAxWzS\\_EDHenJDWQQFn0ECBEQAQ&url=https%3A%2F%2Fec.europa.eu%2Fdocsroom%2Fdocuments%2F34802%2Fattachments%2F1%2Ftranslations%2Fen%2Frenditions%2Fnative&usq=A0vVaw1zu0-DIev41PQeKP3yxh\\_p&opi=89978449](https://www.google.com/url?sa=t&rct=j&q=&esrc=s&source=web&cd=&ved=2ahUKEwih5b-q7mAAxWzS_EDHenJDWQQFn0ECBEQAQ&url=https%3A%2F%2Fec.europa.eu%2Fdocsroom%2Fdocuments%2F34802%2Fattachments%2F1%2Ftranslations%2Fen%2Frenditions%2Fnative&usq=A0vVaw1zu0-DIev41PQeKP3yxh_p&opi=89978449).
- [13] Formula SAE. *History of Formula SAE*. URL: <https://www.fsaeonline.com/page.aspx?pageid=c4c5195a-60c0-46aa-acbf-2958ef545b72>.
- [14] Formula Student Germany. *Formula Student Rules*. 2023. URL: [https://www.formulastudent.de/fileadmin/user\\_upload/all/2023/rules/FS-Rules\\_2023\\_v1.1.pdf](https://www.formulastudent.de/fileadmin/user_upload/all/2023/rules/FS-Rules_2023_v1.1.pdf).
- [15] Oro Station. *Driving Innovation: How Motorsports Has Influenced Automotive Technology*. URL: <https://www.orostation.ca/post/driving-innovation-how-motorsports-has-influenced-automotive-technology>.
- [16] *Squadra Corse Driverless*. URL: <https://squadracorsedriverless.com/>.
- [17] Formula SAE Italy. *Class 1D - Overall results*. 2022. URL: [https://www.formula-ata.it/wp-content/uploads/2022/07/Class1D\\_Overall\\_20220716\\_official\\_rev02-1.pdf](https://www.formula-ata.it/wp-content/uploads/2022/07/Class1D_Overall_20220716_official_rev02-1.pdf).
- [18] MANCA Raffaele. *Design and implementation of an Electric Power Steering system for a Formula Student Driverless vehicle*. 2020.
- [19] SORRENTINO Gennaro. *Design of autonomous control systems for a Driverless race car: Remote Emergency System and Autonomous State Machine*. 2020.
- [20] Brembo. *Formula Student/SAE catalogue*. 2014. URL: [http://www.brembo-technik-center.de/brembo/downloads/racing/brembo-formula-student-katalog-2014\\_1.pdf](http://www.brembo-technik-center.de/brembo/downloads/racing/brembo-formula-student-katalog-2014_1.pdf).
- [21] Brembo. *Racing moto catalogue*. 2012. URL: [https://www.brembo.com/jp/Varie/Brembo\\_RacingMotoCatalogue.pdf](https://www.brembo.com/jp/Varie/Brembo_RacingMotoCatalogue.pdf).
- [22] CIOCCA Samuel. *Design and implementation of autonomous braking system for Formula Student Driverless application*. 2022.
- [23] DANESE Luca. *Design and implementation of an Emergency Brake System (EBS) for a Driverless Vehicle*. 2020.
- [24] BELFORTE Guido. *Manuale di pneumatica*. Milano: Tecniche Nuove, 2005.
- [25] Formula Student East. *Formula Student East Rules*. 2023. URL: [https://fseast.eu/wp-content/uploads/2023/02/FS\\_East\\_2023\\_Rules\\_Formatted\\_v1.1\\_28\\_02\\_2023.pdf](https://fseast.eu/wp-content/uploads/2023/02/FS_East_2023_Rules_Formatted_v1.1_28_02_2023.pdf).
- [26] FERRARESI Carlo and RAPARELLI Terenziano. *Meccanica Applicata*. Torino: C.L.U.T. Editrice, 2007.
- [27] Festo. *Compact cylinders ADN/AEN, to ISO 21287*. 2023. URL: <https://www.festo.com/media/pim/744/D15000100121744.PDF>.

- [28] SKF. *SKF spherical plain bearings and rod ends*. 2013. URL: [https://www.skf.com/binaries/pub12/Images/0901d19680154a05-06116\\_1-EN\\_tcm\\_12-122020.pdf](https://www.skf.com/binaries/pub12/Images/0901d19680154a05-06116_1-EN_tcm_12-122020.pdf).
- [29] BAUR H., MÜLLER S., HIRSCHMÜLLER A., HUBER G., and MAYER F. *Reactivity, stability, and strength performance capacity in motor sports*. 2006. URL: <https://www.ncbi.nlm.nih.gov/pmc/articles/PMC2465029/>.
- [30] Bosch Rexroth. *Screw assemblies*. 2021. URL: [file:///C:/Users/matte/Downloads/R999001185\\_202104\\_EN\\_Gewindetriebe.pdf](file:///C:/Users/matte/Downloads/R999001185_202104_EN_Gewindetriebe.pdf).
- [31] Park Industries. *Rack and Pinion Vs Ball screw*. URL: <https://www.parkindustries.com/stone/blog/rack-and-pinion-vs-ball-screw/>.
- [32] Hiwin. *Viti a ricircolo di sfere & accessori*. 2021. URL: [https://www.hiwin.it/images/download/documenti/Catalogo\\_HIWIN\\_BS-IT\\_2021.pdf](https://www.hiwin.it/images/download/documenti/Catalogo_HIWIN_BS-IT_2021.pdf).
- [33] SKF. *Rolling bearings*. 2018. URL: [https://cdn.skfmediahub.skf.com/api/public/0901d196802809de/pdf\\_preview\\_medium/0901d196802809de\\_pdf\\_preview\\_medium.pdf#cid-121486](https://cdn.skfmediahub.skf.com/api/public/0901d196802809de/pdf_preview_medium/0901d196802809de_pdf_preview_medium.pdf#cid-121486).
- [34] SOMA' Aurelio. *Fondamenti di meccanica strutturale*. Milano: Quine, 2020.
- [35] Maxon. *EC 45 flat catalogue*. 2019. URL: [https://www.maxongroup.it/medias/sys\\_master/root/8833813184542/19-EN-264.pdf](https://www.maxongroup.it/medias/sys_master/root/8833813184542/19-EN-264.pdf).
- [36] CAVAGNINO Andrea. *Macchine Elettriche*. Lecture notes. Politecnico di Torino, 2005.
- [37] NICODEMI Walter. *Acciai e leghe non ferrose*. Bologna: Zanichelli, 2008.
- [38] BUDYNAS Richard G. and NISBETT J. Keith. *Shigley's Mechanical Engineering Design*. New York: McGraw Hill Education, 2020.
- [39] SOMA' Aurelio. *Costruzione di Macchine*. Lecture notes. Politecnico di Torino, 2022.
- [40] Maxon. *Planetary Gearhead GP 32 C*. 2021. URL: [https://www.maxongroup.com/medias/sys\\_master/root/8882774343710/EN-21-396-397-398.pdf](https://www.maxongroup.com/medias/sys_master/root/8882774343710/EN-21-396-397-398.pdf).
- [41] BERRUTI Teresa, BRUSA Eugenio, CURA' Francesca, DELPRETE Cristiana, and ROSSETTO Massimo. *Elementi di Costruzione di Macchine*. Lecture notes. Politecnico di Torino, 2020.
- [42] CALIGARIS Luigi, FAVA Stefano, and TOMASELLO Carlo. *Manuale di meccanica*. Milano: Hoepli, 2016.
- [43] SKF. *SKF bushings, thrust washers and strips*. 2010. URL: [https://www.skf.com/binaries/pub12/Images/0901d19680090e01-SKF-bushings-thrust-washers-and-strips-1-EN\\_tcm\\_12-120169.pdf](https://www.skf.com/binaries/pub12/Images/0901d19680090e01-SKF-bushings-thrust-washers-and-strips-1-EN_tcm_12-120169.pdf).
- [44] BERTOLINO Antonio Carlo, DE MARTIN Andrea, NESCI Andrea, and SORLI Massimo. *Meccatronica*. Torino: C.L.U.T. Editrice, 2021.

- [45] SUBHASH Mishra and SAGAR Janghu. *Balance Bar Design and Motion Analysis of Pushrod*. 2014. URL: [https://globaljournals.org/GJRE\\_Volume14/3-Balance-Bar-Design.pdf](https://globaljournals.org/GJRE_Volume14/3-Balance-Bar-Design.pdf).
- [46] QUAGLIA Giuseppe. *Meccanica delle Macchine Automatiche*. Lecture notes. 2022.
- [47] CHIRONE Emilio and TORNINCASA Stefano. *Disegno tecnico industriale Vol.2*. Torino: Il capitello, 2018.
- [48] FARINA Lorenzo. *Positive systems in the state space approach: main issues and recent results*. 2002.

# Appendix A

## Abbreviations

**ABS** Anti-lock Brake System

**AS** Autonomous System

**ASB** Autonomous System Brake

**EBS** Emergency Brake System

**f** front

**FSG** Formula Student Germany

**MC** Master Cylinder

**r** rear

**RES** Remote Emergency System

**SAE** Society of Automotive Engineers

**SDC** Shutdown Circuit

# Appendix B

## Simulink model

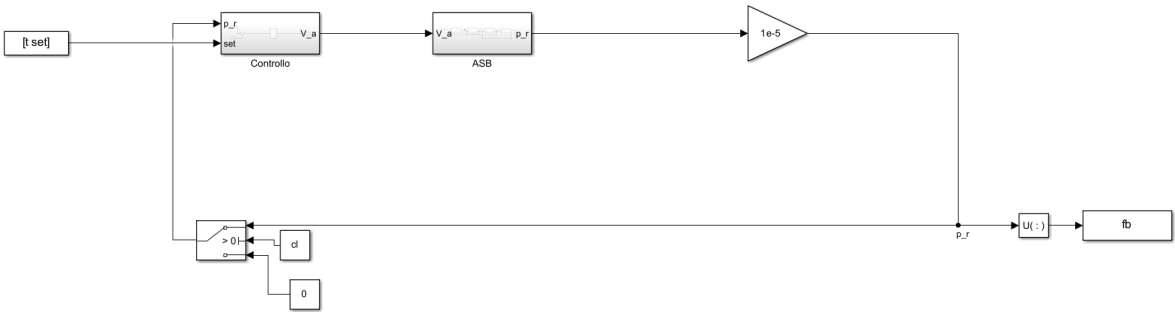


Figure B.1: ASB model

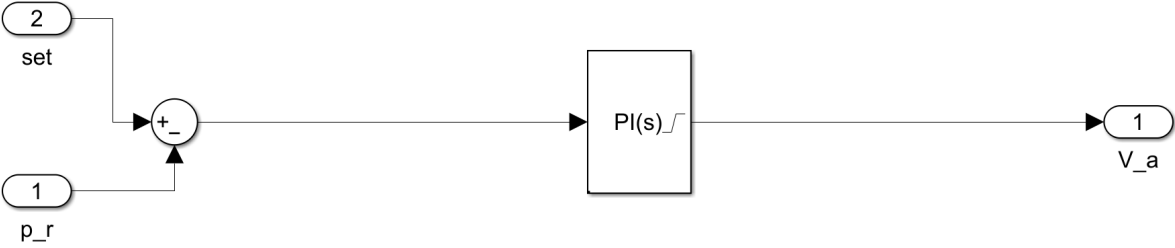


Figure B.2: ASB controller subsystem

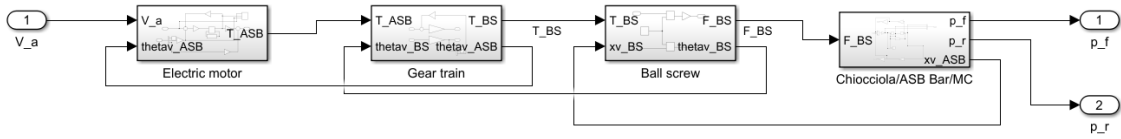


Figure B.3: ASB subsystem

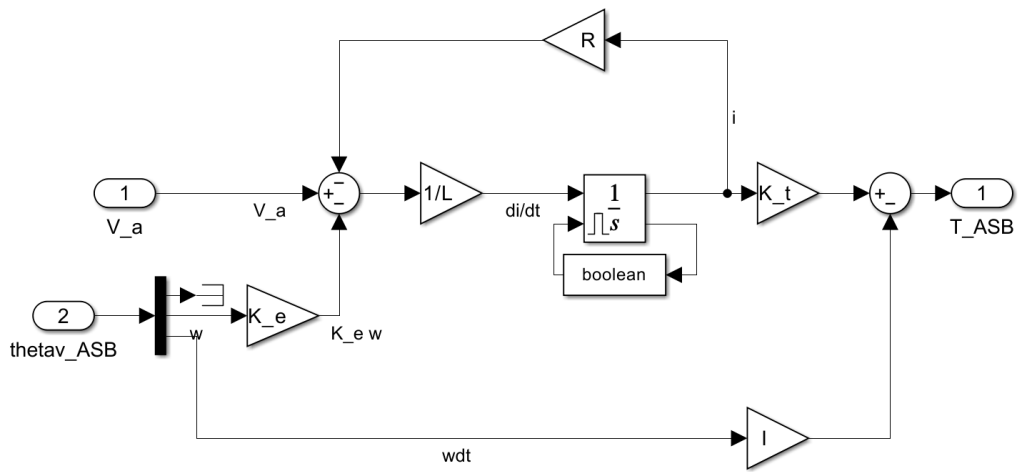


Figure B.4: Electric motor subsystem

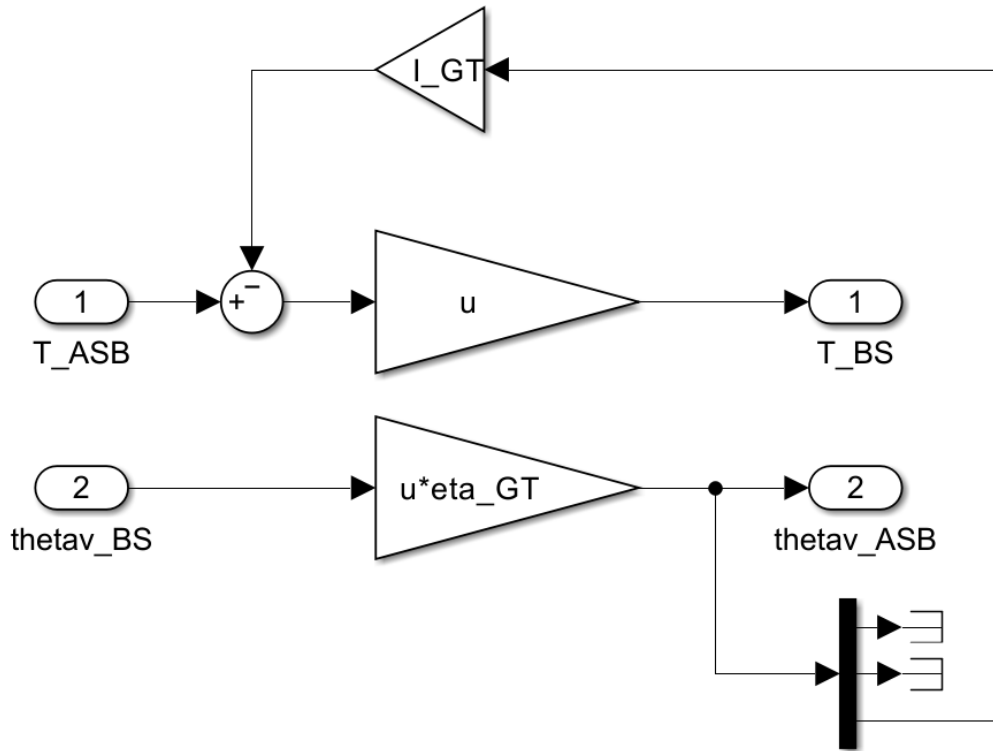


Figure B.5: Gear train subsystem

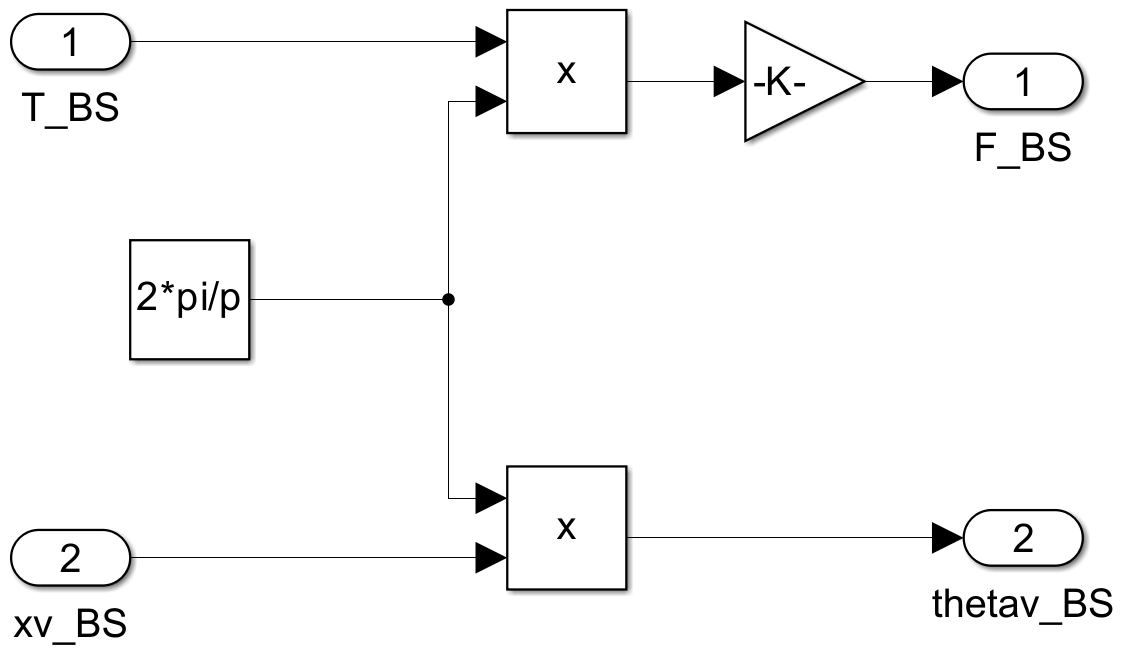


Figure B.6: Ball screw subsystem

